

# Design of Wideband Rotman Lenses with Dummy Ports for Wide-Scan Phased Array Applications

by

Somayeh ADIBIFARD

THESIS PRESENTED TO ÉCOLE DE TECHNOLOGIE SUPÉRIEURE  
IN PARTIAL FULFILMENT FOR A MASTER'S DEGREE  
WITH THESIS IN ELECTRICAL ENGINEERING  
M.A.Sc.

MONTREAL, AUGUST 29, 2018

ÉCOLE DE TECHNOLOGIE SUPÉRIEURE  
UNIVERSITÉ DU QUÉBEC

Copyright © 2018, Somayeh Adibifard, 2018 All right reserved

© Copyright reserved

It is forbidden to reproduce, save or share the content of this document either in whole or in parts. The reader who wishes to print or save this document on any media must first get the permission of the author.

BOARD OF EXAMNERS  
THIS THESIS HAS BEEN EVALUATED  
BY THE FOLLOWING BOARD OF EXAMINERS

Mr. Ammar Kouki, Thesis Supervisor  
Department of Electrical Engineering at École de technologie supérieure

Mr. Georges Kaddoum, President of the Board of Examiners  
Department of Electrical Engineering at École de technologie supérieure

Mr. Naïm Batani, Member of the jury  
Department of Electrical Engineering at École de technologie supérieure

THIS THESIS WAS PRESENTED AND DEFENDED  
IN THE PRESENCE OF A BOARD OF EXAMINERS AND PUBLIC  
AUGUST 21, 2018  
AT ÉCOLE DE TECHNOLOGIE SUPÉRIEURE



## **ACKNOWLEDGMENTS**

There are no proper words to convey my deep gratitude and respect for my thesis and research advisor, Professor Ammar Kouki. He taught me the skills to successfully formulate and approach a research problem. I would also like to thank him for being an open person to ideas, and for encouraging and helping me to shape my interest and ideas.

I would like to thank my family, especially my husband for always believing in me, for their continuous love and their supports in my decisions. Without them, I could not have made it here.



# **LA CONCEPTION D'UNE LENTILLE ROTMAN DE LARGE BANDE AVEC DES PORTS FACTICE POUR DES APPLICATIONS DE RÉSEAU A COMMANDE DE PHASE BALAYAGE LARGE**

Somayeh ADIBIFARD

## **RÉSUMÉ**

Les lentilles micro-ondes de Rotman permettent un balayage angulaire important sur une large bande de fréquences avec une faible erreur de phase. Elles permettent également la mise en forme de faisceaux par un vrai délai temporel. Leurs performances sont particulièrement idéales pour des applications telles que les véhicules télécommandés, les satellites, les radars anticollision, et les systèmes de communications ULB (Ultra Large Bande). L'utilisation des techniques de fabrication de circuits imprimés pour les lentilles Rotman a récemment facilité la conception de réseaux de mise en forme de haute performance avec de bas profils.

Ce mémoire focalise sur l'étude des réseaux d'antennes à commande de phase, à large bande et à large balayage angulaire par un réseau de mise en forme de faisceau basé sur des lentilles Rotman en microbande. Une capacité de balayage de faisceau de 40 degrés est mise en évidence dans la plage de fréquence de 8-12 GHz. Le défi le plus important dans ce travail est la conception d'une lentille Rotman de balayage de faisceaux large tout en maintenant une bonne adaptation d'impédance sur toute la bande de fréquence. À cette fin, il est proposé d'incorporer des ports supplémentaires entre l'entrée et la sortie de la lentille Rotman. Ce faisant le couplage mutuel entre les ports est considérablement réduit, ce qui conduit à une hausse des performances. Trois différentes lentilles Rotman sont modélisées à l'aide du logiciel CST. Une d'entre elles est fabriquée et caractérisée. Les résultats de mesure sont en accord avec ceux des simulations.

Une antenne Vivaldi en réseau à commande de phase et large bande incorporant une des lentilles Rotman développée est conçue et simulée. Une réduction de la taille en maintenant de bonnes performances en termes lobes secondaires et de gain de rayonnement a été effectuée. Les réseaux à commande de phase Rotman-Vivaldi offrent une alternative intéressante pour couvrir de larges bandes fréquentielle et un balayage angulaire important.

**Mots-clés** : réseau de mise en forme de faisceaux, matrice de Butler, lentille Rotman, antenne Vivaldi.





# **DESIGN OF WIDEBAND ROTMAN LENSES WITH DUMMY PORTS FOR WIDE-SCAN PHASED ARRAY APPLICATIONS**

Somayeh ADIBIFARD

## **ABSTRACT**

Microwave Rotman Lenses support wide-angle scanning, wideband, low-phase error, and true time delay (TTD) beam forming. Their performance is ideal for applications such as remote-piloted vehicles, satellites, collision-avoidance radars, and ultra-wideband communications systems. The use of printed circuit technology for Rotman Lenses in recent years has facilitated designing high performance but low profile, and lightweight beam-forming networks (BFNs).

In this thesis, wide-band wide-scan phased arrays are investigated by utilizing the beamforming network that is based on a microstrip Rotman Lens. A wide beam scanning capability of  $\pm 40^\circ$  for the frequency range 8-12 GHz is demonstrated. The most crucial part is to design a wide beam scanning Rotman Lens in conjunction with a good impedance matching over the entire frequency band. To do so, a technique is proposed to place the dummy ports between input ports and output ports of Rotman Lens as mutual coupling between ports are reduced significantly which results in improving the performance of Rotman Lens. Three different Rotman Lenses are designed and full wave simulated in CST (EM Simulation Software). One of them is fabricated and tested to verify the simulations. Good agreement between simulation and measured results is achieved.

A wide-band Vivaldi phased arrays antenna incorporating the designed Rotman lens is also designed and simulated. Size reduction while maintaining good performance in terms of grating lobes and radiation gain was carried out. The design Rotman-Vivaldi phased array offers a good alternative for achieving both wide scanning angles and wide bandwidth coverage.

**Keywords:** Beamforming Networks, Butler Matrix, Rotman Lens, Vivaldi Antenna.



## TABLE OF CONTENTS

	Page
INTRODUCTION .....	1
<b>CHAPTER 1</b> LITERATURE REVIEW .....	<b>5</b>
1.1 Beamforming Networks .....	5
1.1.1 Digital Beam Forming Networks.....	6
1.1.2 Network Beam Forming Networks.....	7
1.1.3 Microwave Lens Beam Forming Networks.....	8
1.2 Principle of Rotman Lenses.....	12
1.2.1 Formulation and analysis of Microwave lens .....	12
1.2.2 Defining Rotman’s characteristics.....	14
1.2.3 Extracting Rotman’s geometric parameter .....	15
1.2.4 Phase errors and their interpretations:.....	18
1.2.5 Drawing Rotman’s geometry and importing to the simulation software..	23
1.2.6 Investigation of the effect of Rotman Lens parameters on performance..	26
1.3 Conclusion.....	29
<b>CHAPTER 2</b> ROTMAN LENS DESIGNS .....	<b>31</b>
2.1 First design: 3x6 Rotman Lens.....	32
2.2 Second design: 5x6 Rotman Lens .....	40
2.3 Third design: conference paper (ANTEM 2016) .....	48
2.4 Measurement results.....	55
2.5 Conclusion.....	60
<b>CHAPTER 3</b> VIVALDI ARRAY ANTENNA.....	<b>61</b>
3.1 Vivaldi antenna single element.....	63
3.2 Substrate selection and size limitation for antenna design .....	63
3.3 Exponential slot design for Vivaldi antenna.....	65
3.4 Feed design for Vivaldi antenna.....	66
3.5 Simulation results of designed Vivaldi antenna in two software “HFSS and CST” ....	70
3.6 Radiation efficiency of Vivaldi antenna.....	78
3.7 Design and simulation of Vivaldi antenna linear array .....	79
3.8 Conclusion.....	81
CONCLUSION.....	83
APPENDIX I INPUT PARAMETERS FOR MATLAB CODE.....	85
APPENDIX II MATLAB CODE FOR ROTMAN DESIGN.....	87
APPENDIX III MATLAB CODE FOR ROTMAN PORT’S DESIGN .....	90
APPENDIX IV VALUE FOR TABLE 2.2 .....	94
APPENDIX V VALUE FOR TABLE 2.5.....	96

	Page
APPENDIX VI VALUE FOR TABLE 2.8 .....	98
LIST OF REFERENCES.....	100

## LIST OF TABLES

	Page
Table 1.1	Transceiver specification for VHF and UHF bands.....15
Table 1.2	Optimal values of parameter $g$ for different $F/D_s$ .....29
Table 2.1	Rotman Lens specifications .....32
Table 2.2	Matlab code's parameters.....32
Table 2.3	Simulation results for Array Factor.....40
Table 2.4	Rotman Lens specifications .....40
Table 2.5	Matlab code's parameters.....41
Table 2.6	Simulation results for Array Factor.....47
Table 2.7	Rotman Lens specifications .....48
Table 2.8	Matlab code's parameters.....48
Table 2.9	Simulation results for Array Factor.....54
Table 2.10	Comparison between measured and simulated results.....59
Table 3. 1	Array design goal .....63
Table 3. 2	simulation results in $\phi=90$ plane (E-palne) .....73
Table I.1	Input parameters for MATLAB code.....85



## LIST OF FIGURES

		Page
Figure 1.1	(a) Quasi light beamforming network (b) Circuitry beamforming network.....	5
Figure 1.2	Digital Beam Forming Networks .....	6
Figure 1.3	Butler Matrix BFN .....	7
Figure 1.4	Rotman Lens BFN.....	8
Figure 1.5	Rotman Lens BFN ports.....	9
Figure 1.6	Using the rectangle waveguide in Rotman Lens ports.....	10
Figure 1.7	Central plane, input and output ports of microstrip Rotman Lens .....	11
Figure 1.8	2D Rotman Lens BFN.....	11
Figure 1.9	The comparison between Non-focal Lens and Focal Rotman Lenses .....	13
Figure 1.10	Phase Errors across Array Aperture of Trifocal and Non-focal Lenses.....	13
Figure 1.11	2D Rotman's geometric parameter .....	16
Figure 1.12	Phase Errors Normalized to F across the Aperture for Single Port, $\alpha=30^\circ$ .....	19
Figure 1.13	Lens Beam and Receiving Contours versus (a) Focal Angle $\alpha$ (b) Maximum Subtended Angle $\theta_m$ .....	20
Figure 1.14	Use $g=1/\beta$ Parameter to Conduct Lens Optimization, $\alpha=30^\circ$ , $F/D=1$ .....	21
Figure 1.15	Lens Beam and Receiving Contours versus Parameter $\beta$ .....	21
Figure 1.16	Phase Error versus Eccentricity of the Beam Counter .....	22
Figure 1.17	Different F/D Reflects Different Levels of Phase Errors .....	22
Figure 1.18	An example of 4x4 Rotman Lens.....	24
Figure 1.19	An example of 6x6 Rotman Lens.....	24
Figure 1.20	Drawing a 4x4 Rotman Lens in CST .....	25

Figure 1.21	Effect of parameter $\alpha$ on Rotman's geometry .....	26
Figure 1.22	Effect of parameter $\theta$ on Rotman's geometry .....	27
Figure 1.23	Phase error in input port for maximum $\theta$ and $\alpha=30$ .....	28
Figure 1.24	Effect of parameter $g$ on Rotman's geometry .....	28
Figure 2.1	Extracted ports from MATLAB codes.....	33
Figure 2.2	Rotman Lens geometry (Red color is related to excitation.....	34
Figure 2.3	ADS-modeling of Rotman Lens.....	34
Figure 2.4	Rotman Lens with delay lines in CST, (b) Rotman Lens with covered dummy ports by absorber, and (c) Absorber material characteristic .....	35
Figure 2.5	The coupling diagrams of Rotman (a) input port 1 to output ports,.....	36
Figure 2.6	Array factor of the Rotman Lens: (a) 8 GHz .....	37
Figure 2.7	Extracted ports from Matlab codes .....	41
Figure 2.8	(a)Rotman Lens with delay lines in CST, and.....	42
Figure 2.9	The coupling diagrams of Rotman (a) input port 1 to output ports,.....	43
Figure 2.10	Array factor of the Rotman Lens: (a) 8 GHz, (b) 9 GHz, .....	46
Figure 2.11	Rotman Lens geometry (Red color is related to excitation.....	49
Figure 2.12	The coupling diagrams of Rotman (a) input port 1 to output ports (b) Input port 2 to output ports .....	50
Figure 2.13	Array factor of the Rotman Lens: (a) 8 GHz, (b) 9 GHz, .....	52
Figure 2.14	Photograph of measured Rotman Lens .....	55
Figure 2.15	The coupling diagrams of Rotman .....	56
Figure 2.16	Array factor of the Rotman Lens: (a) 8 GHz, (b) 9 GHz .....	57
Figure 3.1	An example of (a) Dual-polarized Vivaldi array designed (b) Vivaldi element .....	62
Figure 3.2	Bottom view of designed Vivaldi antenna in HFSS .....	66
Figure 3.3	Main parameters for Vivaldi feed design.....	67



Figure 3.4	50 ohms microstrip line width calculation .....	67
Figure 3.5	Vivaldi antenna with its impedance matching and feed in HFSS .....	68
Figure 3.6	Optimized parameters for desired S11 .....	69
Figure 3.7	Vivaldi element in HFSS.....	70
Figure 3.8	3D radiation pattern for designed Vivaldi antenna (a) 12 GHz .....	70
Figure 3.9	Radiation pattern in E-plane and H-plane .....	72
Figure 3.10	(a)Cross polarization at 8GHz.....	73
Figure 3.11	Simulation results of Vivaldi antenna in CST.....	75
Figure 3.12	Input matching with lumped port excitation in HFSS and CST .....	77
Figure 3.13	Maximum antenna gain vs frequency .....	78
Figure 3.14	Pattern efficiency at different frequencies .....	78
Figure 3.15	Vivaldi antenna array in HFSS.....	80
Figure 3.16	Vivaldi linear array 3D radiation pattern .....	80



## **LIST OF ABBREVIATIONS**

BFN	Beamforming Network
FCC	Federal Communications Commission (FCC)
PCB	Printed Circuit Board
UWB	Ultra-Wideband
EHF	Extremely High Frequency
ESPAR	Electronically Steerable Parasitic Array Radiator
SIW	Substrate Integrated Waveguides
CBFN	Circuitry Beamforming Network
QBFN	Quasi Light Beamforming Network
RL	Rotman Lens



## INTRODUCTION

The continually growing use of radio waves in wireless communications, radars, and personal electronics coupled with the need for higher data speeds has led to the use of higher frequencies and more bandwidth. At higher frequencies, such as millimeter-waves, radio wave propagation becomes more directional. Therefore, there will be needs for beamforming devices that can produce wide-angle, wideband, true-time delay, and steerable antenna beams to transmit and/or receive the information in or from certain directions. Such devices, typically known as Beam Forming Networks (BFN) can be made in various circuit technologies with printed circuit board (PCB) technology being most attractive for its low profile and lightweight.

Phased array antennas utilize BFNs to radiate energy into free space and they are used in many radars and satellite systems to electronically control the beam scanning. Array systems were limited to military application due to their high cost, but in recent years, implementing them in PCB has reduced their cost significantly. Therefore, array-based commercial applications have emerged and have become more and more viable. Wireless point-to-point communications and auto-collision avoidance radar are two examples of such applications. Recently, the Federal Communications Commission (FCC) allocated new bands for commercial ultra-wideband (UWB) (F. C. Commission, 2002) and Extremely High Frequency (EHF) applications (J. Wells, 2006), which brought up the need for low profile and high performance arrays. Such arrays should offer wideband frequency coverage as well as a wide range of scan angles for spatial coverage.

Wideband-wide scan low-cost phased array antennas are increasingly sought after for many commercial and military applications (Steven Christie et al, 2012). Over the past decades, a significant body of research has been conducted on this subject. Low cost phased array antennas based on electronically steerable parasitic array radiator (ESPAR) have been recently been reported, e.g. in (M. Ranjbar Nikkhah et al, 2014) and more such systems are needed. In this context, Rotman-Vivaldi phased arrays may offer a good alternative for achieving both wide-scanning and wideband coverage without the need for steering electronic components.

Indeed, the Rotman Lens allows multiple antenna beams to be formed without the need for phase shifters as these represent a major part of the cost of phased array antennas as well as being a source of losses. Furthermore, based on previously reported designs (Woosung Lee et al, 2011), beams produced by Rotman Lenses tend to vary little with frequency. These interesting features make Rotman Lenses an excellent candidate for wide-band multi-beam phased array antennas as a low-cost beamforming network. Rotman Lenses can be implemented using different structures such as microstrip, substrate integrated waveguides (SIWs), post-wall waveguides, or laminated waveguides. Recently, a fast design of Rotman Lens based on odd and even mode characteristics has been presented (M. Ranjbar Nikkhah, et al, 2015). Still, further design and performance improvements can be achieved and are required.

This thesis aims at designing microwave lens-based beamforming networks and optimizing their performance. Traditional design theory will be improved in terms of input and output matching. Microwave lenses for PCB implementation is emphasized. Accurate simulation and analysis method based on electromagnetic full-wave simulation will be explored. A novel technique that improves the input and output matching is proposed. Two microwave lenses have been designed and prototyping was carried out. Measured results of the prototypes are reported and they validate the proposed designs.

The remainder of this thesis is organized as follows. Chapter 1 presents the basic concepts and the relevant state of the art in the literature on beamforming networks. Besides, understanding the BFNs and previous researchers' works, the content of this chapter provided invaluable basis for this dissertation to propose new formulations, simulation method and optimization strategies. Chapter 2 is dedicated to the design of Rotman Lenses. Three alternative Rotman Lenses designs are explored through electromagnetic field simulation and one of the three designs is prototyped and tested. In Chapter 3, the design of a Vivaldi linear array antenna is carried out using both HFSS and CST full wave simulators. An optimization of the array performance is also carried out with good overall performance achieved in simulation. Concluding remarks and recommendations for future work are presented in the Conclusion.

### **Thesis Contributions**

The major contribution of this thesis are listed below:

A new proposed design technique to improve the input and output matching of a Rotman Lens. A wide-band wide-scan phased array is investigated by utilizing the beamforming network that is based on a microstrip Rotman Lens. A wide beam scanning capability of  $\pm 40^\circ$  for the frequency range 8-12 GHz is demonstrated. The most crucial part is to design a wide beam scanning Rotman Lens in conjunction with a good impedance matching over the entire frequency band. To do so, dummy ports are placed between input ports and output ports of the Rotman Lens and the mutual coupling between ports is reduced significantly, which results in improving the performance of the Rotman Lens.

A Vivaldi antenna array suitable for integration with a Rotman Lens is designed.

Rotman-Vivaldi phased arrays offer a good option for achieving both wide-scanning and wideband frequency coverage. Therefore a Vivaldi array antenna is designed for potential integration with the proposed Rotman Lens.

### **Published paper:**

S. Adibifard and A. Kouki, "Design of a wideband Rotman Lens with dummy ports for wide-scan phased array applications," 2016 17th International Symposium on Antenna Technology and Applied Electromagnetics (ANTEM), Montreal, QC, 2016, pp. 1-2. doi: 10.1109/ANTEM.2016.7550199





# CHAPTER 1

## LITERATURE REVIEW

### 1.1 Beamforming Networks

Nowadays, antenna systems with the ability to produce multiple beams have many applications in satellite communication, electronic war, and radar systems. In such systems the phase and amplitude of each array element can be controlled through the use of either fixed or controllable circuit components, collectively referred to as a Beam-Forming Network (BFN). In general, BFNs can be categorized in two different groups: Circuitry beamforming networks (CBFNs) and Quasi light beamforming networks (QBFNs). In CBFNs, the beam angle and beam width are frequency dependent while in QBFNs the beams are frequency independent. J. Dong et al (2009). The frequency independent nature of QBFNs is useful for achieving wideband coverage. Figure 1.1 illustrates these two classes of beam formers.

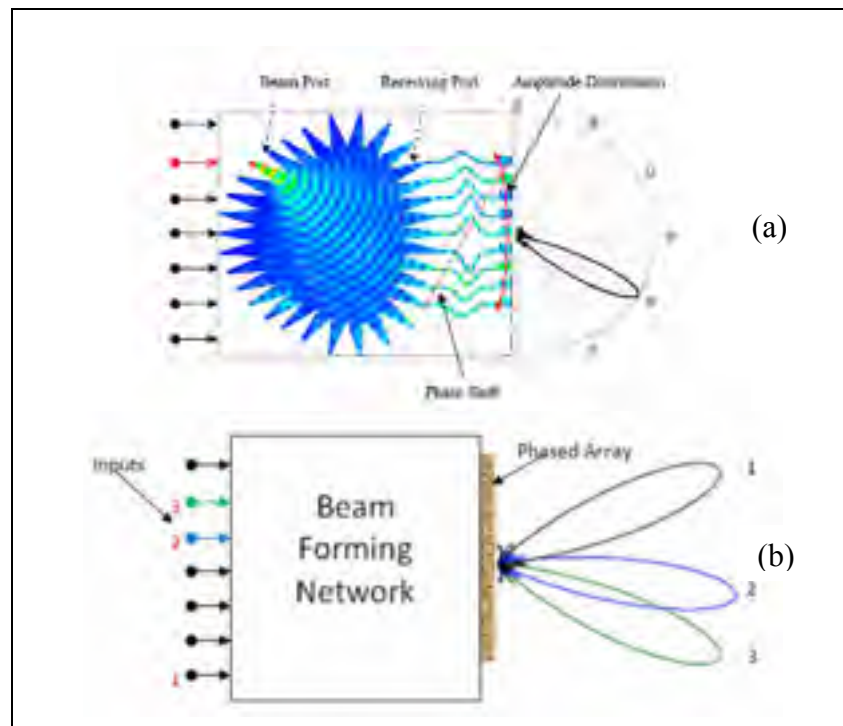


Figure 1.1 (a) Quasi light beamforming network (b) Circuitry beamforming network

Adapted from J. Dong et al (2009)

BFNs can also be categorized according to whether they form a single beam at a single port or multiple beams at multiple ports. There are several ways to design a beam forming network such as: Digital BFNs, network BFNs and microwave lens BFNs. Digital and network methods are circuitry beamforming network and microwave lens method is quasi light beamforming network.

### 1.1.1 Digital Beam Forming Networks

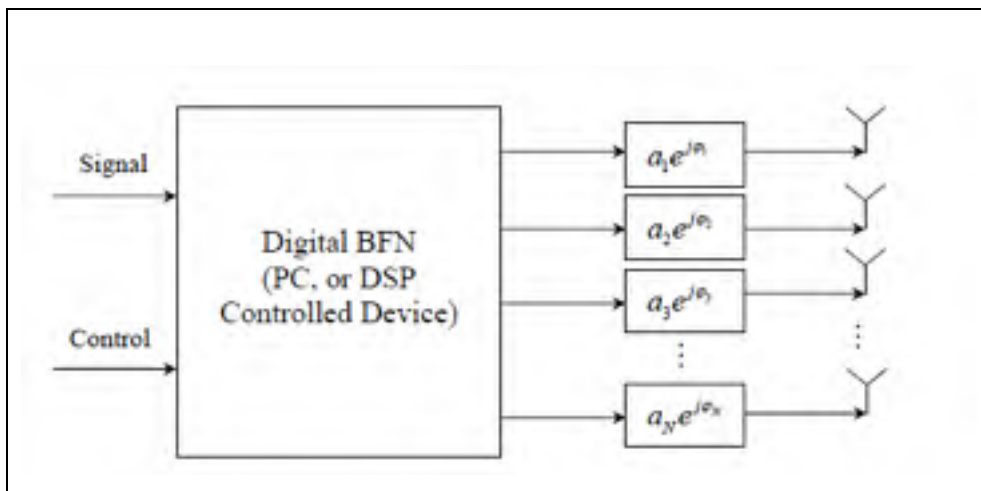


Figure 1.2 Digital Beam Forming Networks  
Adapted from J. Dong et al (2009)

Digital Beam Forming Networks, like the one shown in figure 1.2 will provide the exact amplitude and phase control on the digitized signals for each of the array elements. The advantages of this method are zero phase error, flexible amplitude tapering and complete control over scanning. However, they require multiple RF front-ends, which tends to increase cost.

### 1.1.2 Network Beam Forming Networks

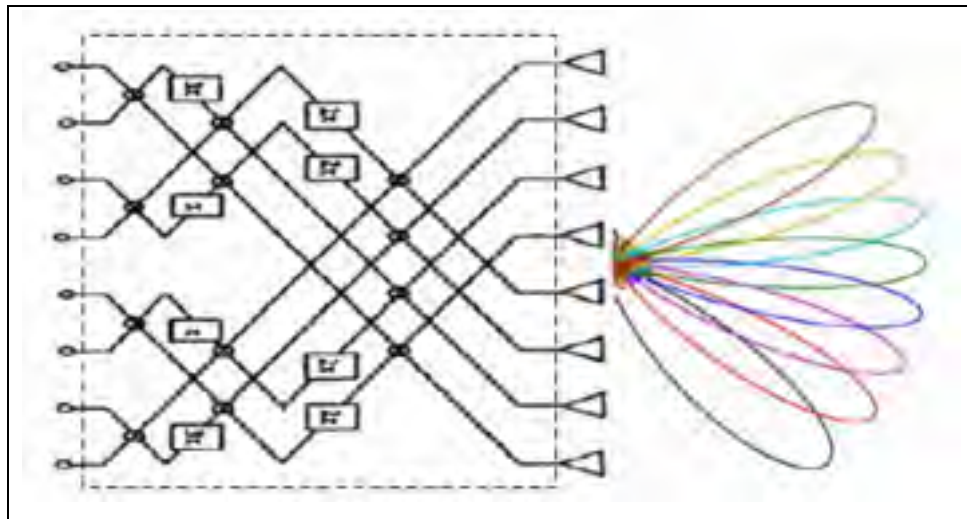


Figure 1.3 Butler Matrix BFN  
Adapted from J. Dong et al (2009)

This is an analog network typically consisting of hybrid junctions and phase shifters. One such network is illustrated in figure 1.3 and is known as a Butler Matrix BFN. Butler Matrix BFN is one of the earliest CBFN. The advantages of a Butler matrix are that it is easy to fabricate and can be made in PCB technology, e.g., microstrip, stripline, coplanar waveguide. Furthermore, the Butler matrix contains less components compared to other CBFNs such as Blass Matrix (R. C. Hansen, 1998). One of the disadvantages of this BFN is its dependency on frequency, i.e., limited bandwidth. Therefore, its performance for large bandwidths is limited by the bandwidth of its components and as frequency changes, the beams that it produces tend to shift in orientation and shape. Furthermore, some of its elements require lines to cross-over which may lead to complicated layouts that require multi-layer technology. Additionally, as the number of ports, i.e., beams, increases so will the number of components. This will lead to more losses in the BFN structure and thus reduced antenna gain.

### 1.1.3 Microwave Lens Beam Forming Networks

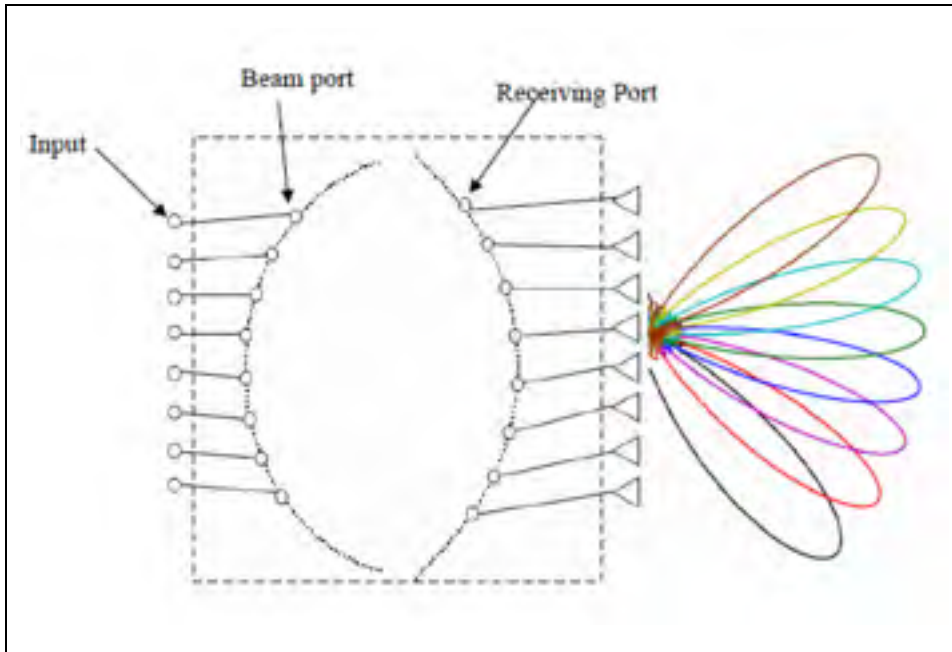


Figure 1.4 Rotman Lens BFN  
Adapted from J. Dong et al (2009)

Microwave Rotman Lens is a type of QBFN. Microwave lens Beam Forming Networks apply path delay mechanism to produce the desired phase at its output ports. This mechanism is independent of frequency, so it is considered as true-time delay device and it can be used for wideband applications. Figure 1.4 shows a general diagram of Rotman Lens BFN. The main advantages of Rotman Lenses compared to Butler and Blass Matrices and other similar structures are:

- 1- Less switching elements are required;
- 2- Feeding the linear and planar arrays with high voltage transfer capability;
- 3- Better form factor, lower weight and fabrication cost.

Therefore, a Rotman Lens is suitable for applications that require both large scan of the radiation pattern and wide frequency range coverage.

The main parameters that can control the amplitude and phase of the signals between the inputs (beam ports/array ports) and outputs (array ports/beam ports) in a Rotman Lens design are as follows:

- 1- The number and location of beam ports;
- 2- The number and location of array ports at output of Rotman Lens;
- 3- The number and location of dummy ports to absorb the reflected signal and improve the matching;
- 4- The length of TEM transmission lines that connect the output ports to the input of array;
- 5- Distance between radiation elements in array;
- 6- Other geometric parameters of Rotman Lens.

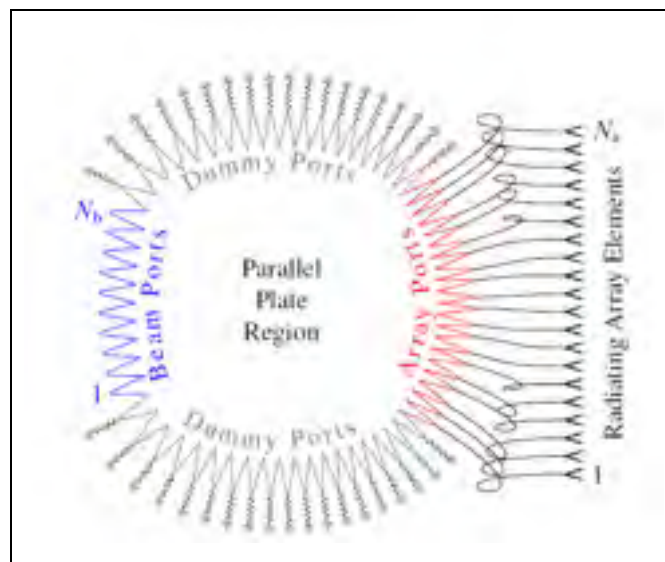


Figure 1.5 Rotman Lens BFN ports  
Adapted from J. Dong et al (2009)

To define the location of the input, output and dummy ports, all the coupling between feeding lines and ports should be considered. It should be noted that the isolation between ports, i.e., reflection from all other ports (beam and dummy) to the array ports, and spill over related to the beam ports are the main parameters that can limit the bandwidth. Therefore, they all have to be considered to be able to design a good Rotman Lens. Figure 1.5 shows the details of Rotman Lens with its beam, dummy and array ports.

Rotman Lenses are typically realized in one of two technologies: waveguides or printed transmission lines. Waveguides can handle higher power while printed striplines can handle wider bandwidth and printed microstrips are low profile. In waveguide technology, there are two parallel plates to form the cavity of the Rotman Lens. The rectangular waveguide with the excitation mode of TE<sub>01</sub> is used for the input and output ports. The method of stepping and tapering of waveguide walls can be used for the matching between ports and Rotman Lens cavity. Finally, microwave absorber materials can be utilized to load the sides of the cavity such that they act as dummy ports. Such structures, as shown in figure 1.6, are mostly used in millimeter wave application due the lower loss of waveguides compared to printed transmission lines.

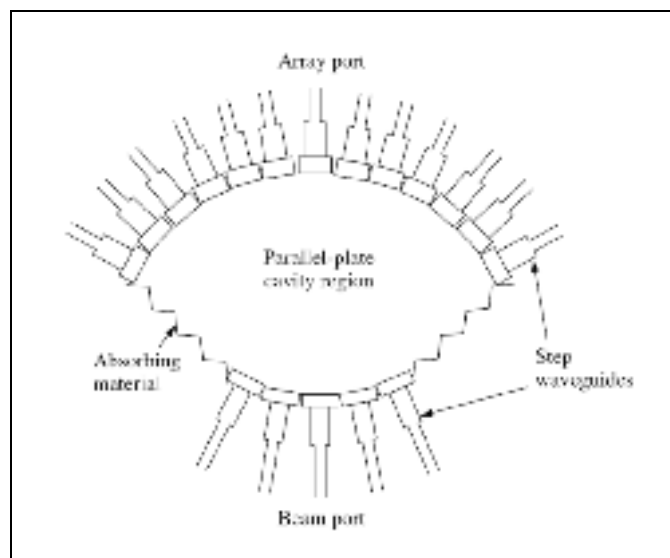


Figure 1.6 Using the rectangle waveguide in Rotman Lens ports  
Adapted from R. C. Hansen (1998)

In printed transmission lines technology, such as microstrip and stripline, the central part of the lens is made of a conducting patch and the input and output ports are connected to it through tapers as shown in figure 1.7. The dummy ports are terminated by matched loads.

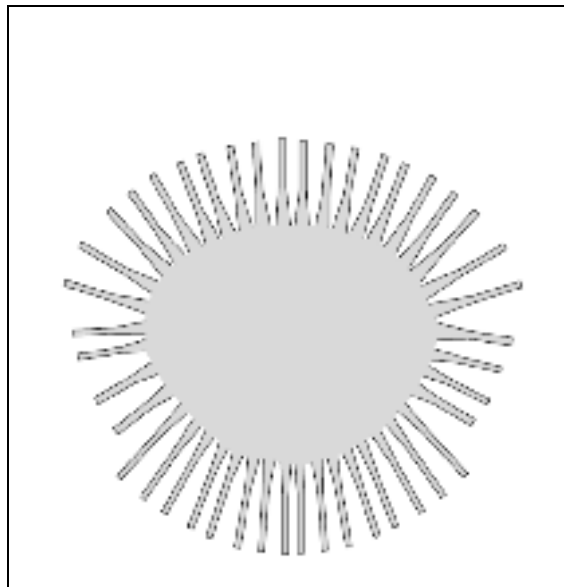


Figure 1.7 Central plane, input and output ports of microstrip Rotman Lens  
Adapted from R. C. Hansen (1998)

A more elaborate BFN can be made by stacking multiple planar Rotman Lenses as shown in figure 1.8. In this arrangement each row and column are able to produce orthogonal beams.

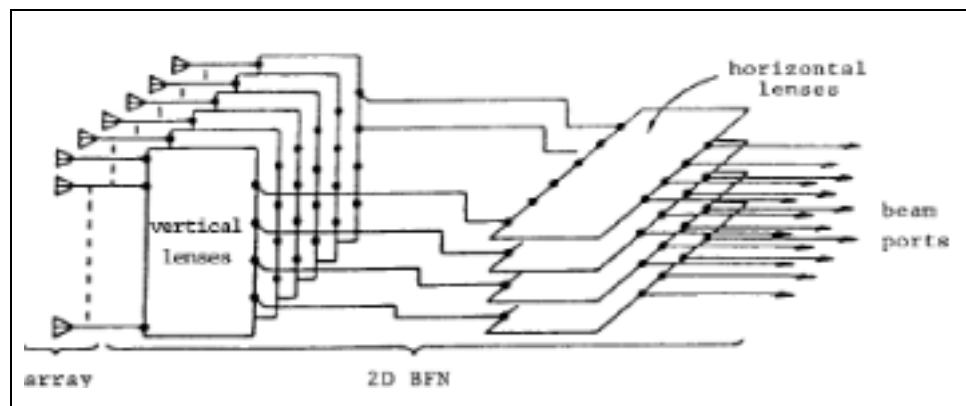


Figure 1.8 2D Rotman Lens BFN  
Adapted from R. C. Hansen (1998)

## 1.2 Principle of Rotman Lenses

A systematic method should be employed in Rotman Lens design. In fact in each step of the design, all the constraints and parameters that can affect the performance of the Rotman Lens should be carefully considered. The Rotman Lens design can be broken down into five steps. These steps include (1) defining the Rotman Lens' characteristics, (2) extracting its geometric parameters, (3) drawing the geometry and adding ports and transmission lines, (4) simulating the resulting structure's performance, and (5) fabrication and testing. In this thesis, the details of each step will be discussed.

### 1.2.1 Formulation and analysis of Microwave lens

The microwave Rotman Lens design starts with theoretical parameters that are determined using geometrical optics. There are three methods to design a Rotman Lens: (1) Trifocal Lens Designs, (2) Quadrifocal Lens Designs, and (3) Non-focal Lens Design. The differences between these methods are the number of design degrees of freedom and the theoretical phase error performance across the lens aperture.

#### 1.2.1.1 Non-focal versus to focal lens design

At this point, it is useful to compare the non-focal with the focal lens design approaches. We consider the lens parameters reported in (Rappaport et al, 1985) with an F/D ratio (Focal to array dimension) of 1. We start by designing a non-focal Rotman Lens that minimizes the phase error over the array aperture J. Dong et al (2009). Next we design trifocal and quadrifocal lenses for the same F/D ratio. Figure 1.9 shows the comparison between non-focal lens and the two focal lenses at the half plane subtended scan angles. As can be seen there are ideal focal points at  $0^\circ$  and  $23^\circ$ , for the trifocal lens, and at  $11^\circ$  and  $25^\circ$ , for the quadrifocal lens. As expected, trifocal and quadrifocal lenses have more phase error for most ports compared to the non-focal lens. Figure 1.10 shows the comparison of the typical phase distributions across the array aperture for the trifocal and non-focal lens at the beam ports.



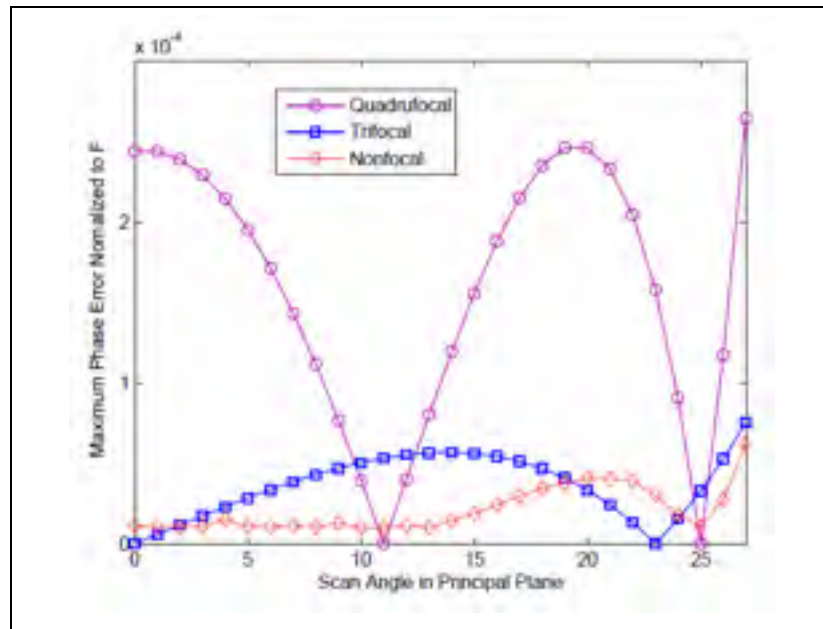


Figure 1.9 the comparison between Non-focal Lens and Focal Rotman Lenses

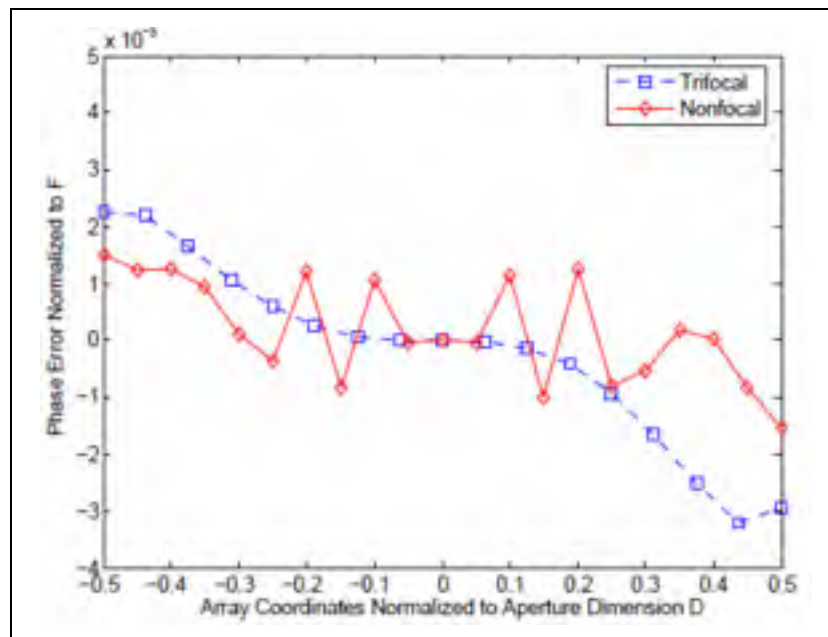


Figure 1.10 Phase Error across Array Aperture of Trifocal and Non-focal Lenses

Figure 1.10 shows that the highest phase errors of the trifocal lens occur at the edge of the receiving ports, while the highest phase error of the non-focal lens occur at centre ports. Also

we can see that non-focal lens has higher errors along a few centre ports. So the non-focal lens phase error reduction becomes significant when we need to feed large aperture array. Such devices which need large aperture has been proposed in photonic beam forming and extremely high frequency sensor designs. In high frequency, the application require extremely narrow beam and the number of array elements may reach hundreds, for example the number of elements for imaging system is 130.

According to the above points, in order that we need a small aperture, we have chosen to design a trifocal Rotman Lens.

### **1.2.2 Defining Rotman's characteristics**

Rotman Lens has two mechanical and electrical characteristics depending on the application. From the mechanical point of view, size, weight, temperature operation range and etcetera should be considered. For example increasing the size improves the performance, but the maximum size can go up to 30x30 cm because of fabrication limitation. The weight is important in portable application. Substrate height can define the tolerable power and mechanical resistivity. In electrical point of view, phase and amplitude error, maximum scanning angle, the number of input and output ports, beam errors over frequency, power reflection from ports, bandwidth, power efficiency, and maximum tolerable power and etcetera should be considered.

In this thesis, three different Rotman Lens with at least 6 beams in space with frequency coverage of 8-12 GHz will be designed. The third design will cover  $\pm 40$  degrees in space. To do this, first the geometric parameters should be defined in which parameters such as phase and amplitude errors, maximum scanning angle, and number of input and output ports affect the final Rotman's geometry. The mentioned parameters are listed in Table 1.1 along with the desired values.

Table 1.1 Transceiver specification for VHF and UHF bands

<b>Transceiver Specification</b>	<b>Spec</b>
Frequency Range	8-12GHz
Space coverage	$\pm 40$ degrees
Number of beams	6
Substrate permittivity	2.2
Substrate thickness	0.5 mm
Amplitude distribution	Uniform
Phase distribution	Linear

### 1.2.3 Extracting Rotman Lens' geometric parameter

Considering Rotman's characteristics, a three focal-points lens will be used. In fact, this kind of lens has three focal points at the input contour, thus it can produce three beams with zero phase error. It is obvious that increasing the number of beams needs more excitation points at the input's contour, which will lead to more phase error at the output. Therefore, in this section we will first introduce Rotman's geometric parameters and formulas to extract the location of the input and output ports. A software code is then used to solve these equations and to draw the resulting lens geometry. The method for choosing the optimal Rotman's geometric parameters and their effect on the Rotman's geometry structure and system phase performance and then discussed. Finally, the optimal 4x4 Rotman Lens and its parameters are presented along with full wave simulations.

Figure 1.11 shows a typical Rotman Lens geometry with its various parameters. It should be noted that the goal in Rotman Lens design is to extract input and output port locations and the distance of each output port to the linear array.

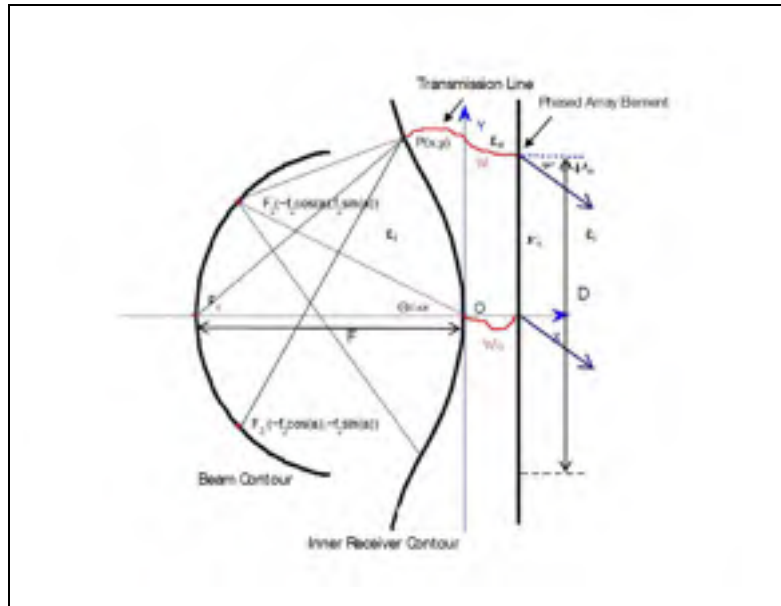


Figure 1.11 2D Rotman's geometric parameters.  
Adapted from J. Dong et al (2009)

The various geometric parameters in figure 1.11 are as follows:

$\alpha$  : Off center focal angle;

$\beta$ : Focal ratio,  $\beta = OF_2/OF_1$ ,  $\beta = f_2/f_1$  in short;

$\Psi$ : Array scan angle;

$\theta$ : Subtended angle for beam port phase centres;

$\gamma$ : Ray to beam angle ratio,  $\gamma = \sin(\Psi_\alpha)/\sin(\alpha)$ ;

$OF_2$ : Side focal length,  $f_2$  in short;  $OF_1$  is the center focal length,  $f_1$  in short;

$\zeta$ : Intermediate parameter =  $Y_3\gamma/f_1$

$Y_3$ : Distance of any array point from the X axis;

$W$ : Transmission line length;

$e$ : Eccentricity of beam contour;

$w$ : Normalized relative transmission line length,  $w = (W - W_0)/f_1$

$\epsilon_r, \epsilon_e, \epsilon_1$ : Dielectric constants for cavity region, transmission line and environment;

$X, Y$ : Undetermined coordinates of inner receiving port phase centers, normalized as  $X, Y$ .

The final equations to extract output contours (inner receiving contours) are listed below J. Brown (1953), J. Brown (1950), R.M.Cox et al (1976), K. Jaeheung (2003), J. Dong et al (2009):

$$\begin{cases} w_{12} = \frac{\sqrt{\epsilon_e} - b - \sqrt{b^2 - 4ac}}{\sqrt{\epsilon_r} \cdot 2a} \\ x = \frac{\epsilon_i y_3^2 \sin^2 \Psi}{2\epsilon_r (\beta \cos \alpha - 1)} + \frac{(1-\beta)w}{\beta \cos \alpha - 1} \sqrt{\frac{\epsilon_e}{\epsilon_r}} \\ y = \sqrt{\frac{\epsilon_i}{\epsilon_r}} \frac{Y_3 \sin \Psi_\alpha}{f_1 \sin \alpha} \left( 1 - \frac{w}{\beta} \sqrt{\frac{\epsilon_e}{\epsilon_r}} \right) \end{cases} \quad (1.1)$$

where,

$$\begin{cases} a = 1 - \left( \frac{1-\beta}{1-\beta c} \right)^2 - \frac{\zeta^2 \epsilon_i}{\beta^2 \epsilon_r} \\ b = -2 + \frac{2\zeta^2 \epsilon_i}{\beta \epsilon_r} + \frac{2(1-\beta)}{1-\beta c} - \frac{\zeta^2 S^2 (1-\beta) \epsilon_i}{(1-\beta c)^2 \epsilon_r} \\ c = \left( -\zeta^2 + \frac{\zeta^2 S^2}{1-\beta c} - \frac{\zeta^2 S^4}{4(1-\beta c)} \right) \frac{\epsilon_i}{\epsilon_r} \\ \beta = f_2 / f_1; \\ \zeta = \frac{Y_3 \sin \Psi_\alpha}{f_1 \sin \alpha} \end{cases} \quad (1.2)$$

Here  $x$ ,  $y$  are the  $X$ ,  $Y$  values normalized to  $f_1$ , and  $w$  is the path-length difference  $W-W_0$  normalized to  $f_1$ , and  $S = \sin \alpha$ ;  $C = \cos \alpha$ .

After defining the output contours geometric parameters, the input contours in the Rotman Lens with more than three ports should be designed. To achieve this, the input ports contour should be considered as a circle or an ellipse that crosses three focal points. The values of  $a$  and  $b$  (ellipse's major and minor axes,  $a=b$  for a circle) and input ports geometric locations can be easily defined using the following equations:

$$X_b = \frac{1}{2} \frac{a[-2a+2ab+2\sqrt{b^2 a^2 - b^2 \tan^2 \theta} + 2b^3 \tan^2 \theta]}{a^2 + b^2 \tan^2 \theta} \quad (1.3)$$

$$y_b = -\tan \theta * X_b \quad (1.4)$$

$$a = \frac{1 - \beta^2 \cos^2 \alpha + 2\beta \cos \alpha + \beta^2 \sin^2 \alpha (e^2 - 1) - 1}{2 \sqrt{1 - e^2} (\beta \cos \alpha - 1)} \quad (1.5)$$

$$e = \sqrt{\frac{a^2 - b^2}{a^2}} \quad (1.6)$$

Where  $\theta$  is the beam subtended angle and  $x_b$  and  $y_b$  are the undetermined beam port coordinates. The eccentricity can be a design parameter controlling this shape of beam contour and it is defined by equation (1.6) J. Dong et al (2009)

#### 1.2.4 Phase errors and their interpretations:

Microwave lens are designed to produce different desired phases and amplitudes for the phase arrays. In order to have multi-beams, we will use more than 3 ports at beam contour. Those ports which are not located at the focal points cause phase errors. In this section, we will discuss the effect of focal angle  $\alpha$ , maximum subtended angle  $\theta_m$ , focal ratio  $\beta$  (or g factor), eccentricity  $e$  and F/D ratio.

There are two ways to view the phase errors:

- 1- Phase error for each beam port produced across the phase front of the aperture.
- 2- Maximum phase error across the aperture for all beams ports.

We will use a lens design with  $\alpha = 30^\circ$ , when  $\theta$  is  $20^\circ$  and  $30^\circ$  and  $40^\circ$ . The maximum phase errors for each  $\theta$  is shown in Figure 1.12. As it shows we will have zero phase error when we use  $\theta = \alpha = 30^\circ$

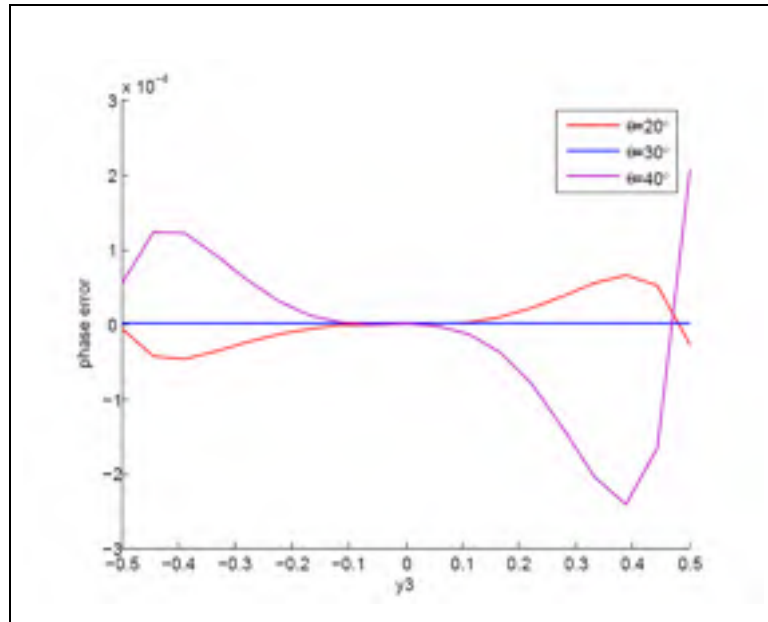


Figure 1.12 Phase Errors Normalized to F across the Aperture for Single Port,  $\alpha=30^\circ$   
Adapted from J. Dong et al (2009)

In figure 1.13 shows the results of beam contours and receiving contour's position versus  $\alpha$  and  $\theta_m$ . In figure 1.13 (a)  $\beta = 0.92$  and  $\theta_m = 20$  and  $\alpha$  changes from  $20^\circ$  to  $50^\circ$ . In figure 1.13 (b)  $\beta = 0.92$  and  $\alpha = 30$  and  $\theta$  changes from  $0^\circ$  to  $40^\circ$ . The beam contour goes toward the centre and the receiving one gets much flatter. In figure 1.13(b) shows that  $\theta_m$  only affect the positions of the beam ports.

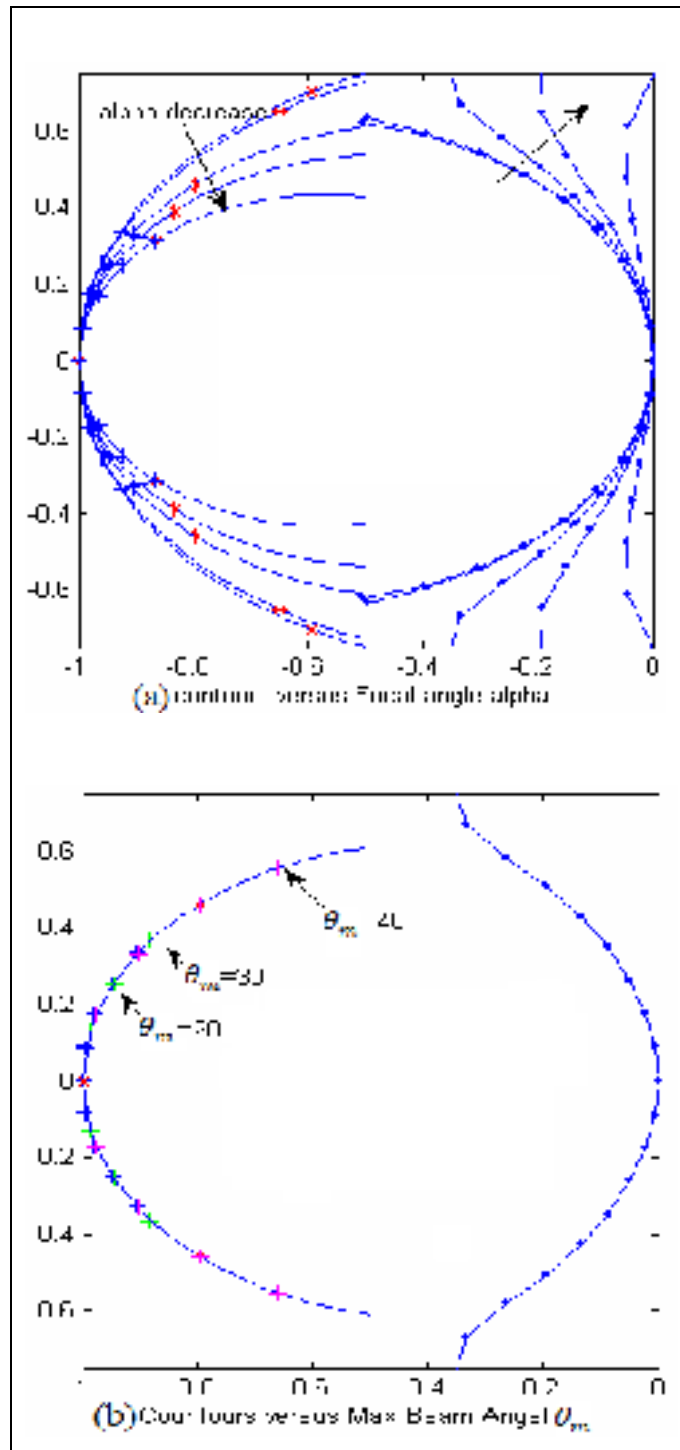


Figure 1.13 Lens Beam and Receiving Contours versus (a) Focal Angle  $\alpha$  (b) Maximum Subtended Angle  $\theta_m$ , Adapted from J. Dong et al (2009)



The  $\beta$  parameter gives different phase performance shown in Figure 1.14. It also changes the lens contours. You can see these changes in figure 1.15. Figure 1.16 shows Phase Error versus Eccentricity of the Beam Counter which doesn't make that much difference.

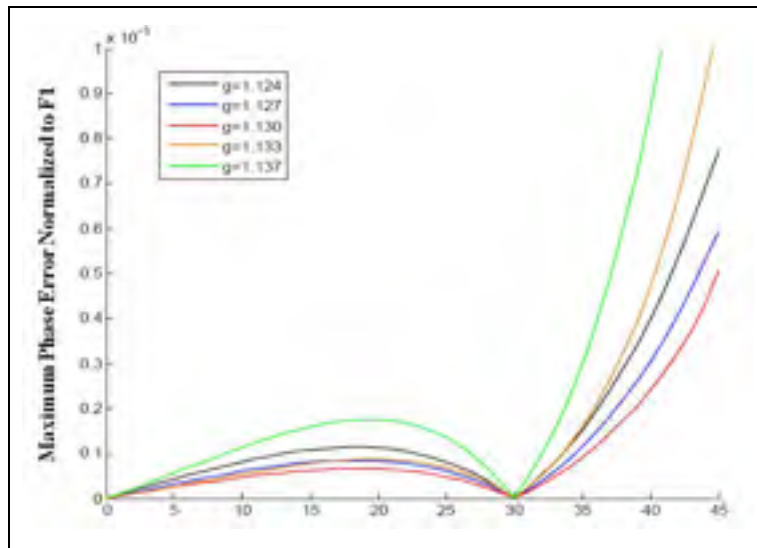


Figure 1.14 Use  $g=1/\beta$  Parameter to Conduct Lens Optimization,  $\alpha=300$ ,  $F/D=1$   
Adapted from J. Dong et al (2009)

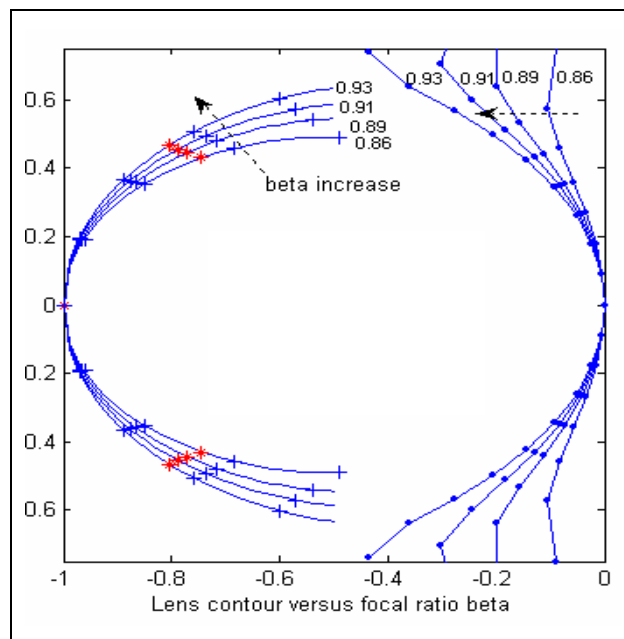


Figure 1.15 Lens Beam and Receiving Contours versus Parameter  $\beta$   
Adapted from J. Dong et al (2009)

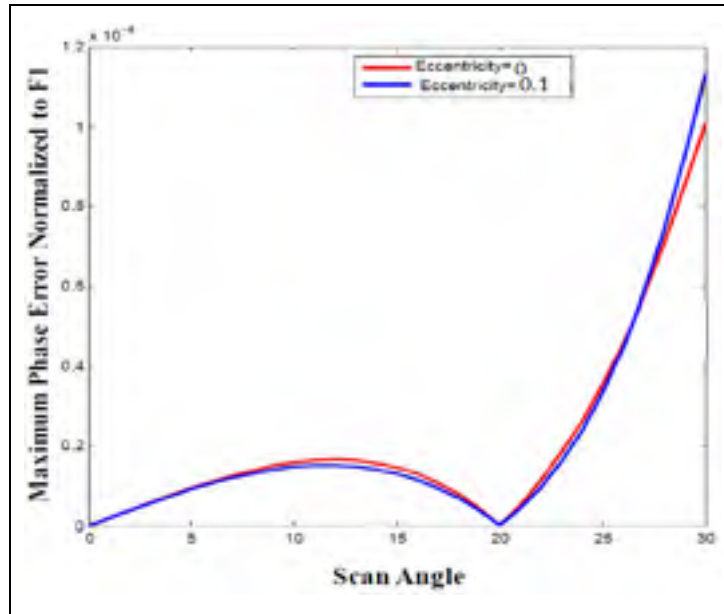


Figure 1.16 Phase Error versus Eccentricity of the Beam Counter  
Adapted from J. Dong et al (2009)

The F/D ratio is one of the important factor in optimizing phase error. Different F/D gives us different levels of phase errors. Figure 1.17 shows this difference. With increasing the F/D factor we will have less phase error but bigger Rotman Lens.

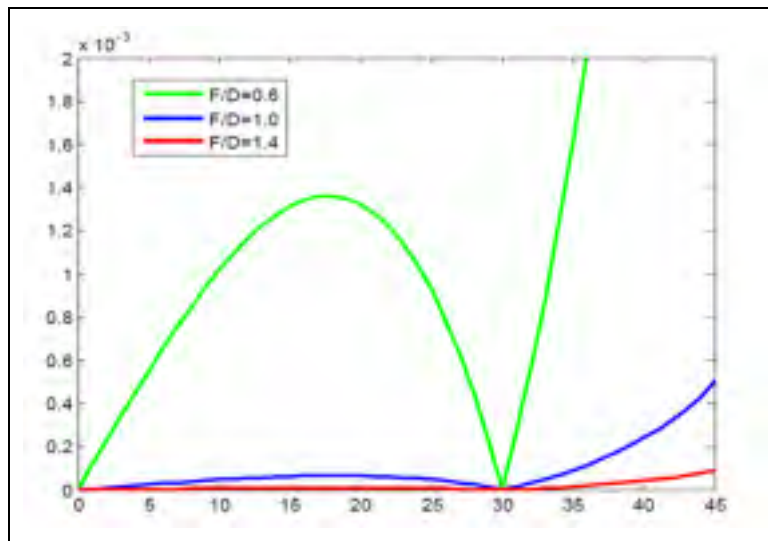


Figure 1.17 Different F/D Reflects Different Levels of Phase Errors  
Adapted from J. Dong et al (2009)

### **1.2.5 Drawing Rotman's geometry and importing to the simulation software**

After defining these equations, it is time to solve them and extract the Rotman's geometry using MATLAB codes. For this purpose, the RotmBRW codes are used, see Appendix II J. Dong et al (2009). It should be noted that the inputs of this code are the geometric parameters related to Rotman Lens design. The inputs of this code are listed in table I.1 in Appendix I. Input and output contours and the length of transmission lines from output ports to the array can be defined by choosing the appropriate input parameters. It should be noted that the parameters in all the above equations are normalized in respect to  $F$  (distance between the center of input and output contours).

The next step after extracting the input and output's geometry is to extract the intended points in CST software. To perform this, we used another software code Appendix III J. Dong et al (2009) to draw the input and output ports. This code will draw the input and output ports in CST by using input and output points from previous code, the transmission line's width in the beginning of taper, and the flares' length for input and output ports. For example, two Rotman Lenses are drawn and shown in figure 1.18 and figure 1.19. It should be noted that the direction of the input ports should be toward the center of the output contour and the direction of output ports should be toward the center of the input contour to improve the amplitude and phase coupling between inputs and outputs. Besides, to optimize the reflection from dummy ports, it is better to consider them as extension of input and output ports.

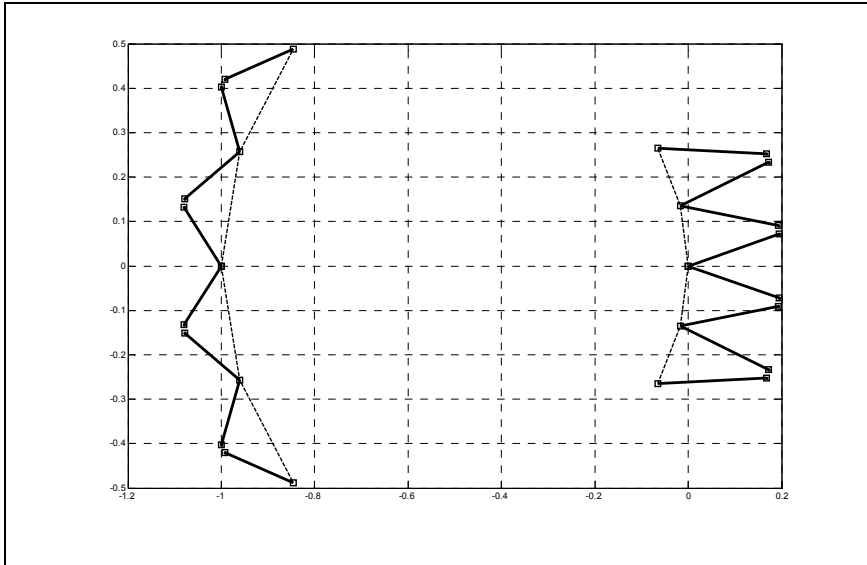


Figure 1.18 An example of 4x4 Rotman Lens

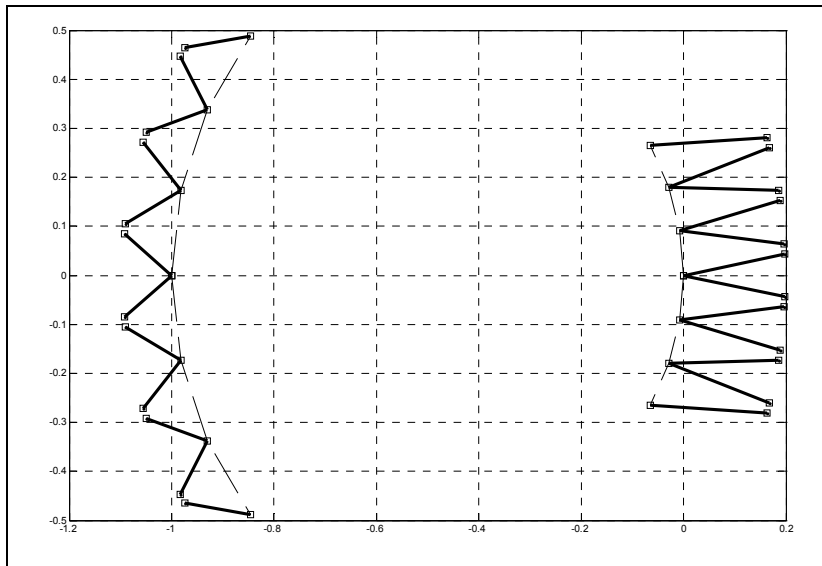


Figure 1.19 An example of 6x6 Rotman Lens

To import these points in CST software, first we need to extract the points of input and output contours and also the points of the beginning of tapers from MATLAB code. As an example, to draw the input contour, we need to put all the points corresponding to the input contour in two separate columns of a text file. It should be noted that the point's longitudinal coordinates should be saved in one column and their cross coordinate in other column and in front of them.

Then this text file can be called in CST software and the ports can be drawn. For example, we have done these steps for figure 1.18 in CST and it shown in figure 1.20.

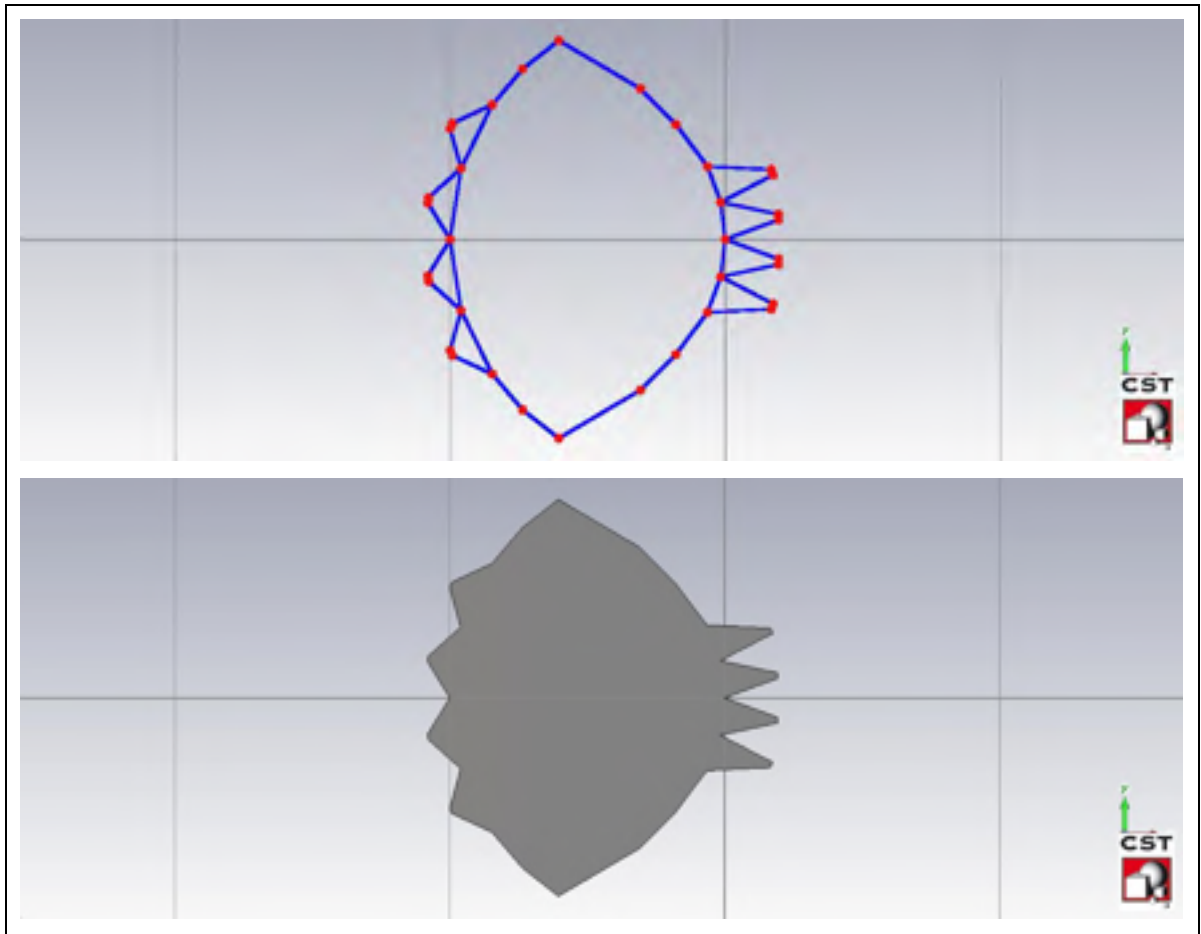


Figure 1.20 Drawing a 4x4 Rotman Lens in CST

The next step after drawing the input and output's contour and their ports in CST, is to draw the transmission lines from output ports to the linear array. To do this, the exact length of each transmission line should be calculated. The length of these lines can be calculated using analytical equation in O. Kilic et al (2005), J. Dong et al (2009), and J. Dong, A. I. Zaghloul (2009). All these equations are included in RotmBRW code and they can be found in variable W. It should be noted that some factors are not considered in these equations such as reflection from input and output and dummy ports, dielectric losses, unwanted modes propagation. Therefore, to consider all these factors to obtain the precise lengths, a full wave simulation

should be used. For this purpose, the full structure of Rotman without output transmission lines are simulated in CST full wave software and then the results are transferred to the ADS software. In next step, the transmission line will be added in ADS and their length will be adjusted to get the ideal phase differences between output ports for each beam. This can be done using optimization techniques in ADS. In this way, we can model all the full wave effects on the transmission lines length's calculation.

### 1.2.6 Investigation of the effect of Rotman Lens parameters on performance

As we saw before in this chapter, Rotman's geometric parameters such as focal angle ( $\alpha$ ), maximum angle of input ports on input contours ( $\theta$ ), focal ratio ( $g$ ), eccentric Oval ( $e$ ), and F/D ratio, have effects on Rotman's geometry and phase error. Figure 1.21 shows the effect of parameter  $\alpha$  on input and output contours which is came from RotmBRW codes.

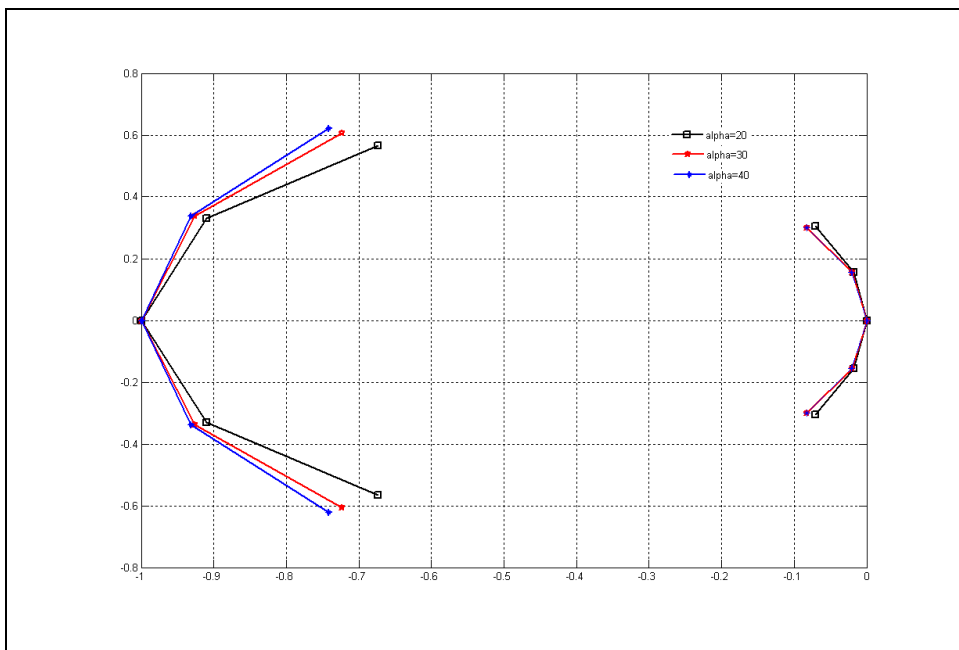


Figure 1.21 Effect of parameter  $\alpha$  on Rotman's geometry

As it can be seen in figure 1.21, increasing parameter  $\alpha$  will squish the output contours toward center while the curvature of input contours will be reduced. Figure 1.22 shows the effect of maximum angle of  $(\theta)$  on input contours. As it can be seen in figure 1.22, variation on  $\theta$  has no effect on output contours while will cause input ports movement on input contours.

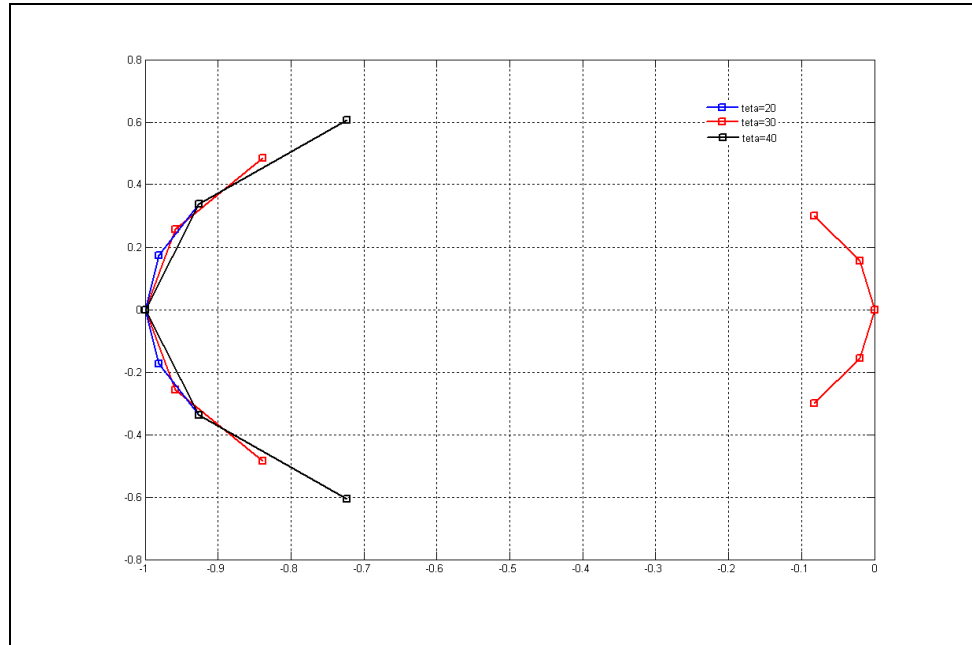


Figure 1.22 Effect of parameter  $\theta$  on Rotman's geometry

As mentioned before the outermost input port will be located along with  $\theta_m$  angle. Therefore, we can make the focal angle  $\alpha$  and  $\theta_m$  equal to reduce the phase error. In this way, two ports will be located on focal points thus the phase error of the two outer ports will be zero. This effect on one of the outer ports is shown in figure 1.23.

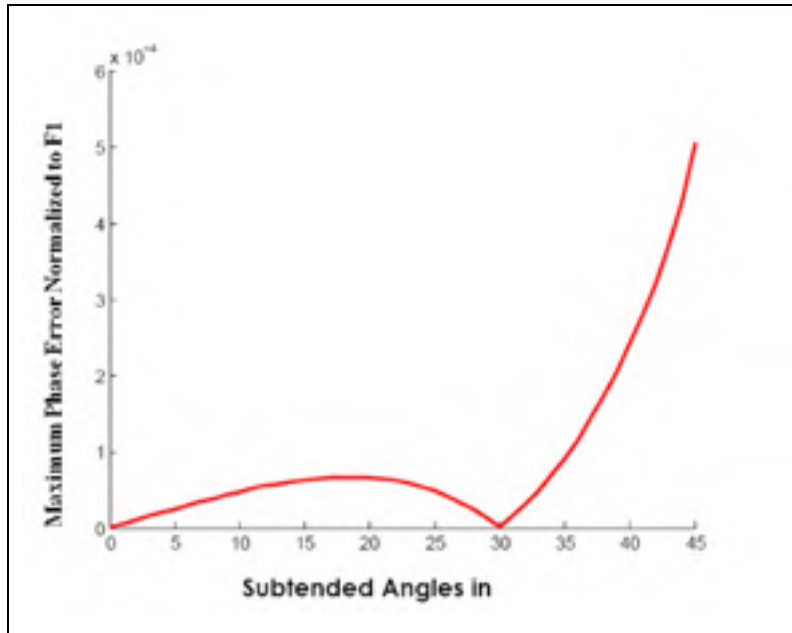


Figure 1.23 Phase error in input port for maximum  $\theta$  and  $\alpha=30$

In literature, parameter  $g$  (focal ratio) is considered as optimization parameter to minimize the phase error. Figure 1.24 shows the effect of this parameter on Rotman's geometry.

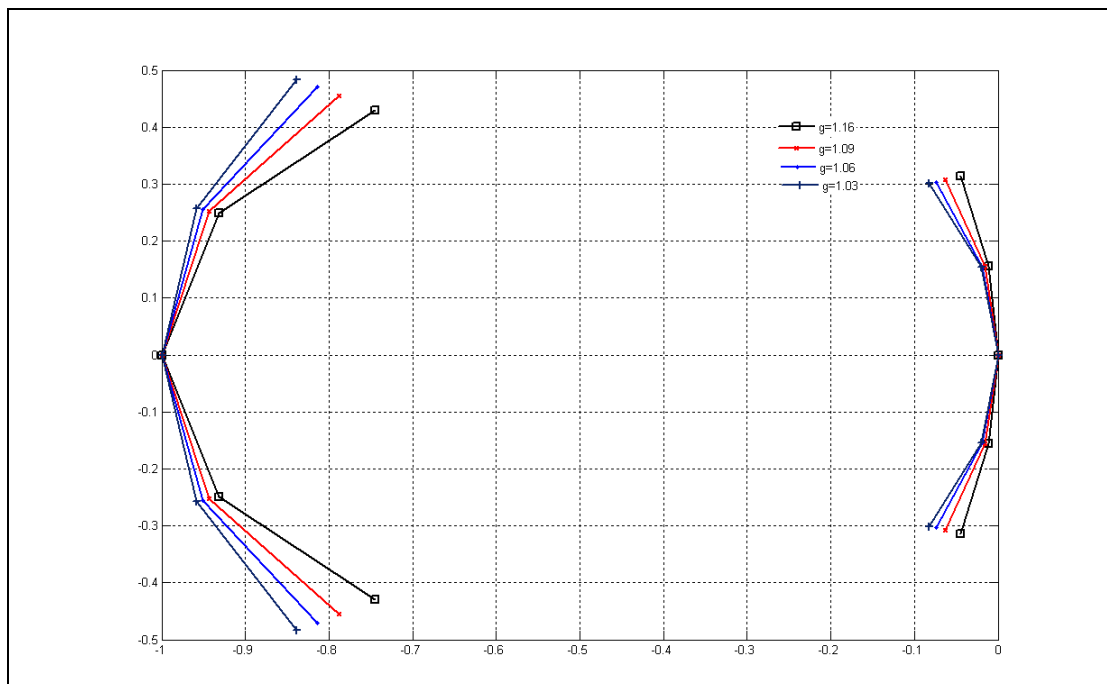


Figure 1.24 Effect of parameter  $g$  on Rotman's geometry



Variation on this parameter has a considerable effect on phase error. Rotman and Turner in (W.Rotman et al, 1963)), present the optimal  $g$ , as below for  $F/D=1$ .

$$g = 1 + \frac{\alpha^2}{2} \quad (1.7)$$

Table 1.2 presents the optimal values of this parameter for different  $F/D$ s J. Dong et al (2009).

Table 1.2 Optimal values of parameter  $g$  for different  $F/D$ s  
Adapted from J. Dong et al (2009)

<b>Best <math>g</math> (Phase Error)</b>	<b>F/D=0.6 (High)</b>	<b>F/D=1 (Medium)</b>	<b>F/D=1.4 (Low)</b>
Alpha=10 degrees	1.009	1.013	1.014
Alpha=20 degrees	1.034	1.055	1.060
Alpha=30 degrees	1.073	1.130	1.143
Alpha=40 degrees	1.120	1.161	1.278

Parameter  $e$  has negligible effect on phase error if the optimal amount of parameter  $g$  is chosen. Parameter  $F/D$  is as important as parameter  $g$ . The investigation shows that the phase error will be reduced if  $F/D$  increases. This phenomena is shown in figure 1.17. In addition, the number of dummy port and their contour curvature and their arrangement have considerable effect on the final phase error.

### 1.3 Conclusion

At this section we discussed about the different type of Beam Forming Networks and discover the advantage of Rotman Lens compare to the other BFNs. Also we discussed about the different type of Rotman Lenses and we figured out that the best designing type for our target is the three focal Rotman Lens which has less phase error compare to quadri-focal lens and also since we have small amount of number of input ports, we will ignore non-focal lens to get better phase error performance. We took a look at some geometric parameters and also

designing formulas and see the related Matlab codes. We saw the effect of this parameter to phase error. In next chapter we will continue to use these formulas and design a three focal Rotman Lens.

## CHAPTER 2

### ROTMAN LENS DESIGNS

The goal of this chapter is to design a Rotman Lens operating in the 8-12 GHz band. The most crucial part is to design a wide beam scanning Rotman Lens in conjunction with a good impedance matching over the entire frequency band.

The essential design equations for Rotman Lenses can be found in (W. Rotman and R. Turner, 1963) and (Hansen R. C, 1991) as mentioned in previous chapter. These equations are demonstrated by ray-optical modeling of the parallel plate waveguide with feeding points on the array port and beam port contour. Ray-optical modeling is not sufficient and accurate for wideband Rotman Lens design because the reflections off the side wall of the dummy ports and the coupling among the microstrip feed lines aren't considered by this method. It should be noted that in our design the Rotman Lens is designed by geometrical optics (GO) equations in (W. Rotman and R. Turner, 1963) and then side wall contours are modified for reducing the multiple reflection from the side wall. It is interesting to point out that multiple reflections significantly decrease if the dummy ports point to the middle of array ports and the beam ports contour. Moreover, the orientations of dummy ports inside the wall are very important to design the Rotman Lens using full wave optimization. To reduce the size of Rotman Lens,  $F/D=1$  is chosen and also the focal angle parameter is set equal to the maximum scan angle.

Here we propose three designs of a Rotman Lenses. The targeted maximum scan angle is  $\pm 40^\circ$  while the targeted frequency range is between 8 and 12 GHz. The commercial simulator CST was used to simulate the design and calculate its bandwidth by computing structure's scattering parameters and optimizing their geometry until these goals are met.

## 2.1 First design: 3x6 Rotman Lens

This lens has three beam ports and six array ports. It will have three beam scanning at -6, 0, 6 degrees, therefore the scan angle will be 12 degrees. We used the Rogers5880. Table 2.1 shows the Rotman Lens specifications. Following the steps outlined in chapter 1, first we used RotmBRW code to get all port's coordinates. Then we used another Matlab code (Appendix III) which uses those points from previous code and tapered transformer line's specifications (flare's length and the taper's width from the input side), so it will be able to draw output and input ports. Table 2.2 shows the value for Matlab code's parameters for this design (Appendix IV):

Table 2.1 Rotman Lens specifications

<b>Rotman Lens specifications</b>	<b>spec</b>
Operation frequency (GHz)	8-12
Scan angle (degrees)	12
Number of beams	3
Substrate permittivity	2.2
Substrate high(mil)	30

Table 2.2 Matlab code's parameters

<b>Matlab code's parameters</b>	<b>3x6 Rotman Lens</b>
Ray to beam angle ratio $\gamma$ (gamma)	1.99
Off centre focal angle $\alpha$ (ap)	6
Array scan angle $\Psi$ (phim)	14
F/D	1
Focal ratio $\beta$ (g)	1.001

All the port points are extracted from MATLAB code and imported in CST as shown in figure 2.1. Then all the dummy ports are added to reduce the reflection as shown in figure 2.2 (Red

color is related to excitation ports and blue color is related to dummy ports). In this step the dummy port's position is so important. In fact with optimizing the dummy ports, the coupling between input and output ports will be desired. It should be noted that with using these codes, some factors including returning power from inputs and outputs and dummies, dielectric loss, unwanted mode propagations are not considered. Therefore to obtain the accurate values of each these widths, we have to do a full-wave simulation which consider all of these factors. We will do a full-wave simulation by CST for the whole lens structure without the output transmission lines. Then the S-parameters of Rotman Lens will be extracted from CST and imported to ADS. In next step, we have to select the transmission line's length in order to get a desired output phases at the output of Rotman Lens. We can use optimization in ADS software. Figure 2.3 shows the ADS-modeling of Rotman Lens with delay lines for output ports.

When we find the desired transmission lines, we added them to Rotman Lens in CST and simulated the final S-parameter and again used ADS to see the array factor to make sure about the beam's positions. Figure 2.4 shows the final CST simulation which we will use it later to build this Rotman Lens. In this figure we used the absorber material covered the dummy ports to absorb the reflection and also make it easier and cheaper instead of using the 50 ohms terminations. Size of this design is  $29 \times 35$  CM.

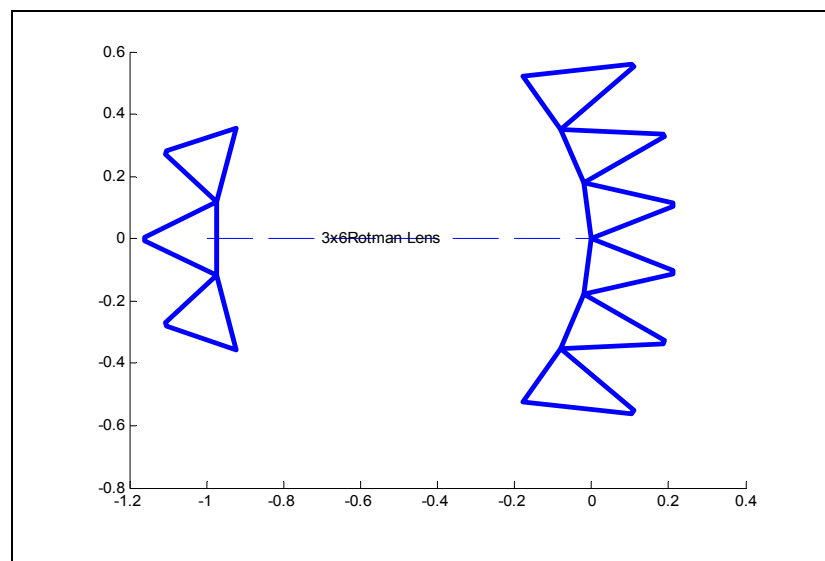


Figure 2.1. Extracted ports from MATLAB codes

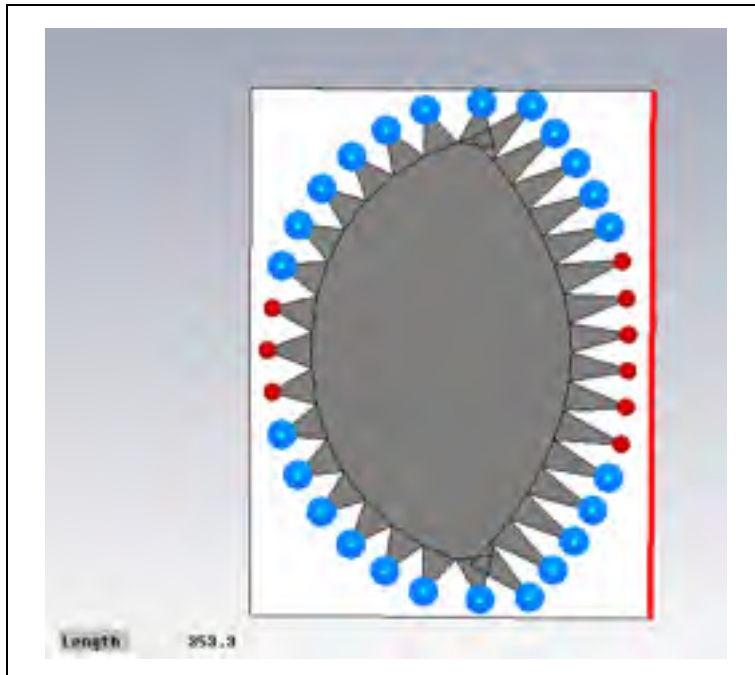


Figure 2.2 Rotman Lens geometry (Red color is related to excitation ports and blue color is related to dummy ports)

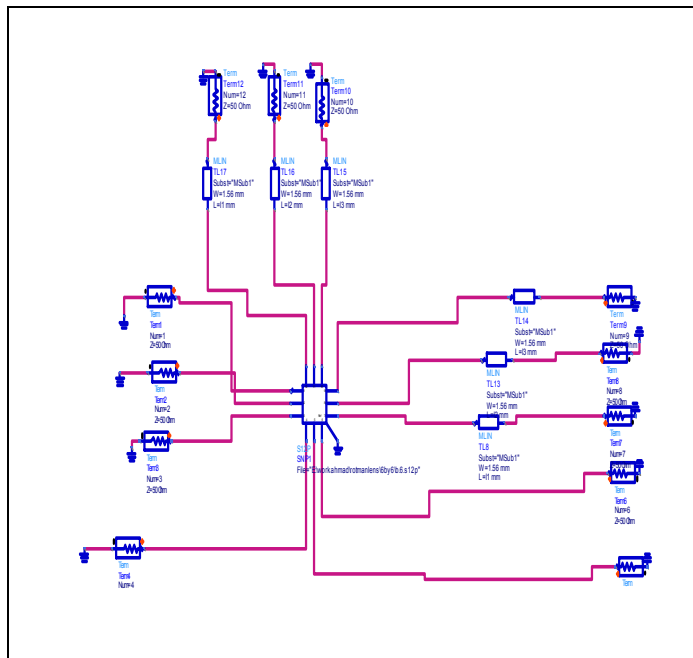


Figure 2.3 ADS-modeling of Rotman Lens (Delay lines of output ports are included in the simulation)

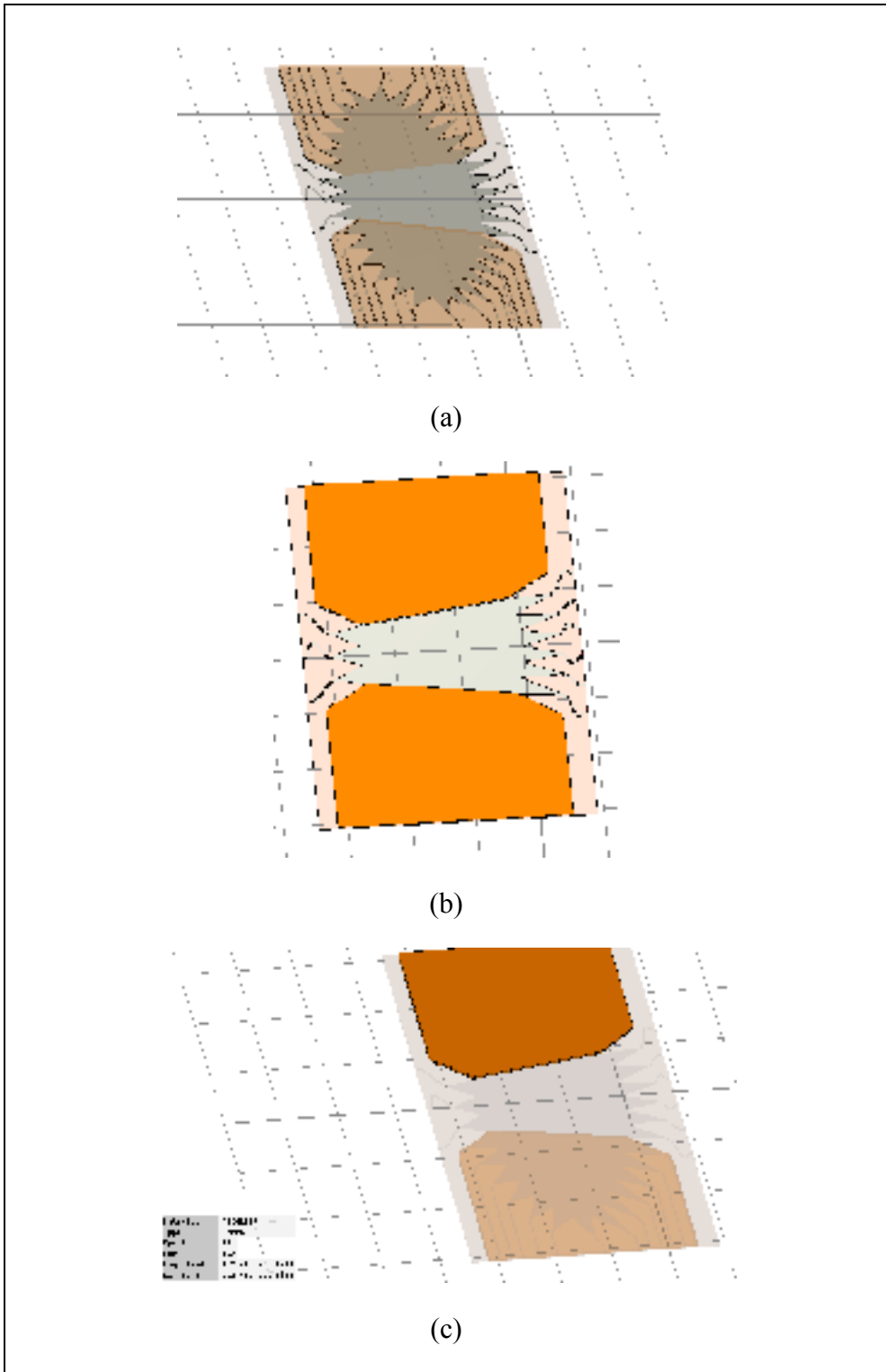


Figure 2.4 Rotman Lens with delay lines in CST, (b) Rotman Lens with covered dummy ports by absorber, and (c) Absorber material characteristic

The S-parameters of this proposed Rotman Lens are shown in figures 2.5 (a, b, c). In this lens design, we tried to have less changes in coupling between input and output ports versus frequency as with increasing these changes we will have more scan loss and side lobe level (SSL). We can see that the coupling between ports for this lens at operation frequency (8-12GHz) is roughly between -9.5dB to -13dB. Also the input and output matching results show that the S-parameters are almost less than -9dB which shows a good matching.

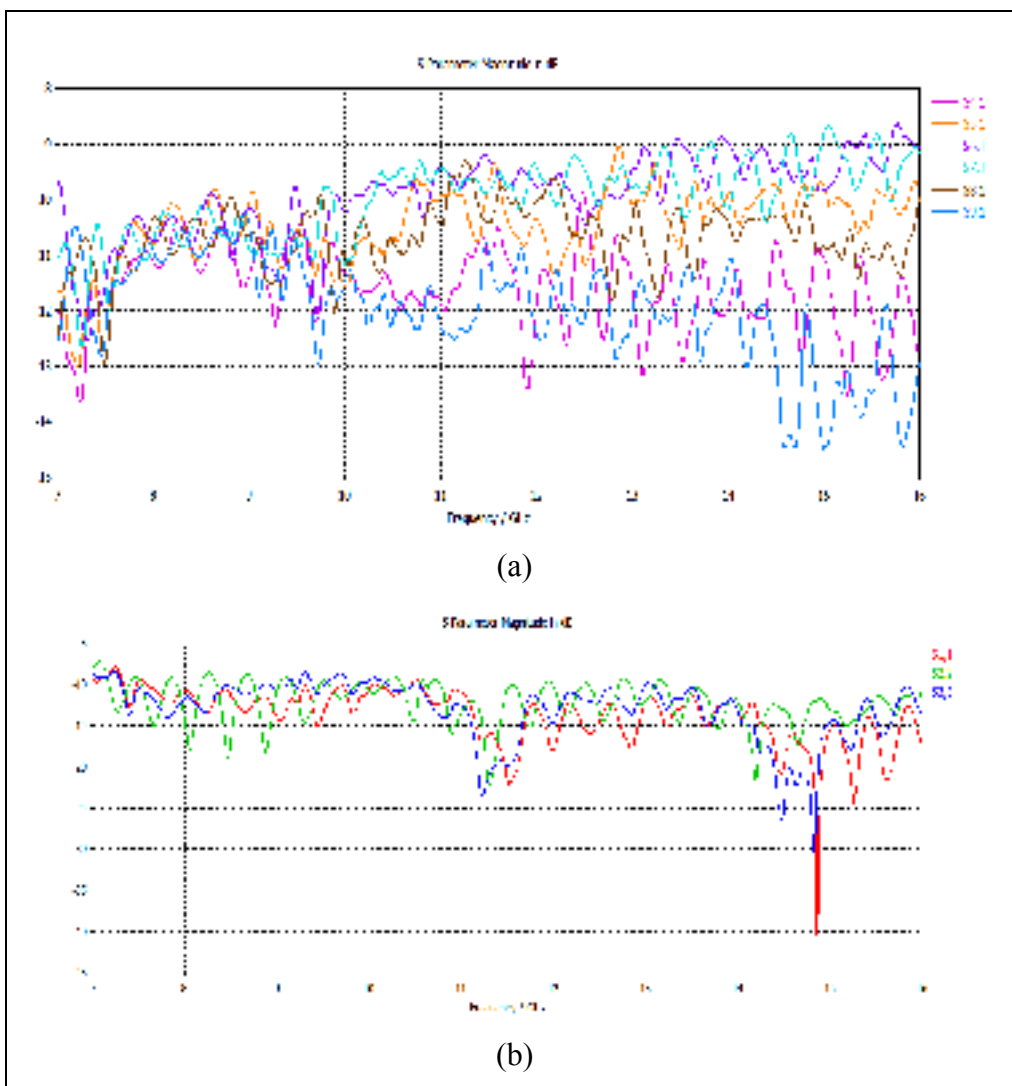


Figure 2.5 The coupling diagrams of Rotman (a) input port 1 to output ports, (b) Impedance matching of the input ports of the Rotman Lens



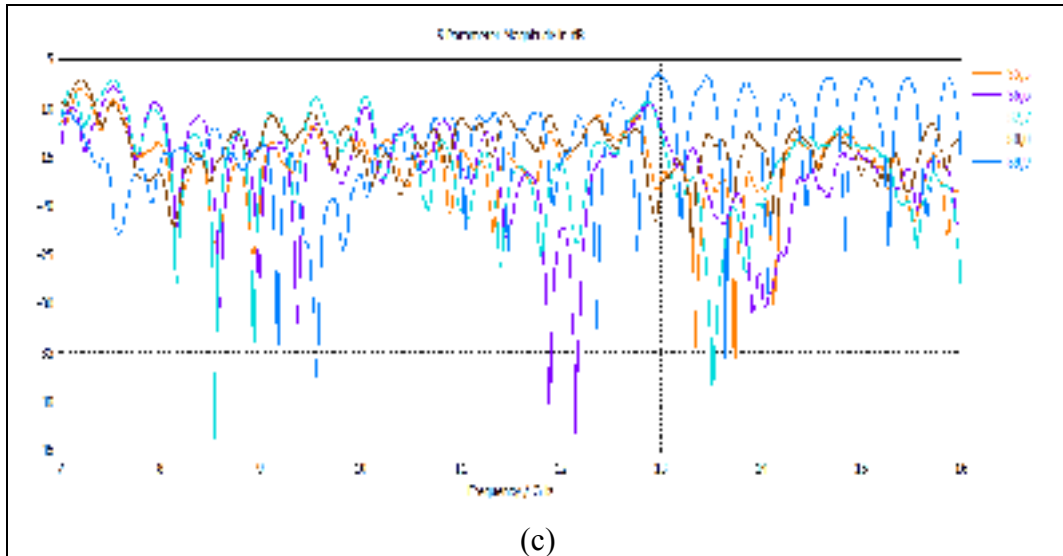


Figure 2.5 (c) Impedance matching of the output ports of the Rotman Lens

The scanning direction is estimated by computing the array factor of the proposed Rotman Lens. The computed array factors of the lens at different frequencies are shown in figure 2.6. These figures demonstrate that the beam shape is approximately constant versus frequency and as we expect we have three beams at -6, 0, 6 degrees. Table 2.3 is a summary of the simulation's results. This table shows the side lobe levels and scan losses for each frequency at beam locations.

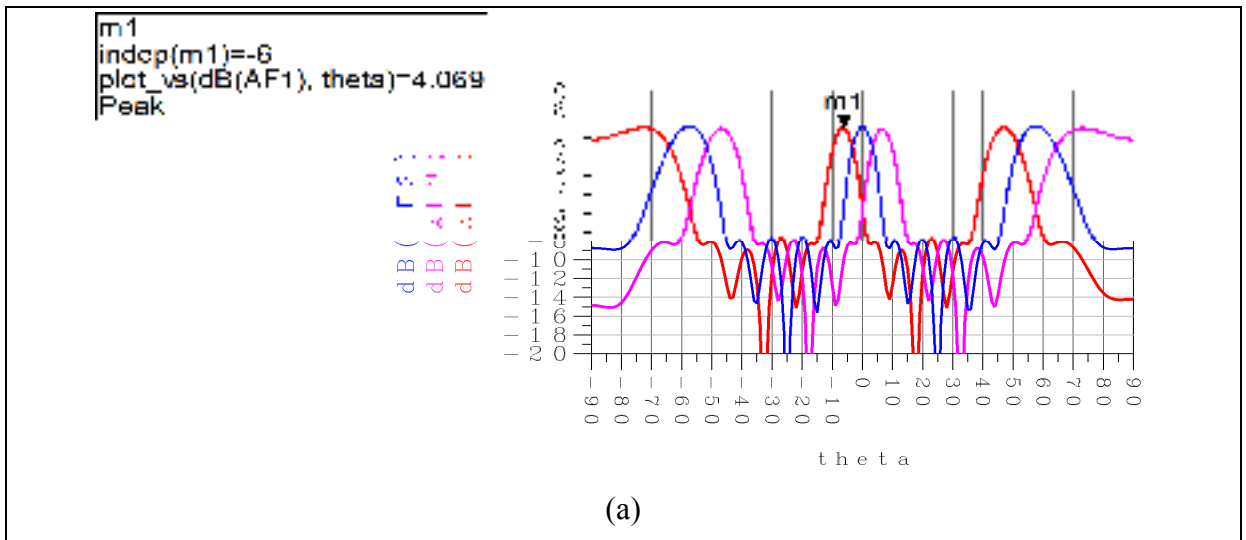
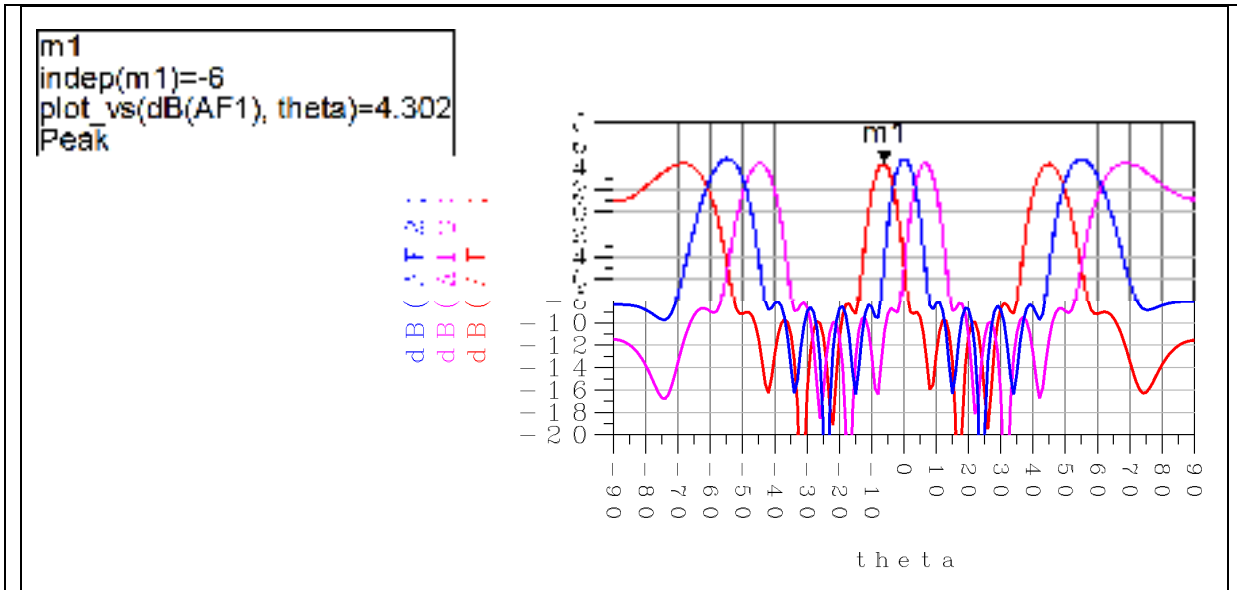
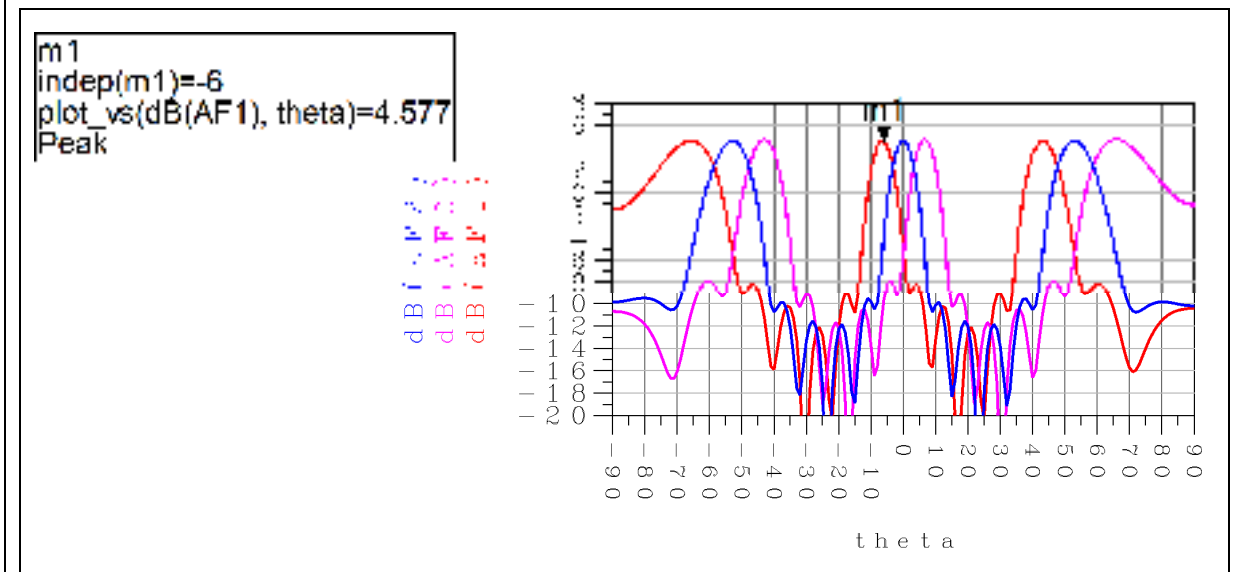


Figure 2.6 Array factor of the Rotman Lens: (a) 8 GHz

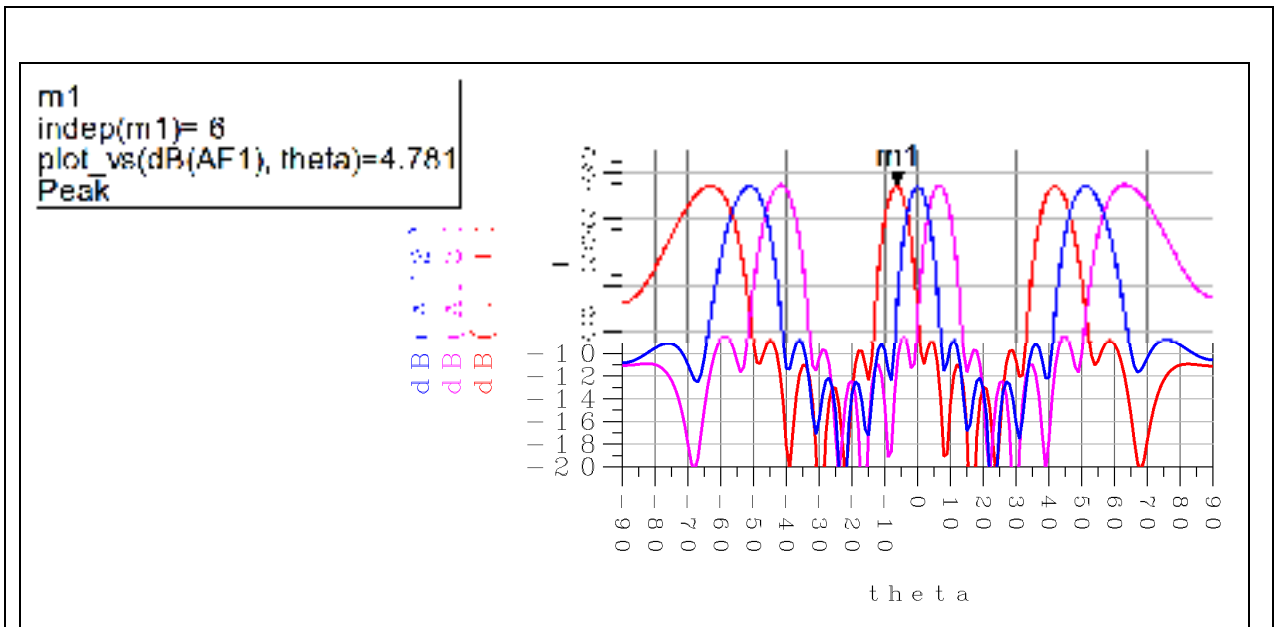


(b)

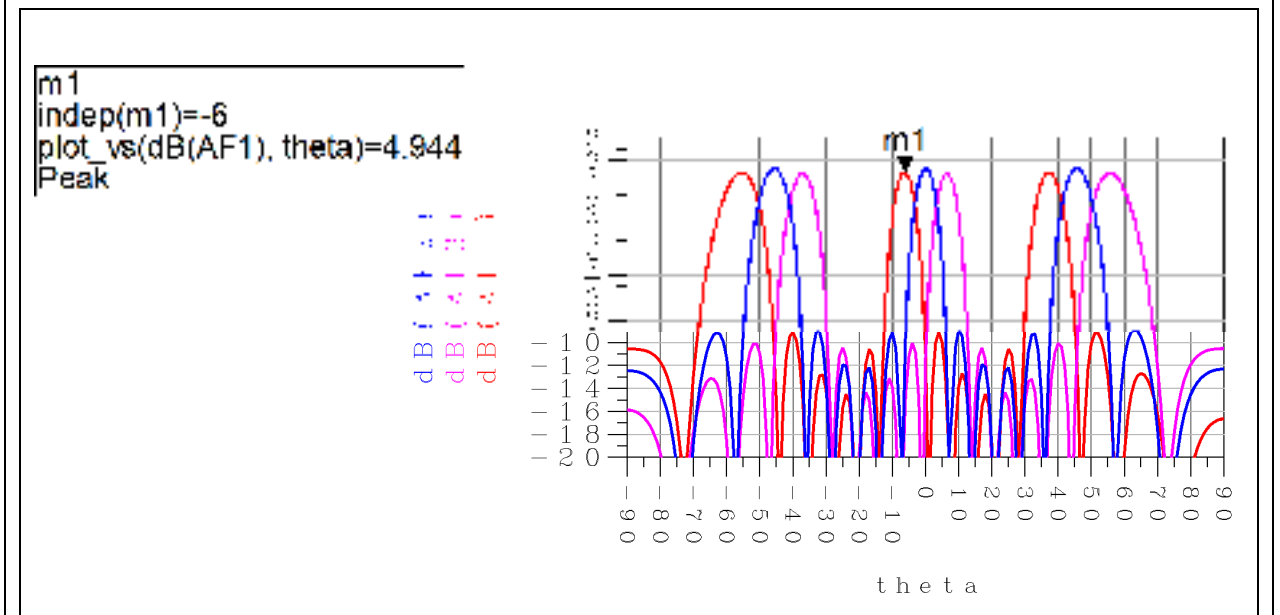


(c)

Figure 2.6 Array factor of the Rotman Lens: (b) 9 GHz (c) 10 GHz



(d)



(e)

Figure 2.6 Array factor of the Rotman Lens: (d) 11 GHz, (e) 12 GHz

Table 2.3 Simulation results for Array Factor

Frequency(GHz)	Beam position	SSL	Scan Loss
8	-6, 0, 6	12.25	0.36
9	-6, 0, 6	13.65	0.04
10	-6, 0, 6	12.7	0.03
11	-6, 0, 6	13.5	0.02
12	-6, 0, 6	13.98	0.38

## 2.2 Second design: 5x6 Rotman Lens

The same methodology has been used to design the second Rotman Lens. This lens has five beam ports and six array ports. The scanning angle will be 80 degrees. The beams will be located at -40, -20, 0, 20, 40 degrees. Table 2.4 shows the spec for this design. Table 2.5 shows the values that we used in Matlab codes (AppendixV). Figure 2.7 shows the port points extracted from Matlab code which will be imported in CST and figure 2.8 shows the complete Rotman Lens in CST including all the input and output delay lines and absorber. Lens's size is 40.3x33.3 mm. The S-parameters of this proposed Rotman Lens are shown in figures 2.9.

Table 2.4 Rotman Lens specifications

Rotman Lens specifications	spec
Operation frequency (GHz)	8-10
Scan angle (degrees)	$\pm 40$
Number of beams	5
Substrate permittivity	2.2
Substrate high(mil)	30

Table 2.5 Matlab code's parameters

Matlab code's parameters	5x6 Rotman Lens
Ray to beam angle ratio $\gamma(\text{gamma})$	1.3
Off centre focal angle $\alpha(\text{ap})$	40
Array scan angle $\Psi(\text{phim})$	83
F/D	1
Focal ratio $\beta(\text{g})$	1.15

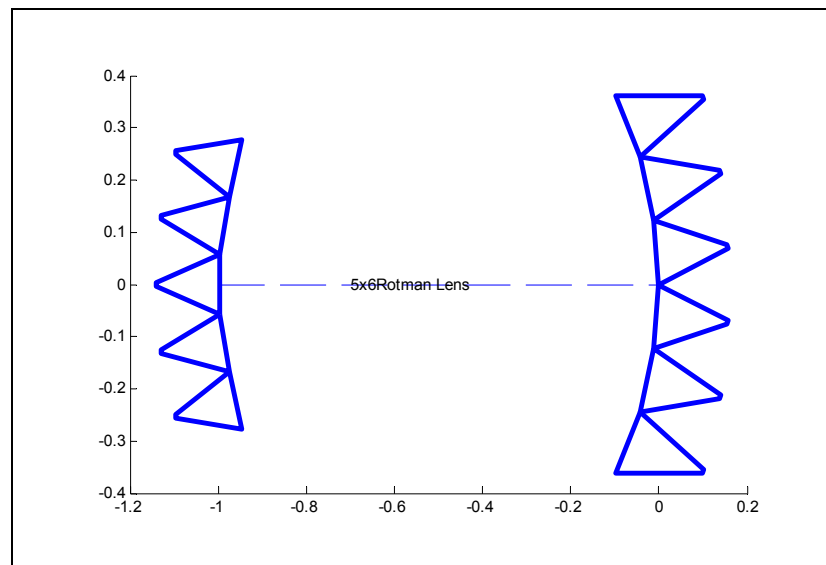


Figure 2.7 Extracted ports from Matlab codes

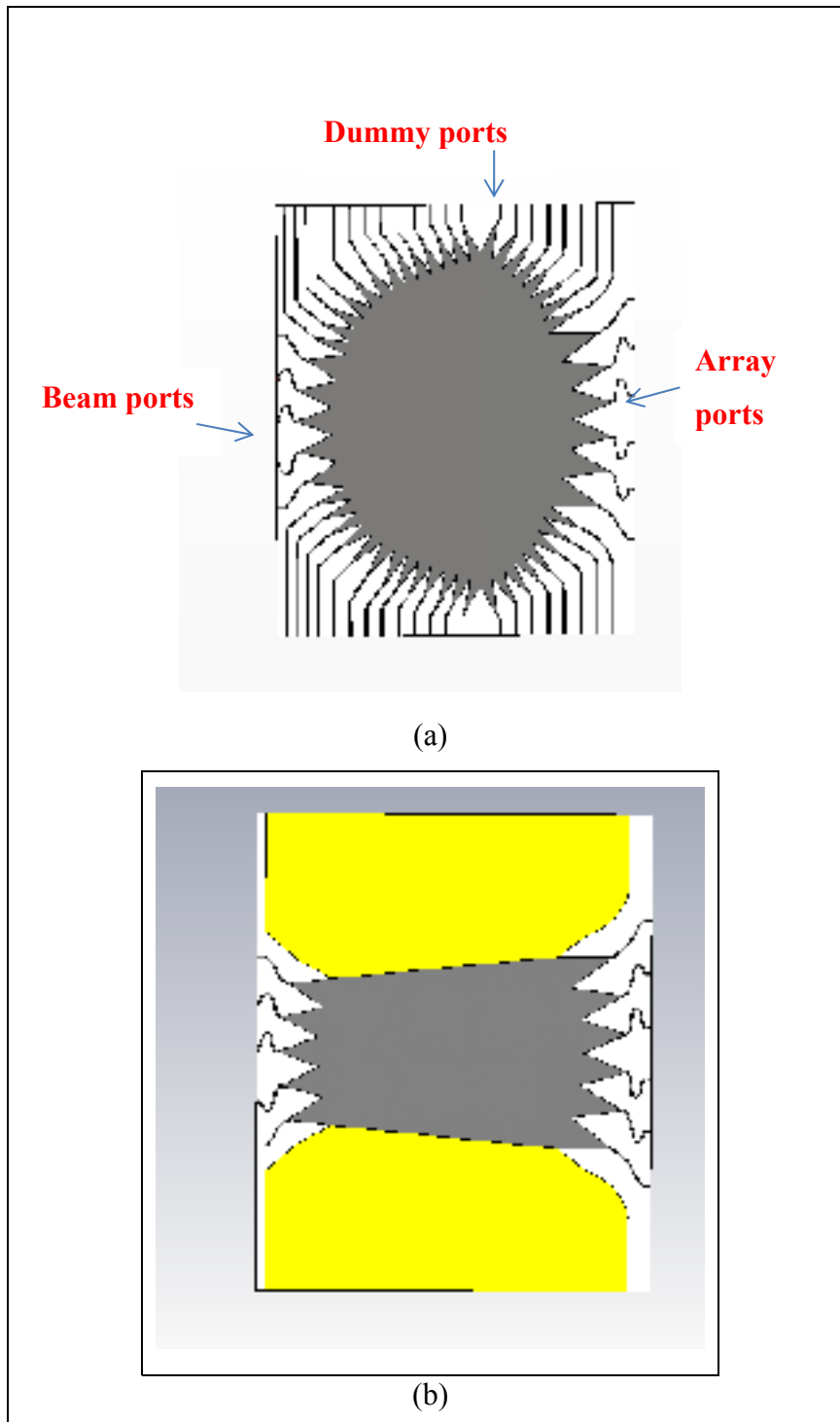


Figure 2.8 (a) Rotman Lens with delay lines in CST, and (b) Rotman Lens with covered dummy ports by absorber

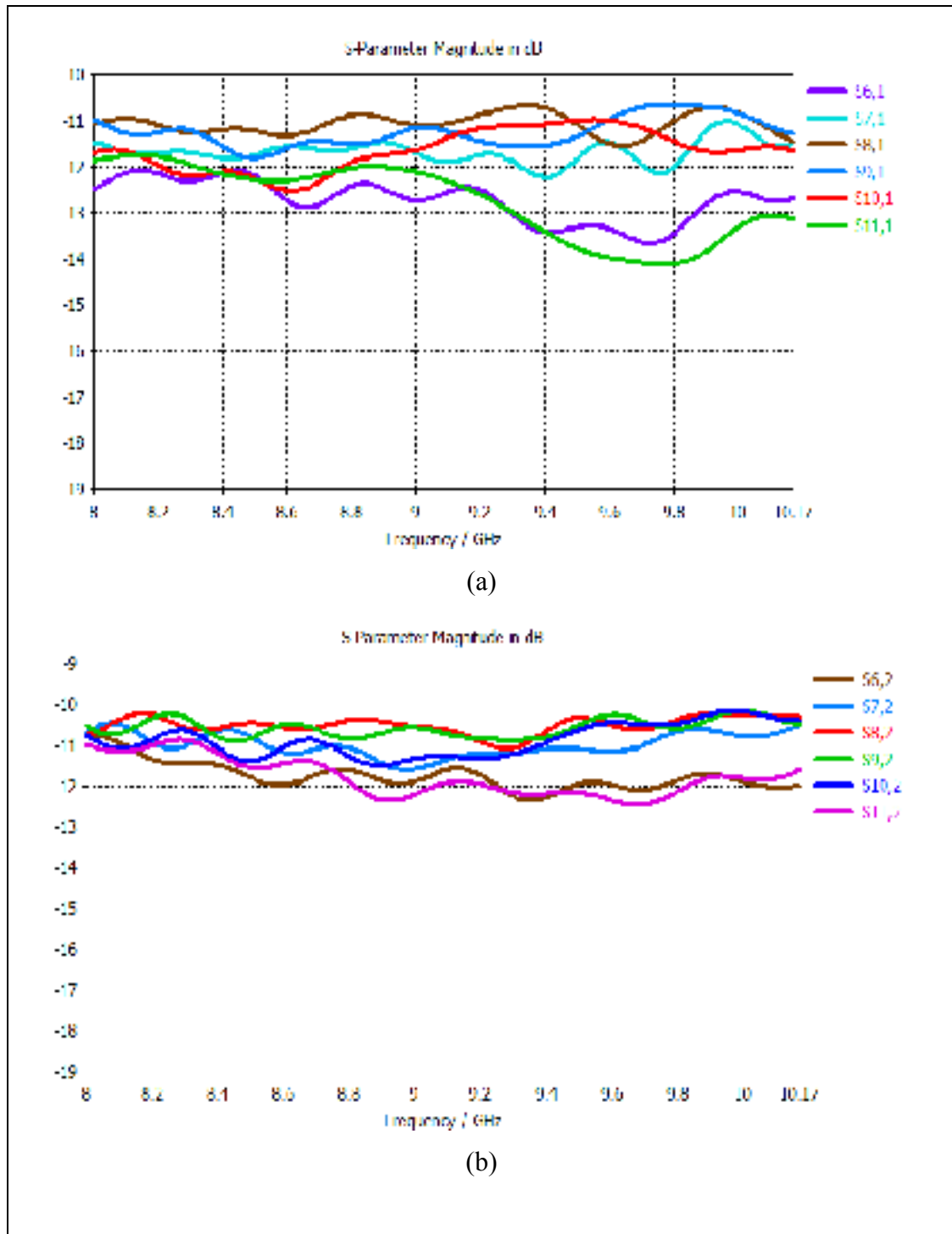


Figure 2.9 The coupling diagrams of Rotman (a) input port 1 to output ports, (b) Input port 2 to output ports

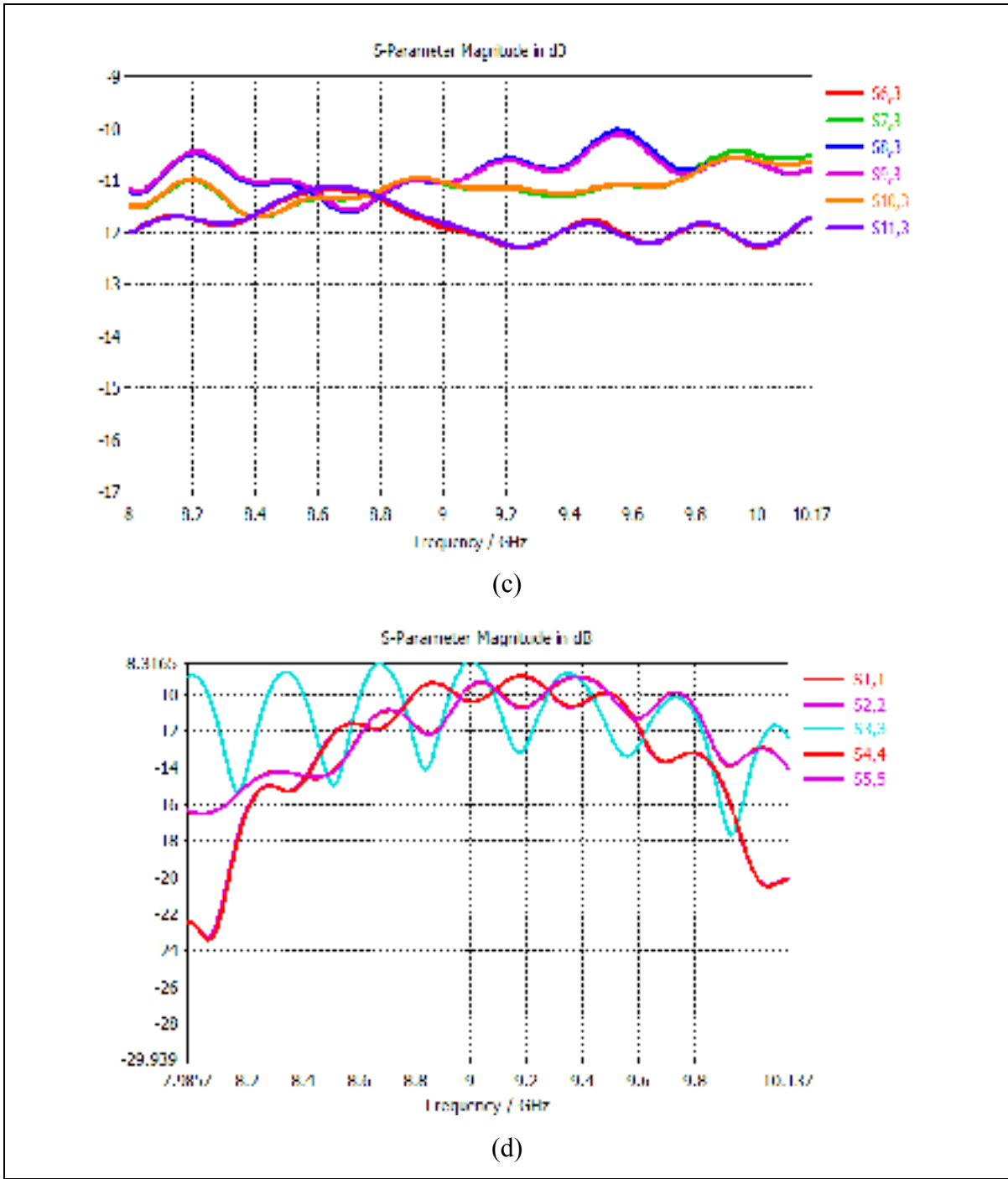


Figure 2.9 The coupling diagrams of Rotman (c) input port 3 to output ports, (d) Impedance matching of the input ports of the Rotman Lens



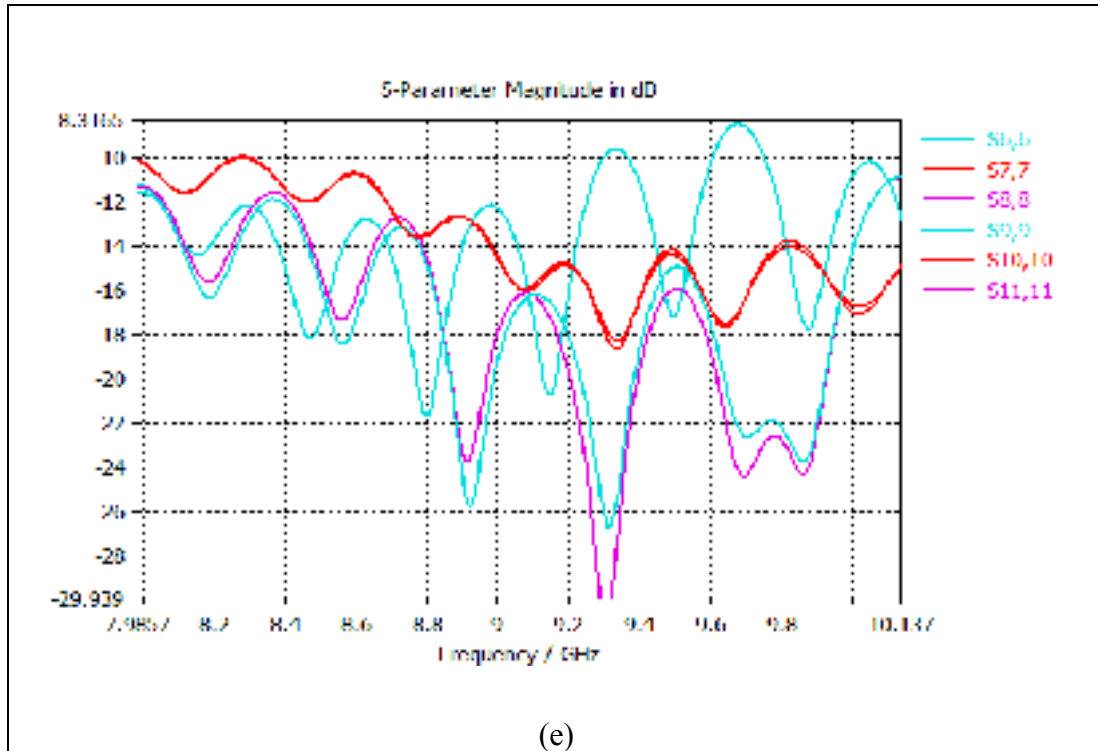


Figure 2.9 The coupling diagrams of Rotman  
(e) Impedance matching of the output ports of the Rotman Lens

As we can see in the above figures, the coupling from input to output ports smoothly changed versus frequency which is representing a good lens. Also this lens has a good input and output matching as shown in figures 2.9 (d, e).

The scanning direction is estimated by computing the array factor of the proposed Rotman Lens. The computed array factors of the lens at different frequencies are shown in figure 2.10. These figures demonstrate that the beam shape is approximately constant versus frequency. We can see that the main beams is located correctly at -40, -20, 0, 20, 40 degrees. Table 2.6 shows a summary of simulation's results.

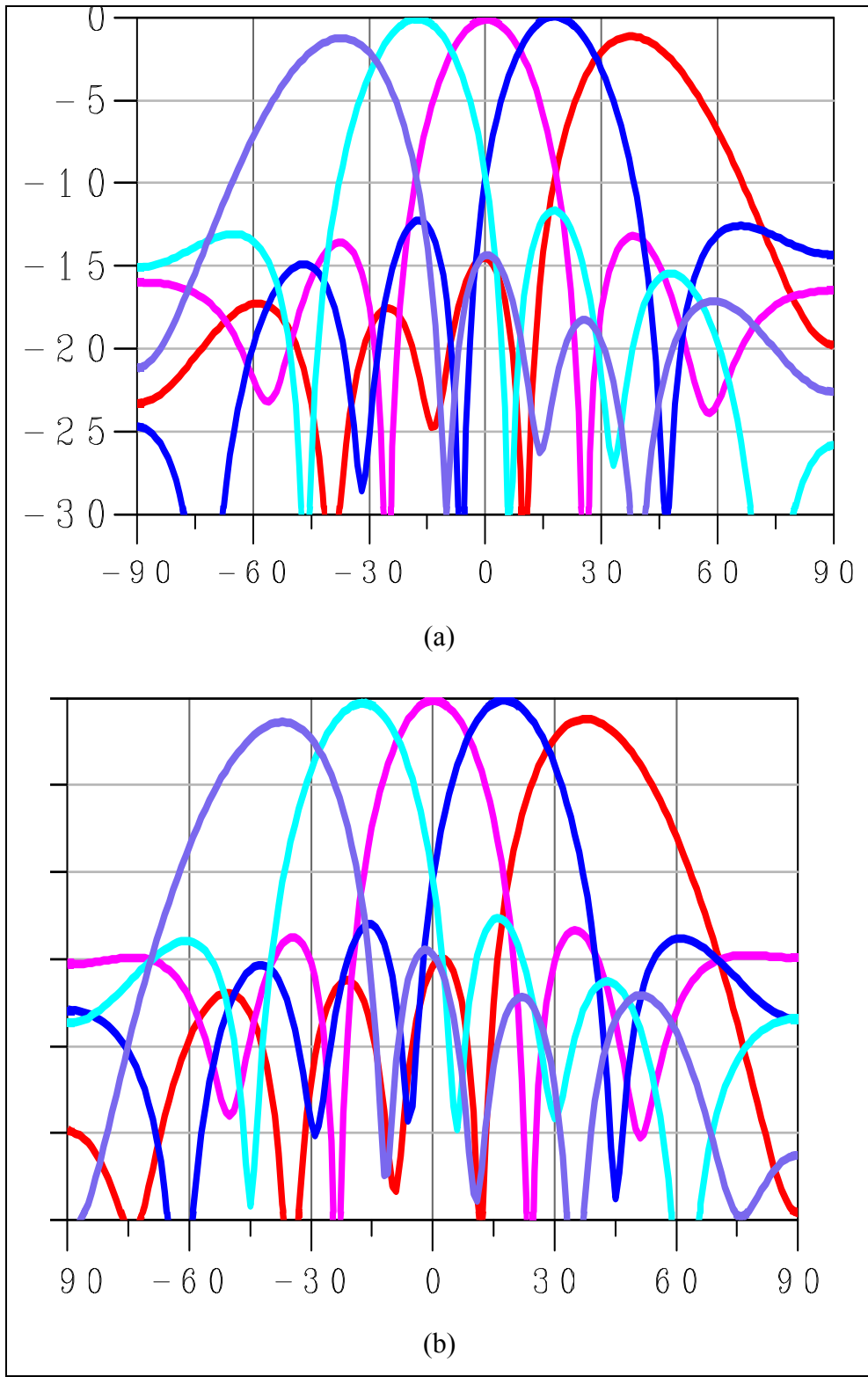


Figure 2.10 Array factor of the Rotman Lens: (a) 8 GHz, (b) 9 GHz,

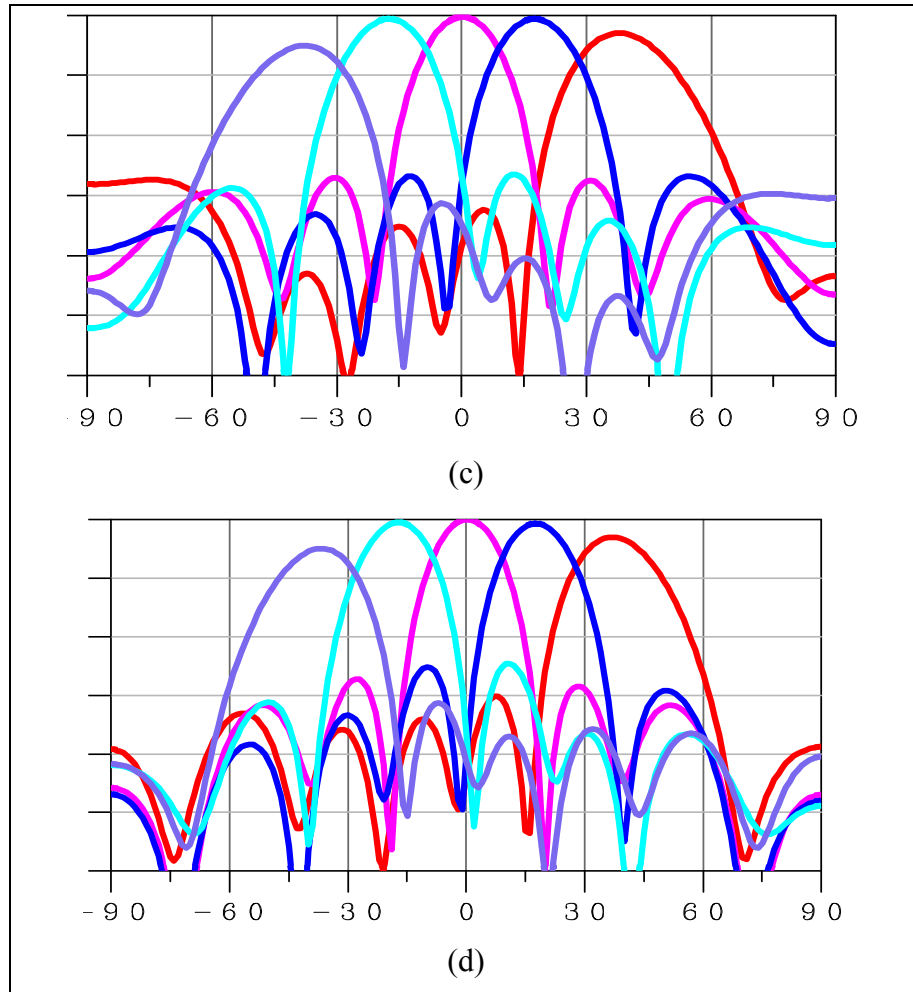


Figure 2.10 Array factor of the Rotman Lens: (c) 10 GHz, and (d) 11 GHz

Table 2.6 Simulation results for Array Factor

Frequency (GHz)	Beam position	SSL	Scan Loss
8	-40, -20, 0, 20, 40	11.92	1.12
9	-40, -20, 0, 20, 40	12.5	1.25
10	-40, -20, 0, 20, 40	13.95	2.5
11	-40, -20, 0, 20, 40	12.91	2.3

### 2.3 Third design: conference paper (ANTEM 2016)

The same methodology has been used to design the third Rotman Lens. Furthermore, to reduce the phase error for array ports of the Rotman Lens, the dummy ports are placed between each beam and receiving ports in the proposed Rotman Lens. These dummies will help to absorb some reflections and reduce the mutual coupling between ports significantly which in turn results in improved performance of the Rotman Lens. This lens has six beam ports and six array ports, shown in red in figure 2.11. The scanning angle is 80 degrees and the beams will be located at -40, -24, -8, 8, 24, and 40. Table 2.7 shows the specifications for this lens. Table 2.8 shows the used values for Matlab codes. (Appendix VI)

Table 2.7 Rotman Lens specifications

<b>Rotman Lens specifications</b>	<b>spec</b>
Operation frequency (GHz)	8-12
Scan angle (degrees)	80
Number of beams	6
Substrate permittivity	2.2
Substrate high(mil)	30

Table 2.8 Matlab code's parameters

<b>Matlab code's parameters</b>	<b>6x6 Rotman Lens</b>
Ray to beam angle ratio $\gamma$ (gamma)	1.33
Off centre focal angle $\alpha$ (ap)	40
Array scan angle $\Psi$ (phim)	75
F/D	1
Focal ratio $\beta$ (g)	1.55

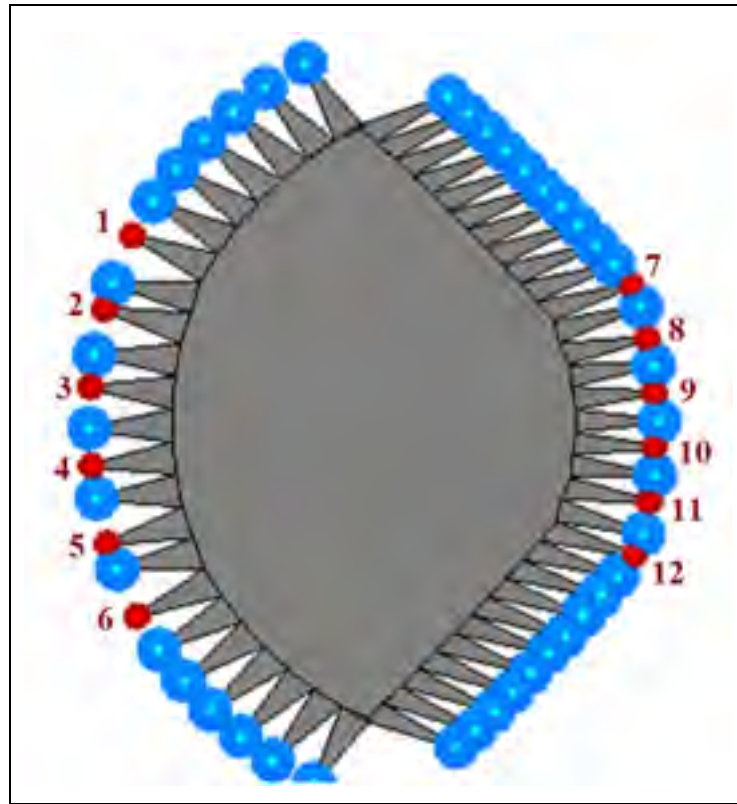


Figure 2.11 Rotman Lens geometry (Red color is related to excitation ports and blue color is related to dummy ports)

The S-parameters of the proposed Rotman Lens are shown in figure 2.12. Figure 2.12 (a, b, c) show that the coupling S-parameters ( $S_{ij}$ ) from input to output ports are smoothly changed over desire frequency range. Figure 2.12d shows the input matchings which are better than -8.2 dB.

The scanning direction is estimated by computing the array factor of the proposed Rotman Lens. The computed array factors of the lens at different frequencies are shown in figure 2.13.

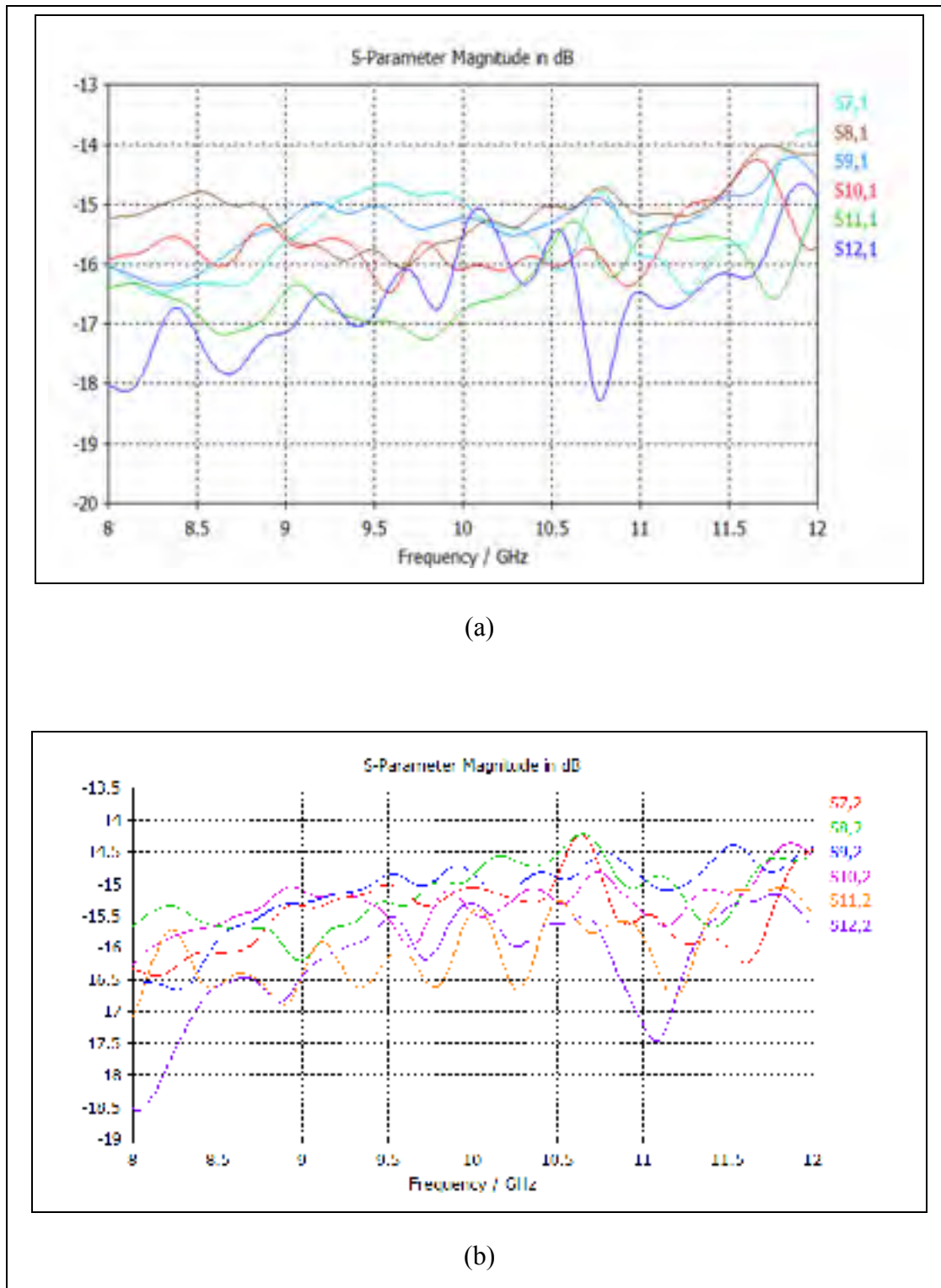


Figure 2.12 The coupling diagrams of Rotman (a) input port 1 to output ports  
(b) Input port 2 to output ports

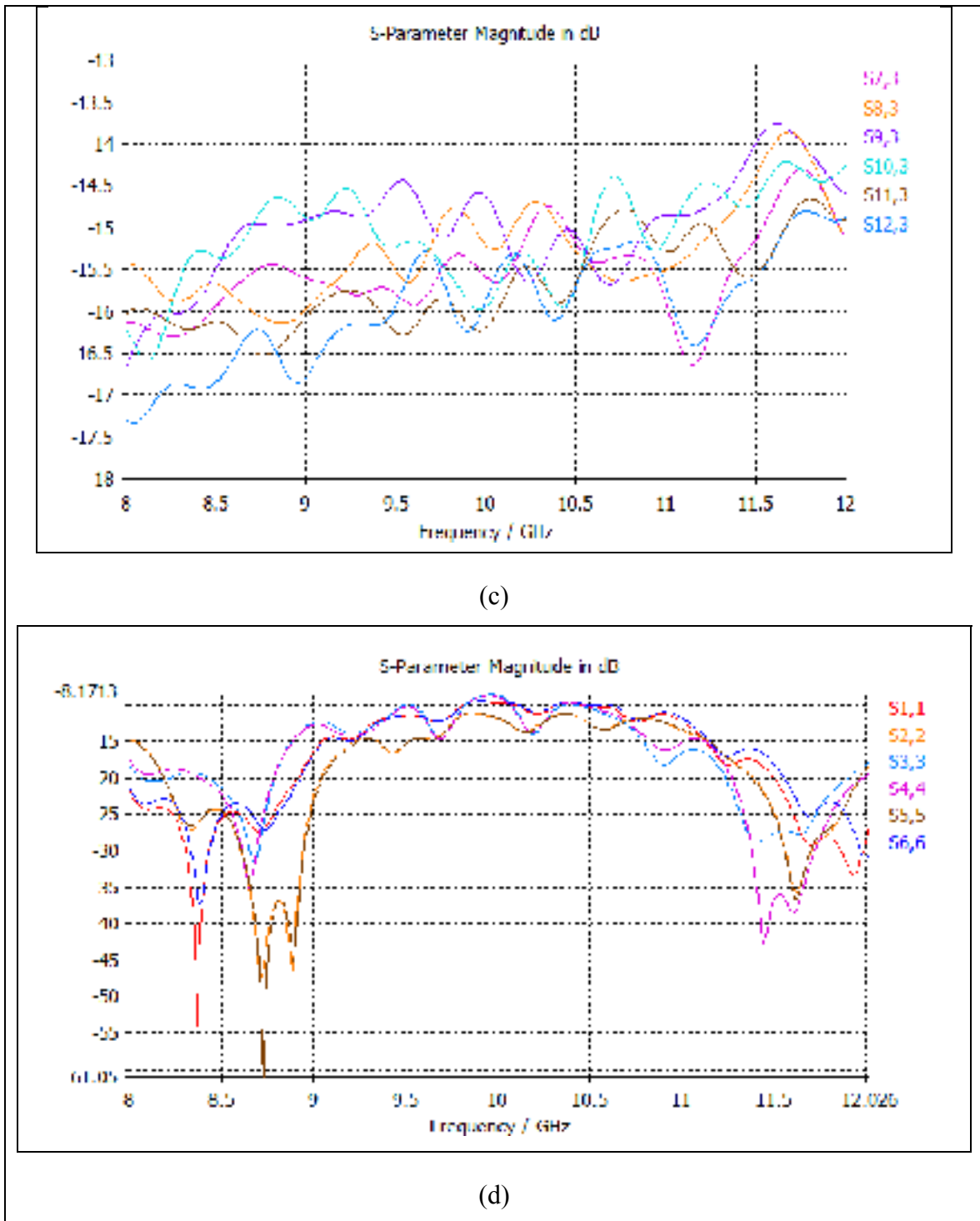


Figure 2.12 The coupling diagrams of Rotman  
 (c) Input port 3 to output ports (d) Impedance matching of the input ports of the Rotman Lens

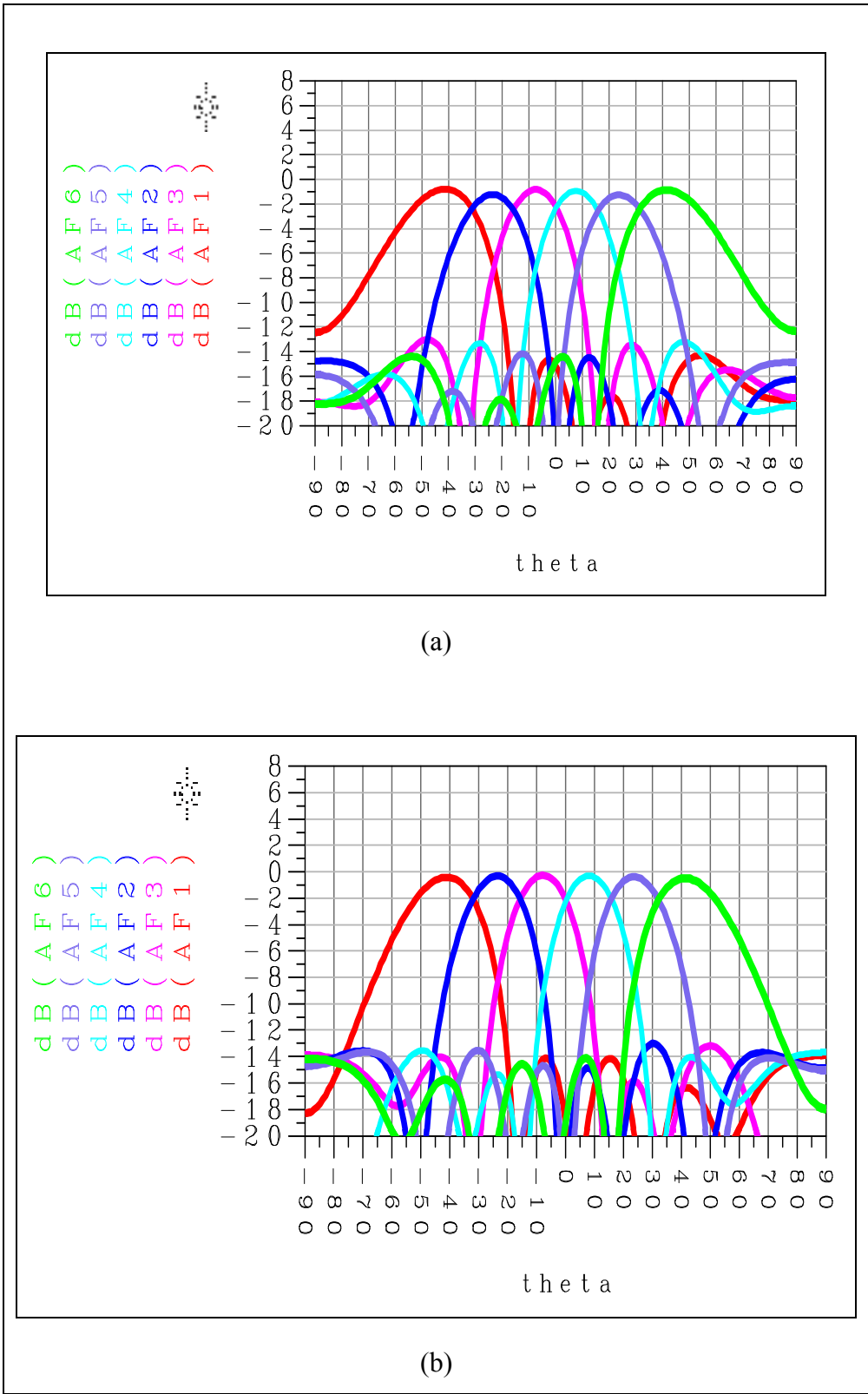


Figure 2.13 Array factor of the Rotman Lens: (a) 8 GHz, (b) 9 GHz,



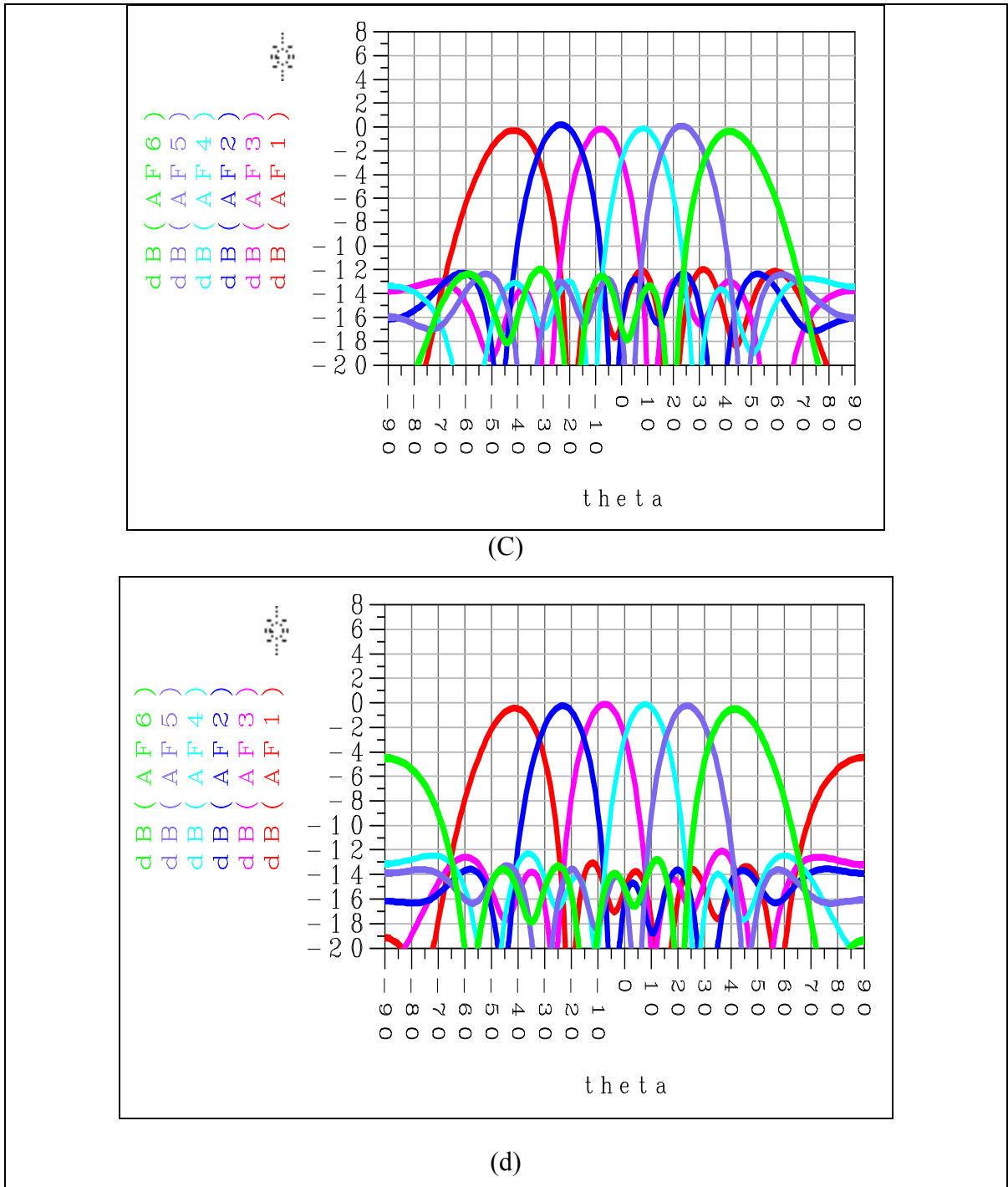


Figure 2.13 Array factor of the Rotman Lens: (c) 10 GHz, (d) 11 GHz

We can see that the main beams is located correctly at  $-40, -24, -8, 8, 24, 40$ . Also we have good scan loss and SLL as you can see table 2.9.

These figures demonstrate that the beam shape is approximately constant versus frequency. However, at higher frequencies, if the distance between the array elements exceeded a wavelength, grating lobes will show up and that would be the limiting factor in increasing the frequency range. Therefore, array element spacing is limited by this constraint. Here  $\theta_m$  is the maximum scanning angle which is  $40^\circ$  and the  $\lambda$  is the minimum wavelength which is 24mm.

$$d/\lambda < \frac{1}{1+\sin\theta_m} \quad (2.1)$$

$$\theta_m = 40^\circ \quad \rightarrow \quad \frac{d}{\lambda} = 0.608 \quad \text{and} \quad \lambda_{min} = 24\text{mm}$$

$$d=15\text{mm}$$

Table 2.9 Simulation results for Array Factor

Frequency (GHz)	Beam position	SSL	Scan Loss
8	-40, -24,-8,8,24, 40	12.2	0.2
9	-40, -24,-8,8,24, 40	12.91	0.1
10	-40, -24,-8,8,24, 40	12.19	0.02
11	-40, -24,-8,8,24, 40	12	0.01

## 2.4 Measurement results

After completion of all the simulations, we decided to build the first design since it has only 3 input ports and also I had size limitation. This lens has three beam ports and six array ports. Its operation frequency is at 8-12 GHz. The beam scanning will be located at -6, 0, 6 degrees, therefore the scan angle will be 12 degrees. It is printed on Rogers 5880 Substrate with substrate permittivity 2.2 and substrate thickness is 30mil.

Figure 2.14, 2.15, and 2.16 show the photograph of Rotman Lens (First design), the measured matchings, and array factors of measured Rotman Lens respectively.

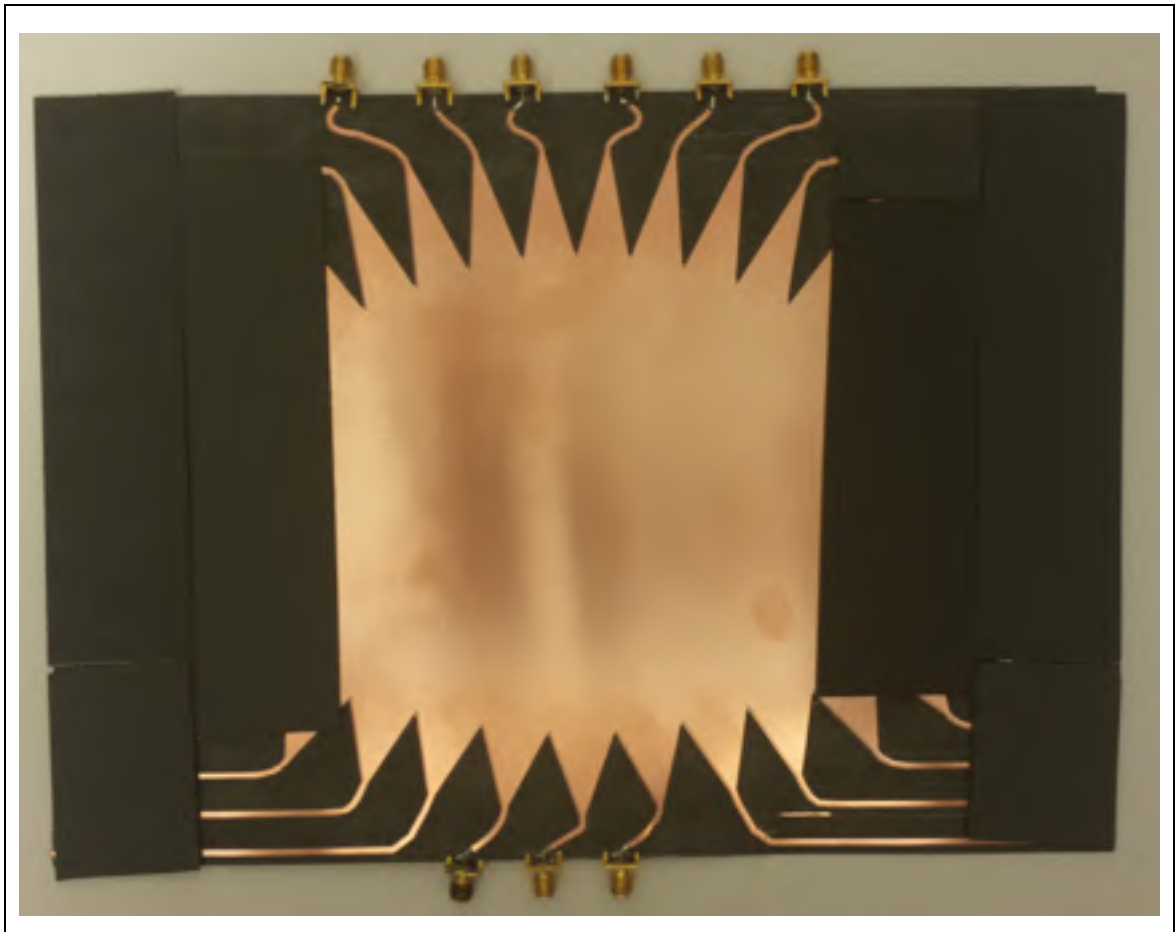
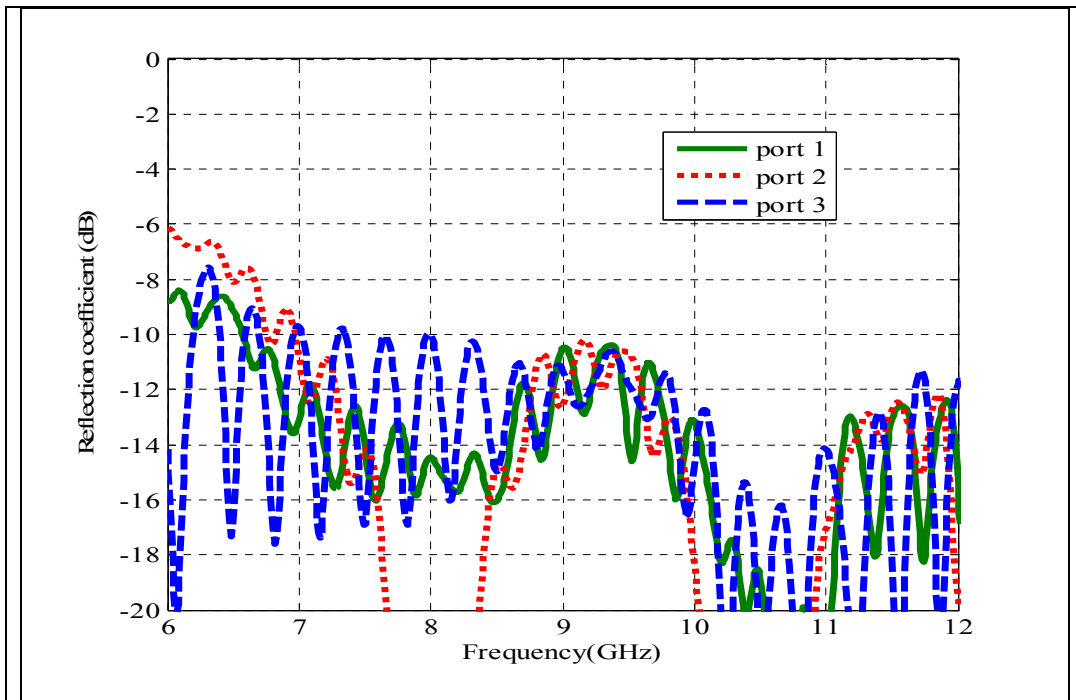
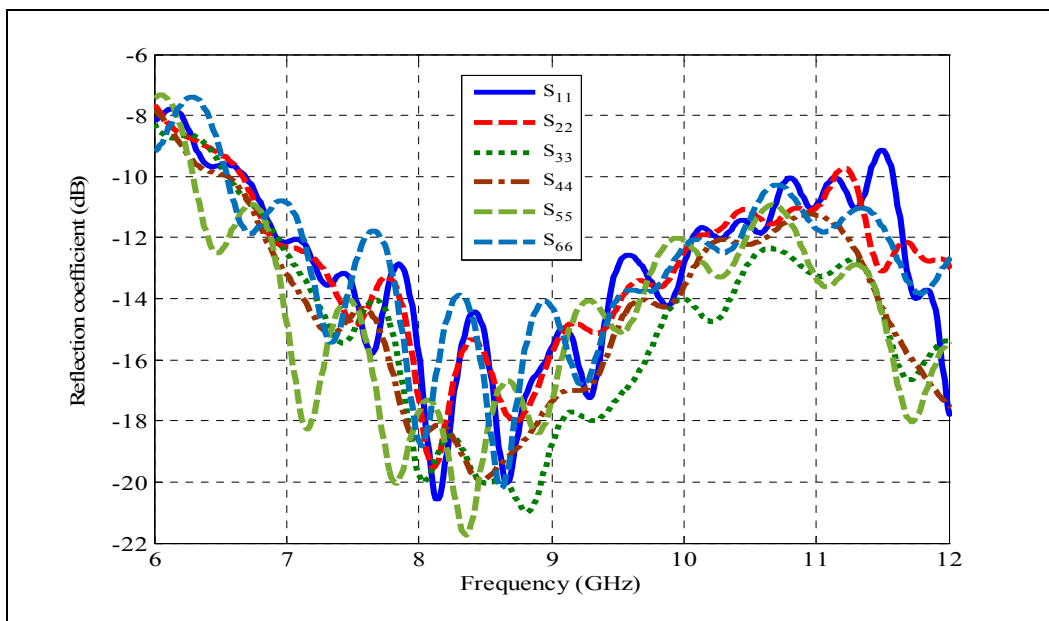


Figure 2.14 Photograph of measured Rotman Lens



(a)



(b)

Figure 2.15 The coupling diagrams of Rotman  
 (a) Measured impedance matching of the input ports of the Rotman Lens,  
 (b) Measured impedance matching of the output ports of the Rotman Lens

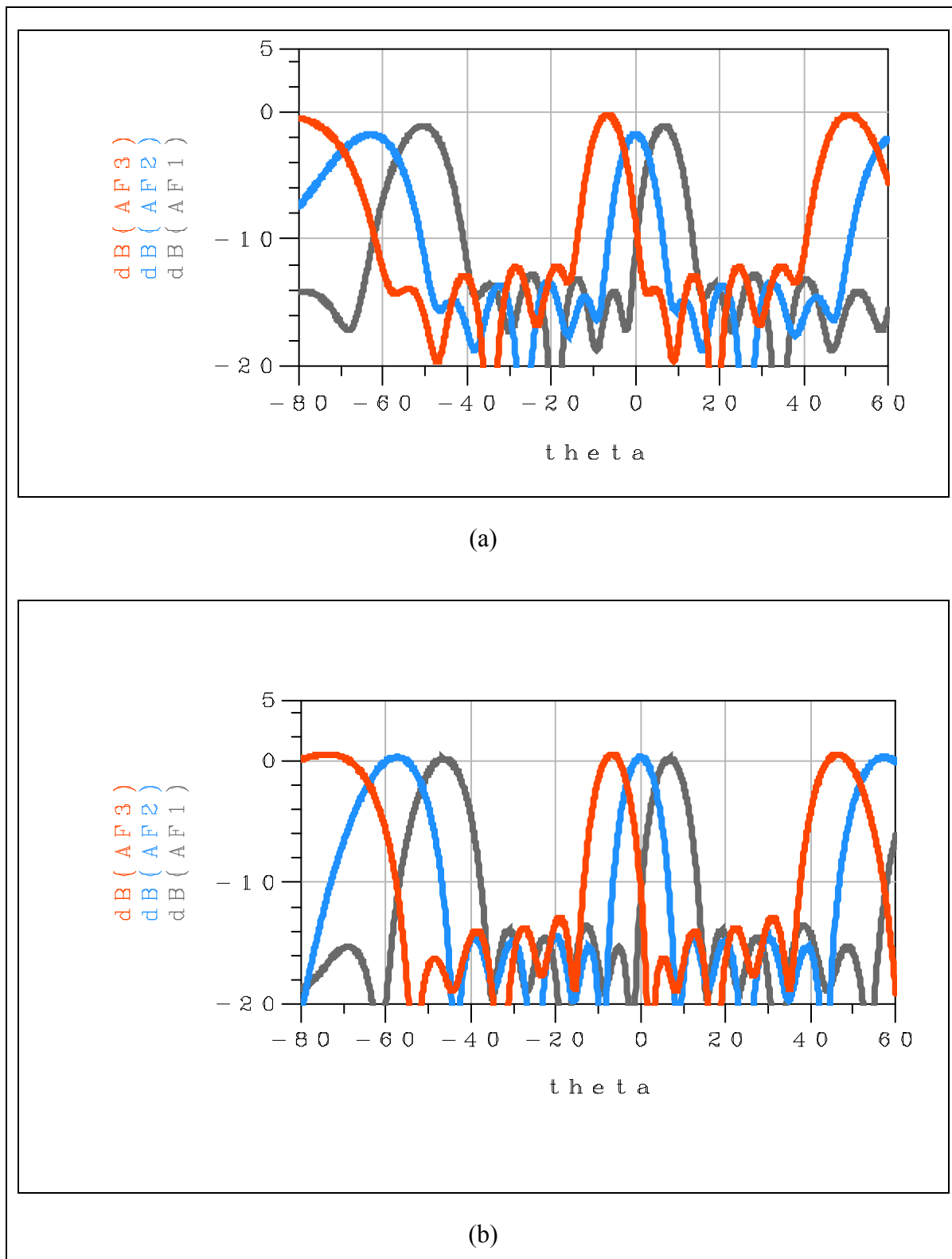


Figure 2.16 Array factor of the Rotman Lens: (a) 8 GHz, (b) 9 GHz

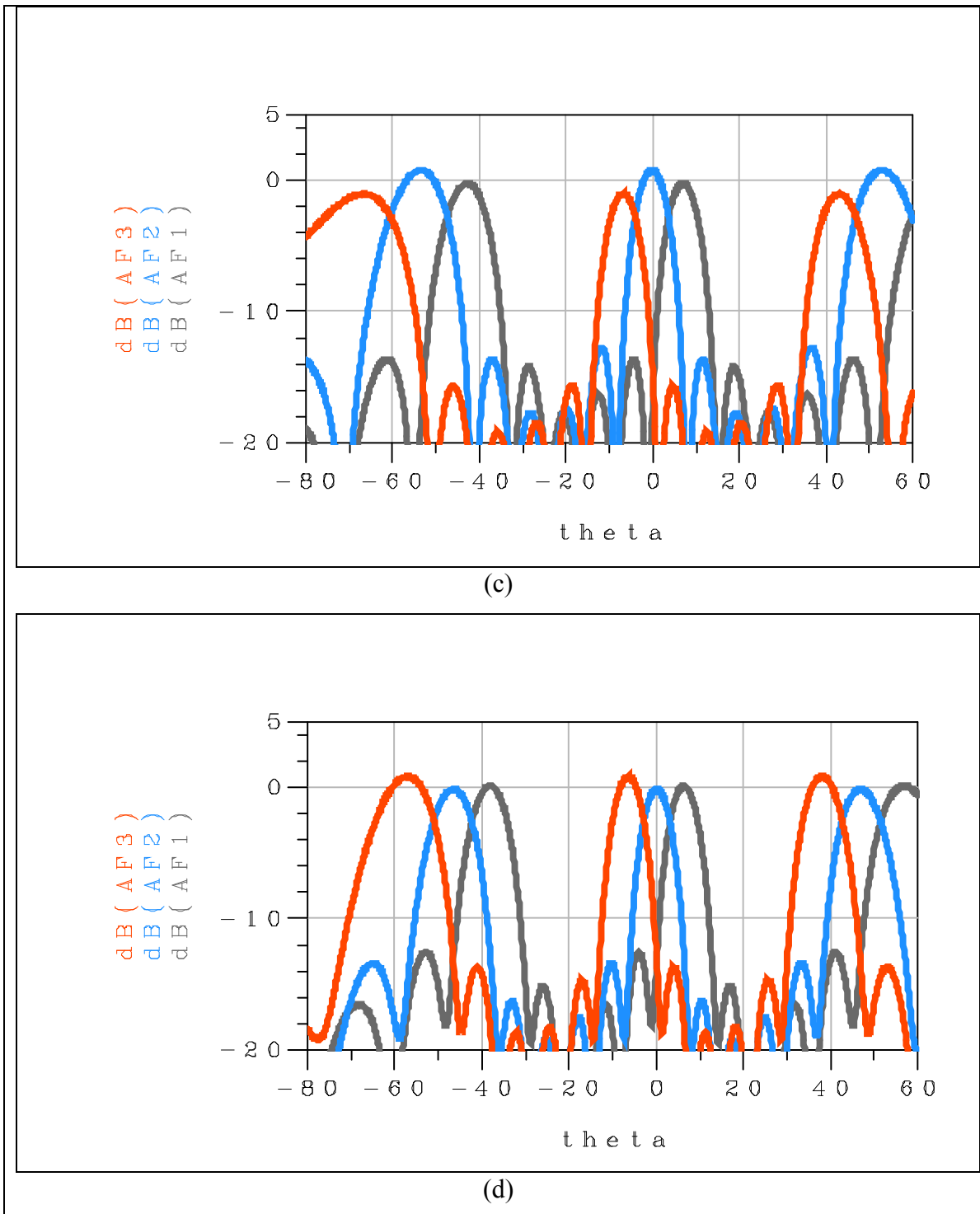


Figure 2.16 Array factor of the Rotman Lens (c) 10 GHz, (d) 11 GHz

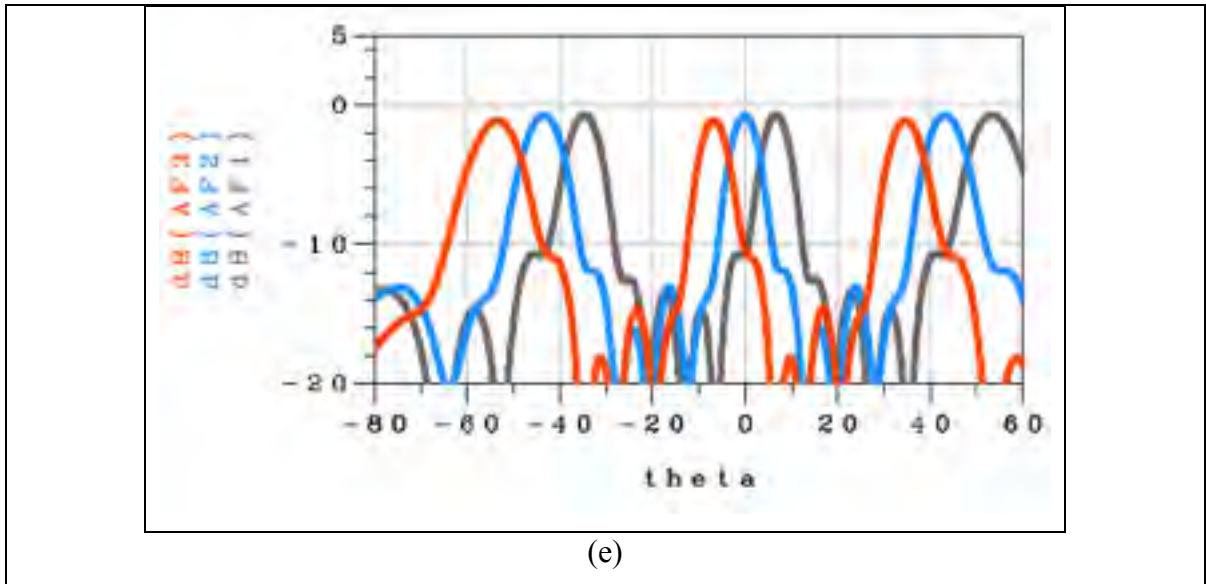


Figure 2.16 Array factor of the Rotman Lens (e) 12 GHz

These figures 2.16 demonstrate that the beam shape is approximately constant versus frequency. The measured and simulated results are compared in table 2.10. As it can be seen simulation and measurements are in a good agreements.

Table 2.10 Comparison between measured and simulated results

Freq	Simulation			Measurement		
	Beam position	SLL	Scan Loss	Beam position	SLL	Scan Loss
8	-6, 0, 6	12.25	0.36	-6.7, 0, 6.7	12	1.5
8.5	-6, 0, 6	13.1	0.1	-6.6, 0, 6.6	13.1	1.5
9	-6, 0, 6	13.65	0.04	-6.8, 0, 6.8	13.5	0.3
9.5	-6, 0, 6	13.92	0.08	-6.7, 0, 6.8	15	0.18
10	-6, 0, 6	12.7	0.03	-6.7, 0, 6.8	14.7	1.12
10.5	-6, 0, 6	13.85	0.04	-6.7, 0, 6.9	13.45	0.85
11	-6, 0, 6	13.5	0.02	-6.4, 0, 6.5	12.7	1.05
11.5	-6, 0, 6	13.36	0.45	-6.4, 0, 6.3	14.7	0.8
12	-6, 0, 6	13.98	0.38	-6.8, 0, 6.7	14	0.4

## 2.5 Conclusion

In this chapter we design three Rotman Lens. First design was 3x6 lens with capability of scanning angle was 12 degrees. 5x6 and 6x6 lenses had a scanning angle of 80 degrees ( $\pm 40^\circ$ ). For all these design we show the matching and coupling and array factor in operation frequency. For each one we compare the SLL and Scan loss. We built first design and used the absorber material in top of dummy ports. We compared the results with simulations and they were in good agreements. In Rotman Lens 6x6, dummy ports are placed between inputs ports and output ports of Rotman Lens as mutual coupling between input ports are reduced significantly which results in improving the performance of Rotman Lens.



## CHAPTER 3

### VIVALDI ARRAY ANTENNA

In these days the ultra-wide band antenna (UWB) is widely used in applications such as wireless communications, microwave imaging, and also in biomedical field. UWB type of antennas belong Biconical, Helical, Bow-tie antennas, Rectangular Loop antennas, Diamond Dipole antennas or Vivaldi antennas.

Here we used Vivaldi antenna because they have simple structures, wideband, light weight, small size, high efficiency, and high gain characteristics. Also they are good candidate for array applications since they have wideband input matching.

The Tapered Slot Antenna (TSA) which is also called Vivaldi antenna is a wideband slot antenna. This antenna can be made of printed circuit board material. They can be made on the same circuit board as an array antenna. This antenna consists of the tapered slot and the feeding is on the narrow side slot. This antenna has three main categories:

- In coplanar Vivaldi antenna two radiator planes are the same side of dielectric material. The antenna can be fed by aperture coupling from other side. In this chapter we designed this type of Vivaldi antenna;
- Antipodal Vivaldi antenna (AVA). In this type of Vivaldi antenna one of the layers is printed on top and the other one which is tapered in opposite direction is printed on the bottom of the dielectric substrate material;
- The balanced antipodal Vivaldi antenna (BAVA) consists of three copper layers. A dielectric layer has been added on the top of the antipodal structure and an additional metal plate just like the one in the bottom of the antenna has been printed on top of the newly added layer.

Here we will design the coplanar Vivaldi antenna as it gets higher gain than AVA and BAVA. Also side lobe level (SLL) for coplanar Vivaldi antenna has better performance than AVA and BAVA. Nurhayati et al (2016)

An example of single element of this antenna as well as its phased array are shown in figure 3.1. It should be noted that, as shown in figure 3.1a, this antenna can be used for both horizontal and vertical polarization and any combination of them. M. Stasiowski et al. (2008)

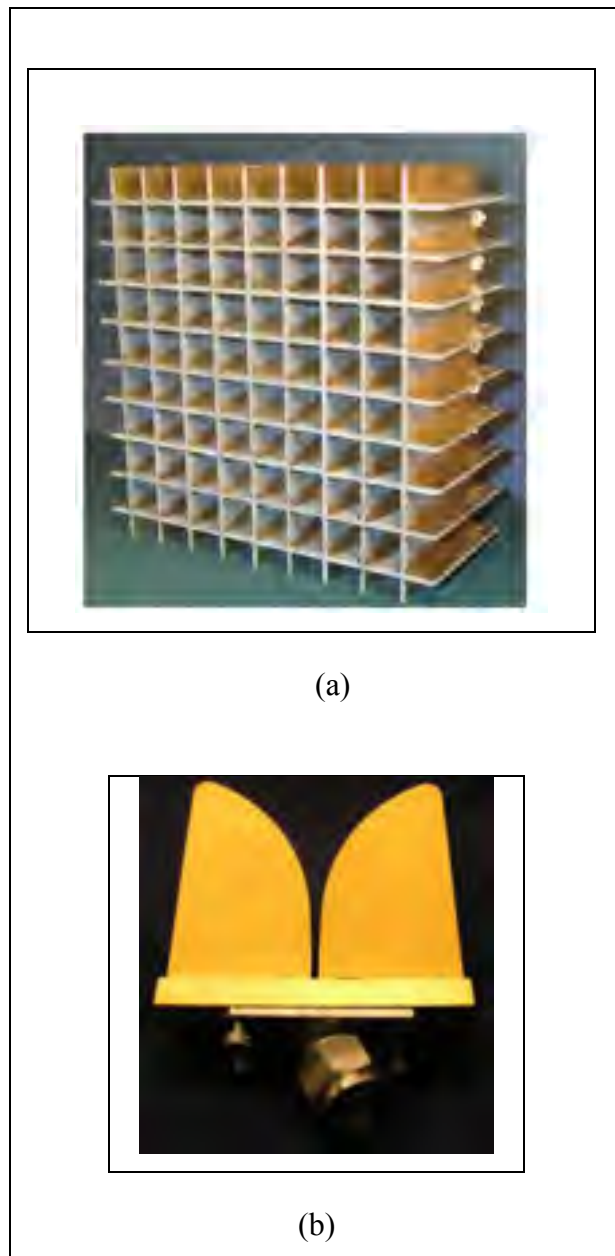


Figure 3.1 An example of (a) Dual-polarized Vivaldi array designed (b) Vivaldi element  
Adapted from M. Stasiowski et al (2008)

In this chapter we want to explain how we design a Vivaldi array antenna  $1 \times 6$  which can be integrate with our Rotman Lens ( $3 \times 6$ ) with the bellow specification.

Table 3. 1 Array design goal

<b>Frequency(GHz)</b>	8-12
<b>Gain</b>	13
<b>Weight</b>	Minimise
<b>Size</b>	6 elements
<b>Gain per Element</b>	5

### 3.1 Vivaldi antenna single element

As mentioned before in this thesis, Vivaldi antenna has high degrees of freedom in design, therefore it does not have grating lobe issue to get the desired gain. However to get a wideband input matching the size of the antenna should be increased which will degrade the grating lobe. To tackle this issue, all the degrees of freedom that have significant effect on antenna's performance have to be optimized. Next, the steps for design will be explained.

### 3.2 Substrate selection and size limitation for antenna design

The exponential shape slots play an important role in Vivaldi antenna design by generating a traveling wave between themselves. Based on our explanation to design a wideband Vivaldi antenna, the exponential slots have to be carefully designed. In this section we will explain which parameter has an effect on antenna's performance.

### 3.2.1 Parametric effect on Vivaldi:

#### Substrate:

Substrate can be considered in terms of dielectric constant and thickness.

- **Dielectric constant:**

Higher dielectric constant substrate made the antenna smaller. Besides, lower dielectric constant provide wider bandwidth. R. Dhawan et al (2016)

- **Thickness:**

Thicker substrate improve gain and main bandwidth of antenna due to decrease in antenna reactance. R. Dhawan et al (2016)

In this work Rogers RT/duroid 5880™ with constant permeability of 2.2 and thickness of 30mil is chosen.

#### Cavity diameter:

Use of circular cavity at the end of slot line offers the freedom to tune the impedance matching (D. H. Schaubert et al,1999) and it will affect the bandwidth of antenna. R. Dhawan et al (2016)

#### Taper:

- **Taper length:**

It depended on wavelength and cavity diameter and antenna length. Bigger taper length improves the bandwidth. R. Dhawan et al (2016)

- **Taper rate:**

It can be define by an exponential which we will show it later. It effects on the bandwidth of input impedance. R. Dhawan et al (2016)

### 3.2.2 Designing parameter:

#### Antenna length:

Antenna length should be greater than the average value of the minimum and maximum wavelength. R. Dhawan et al (2016)

$$F_{max} = 12GHz ; F_{min} = 8GHz$$

$$\lambda_{min} = 24.9 mm ; \lambda_{max} = 37.4 mm$$

$$L > \frac{\lambda_{min} + \lambda_{max}}{2} \rightarrow L = 29mm$$

#### Antenna width:

It should be greater than half of average value of maximum and minimum wavelength. R. Dhawan et al (2016)

$$W > \frac{\lambda_{min} + \lambda_{max}}{4} = 15mm$$

#### Mouth opening:

It should be between  $W_{min}$  and  $W_{max}$ . R. Dhawan et al (2016)

$$W_{min} = \frac{\lambda_{min}}{2} = 12.4 mm$$

$$W_{max} = \frac{\lambda_{max}}{2} = 18.7 mm$$

So an optimum width value is 14mm.

### 3.3 Exponential slot design for Vivaldi antenna

Mathematic equation of exponential slot can be considered as following .Y. Yang, etal (2008):

$$y = c_1 e^{Rz} + c_2 \quad (3.1)$$

It should be noted that that parameter R defines the power of exponential slot or taper rate thus it affects the bandwidth of input impedance. In the above equation the C1 and C2 are defined as below:

$$c_1 = \frac{y_2 - y_1}{e^{Rz_2} - e^{Rz_1}} \quad (3.2)$$

$$c_2 = \frac{y_1 e^{Rz_2} - y_2 e^{Rz_1}}{e^{Rz_2} - e^{Rz_1}} \quad (3.3)$$

$y_1, y_2, z_1,$  and  $z_2$  indicate the slot line start and end points. We will use these formulas in HFSS to draw the taper of the slot line. Figure 3.2 shows the bottom view of designed single element of Vivaldi antenna for 8-12 GHz.

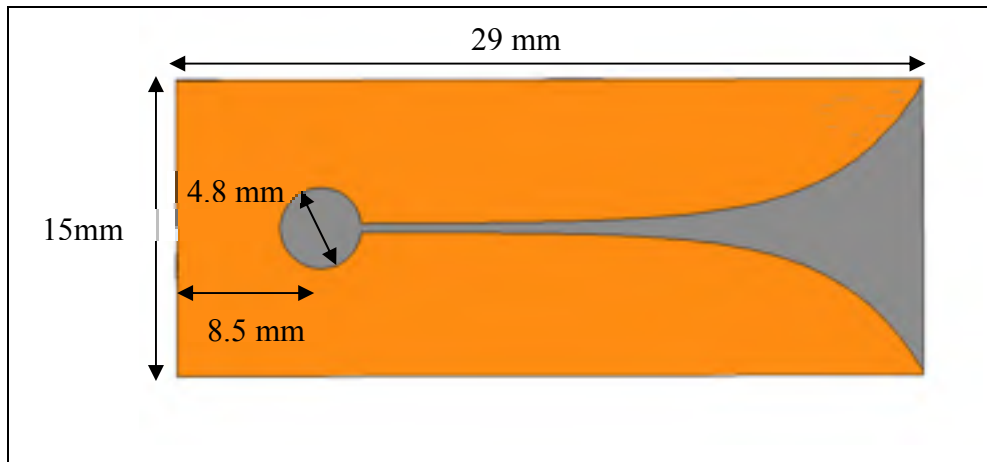


Figure 3.2 Bottom view of designed Vivaldi antenna in HFSS

### 3.4 Feed design for Vivaldi antenna

There are numerous versions of Vivaldi antenna, which are different in the feeding techniques. Here an aperture coupled feed is considered. The feeding line excites a circular space via a microstrip line, terminated with a circular shaped area. From the circular resonant area the energy reaches an exponential pattern via a slot line. The main idea of such a coupling is to feed the antenna by the transformation of micro-strip line to slot line. The metallization of the antenna serves as a ground plane for the microstrip line. Since the antenna will be used an

antenna array, it is good to have the feeding on the back of the structure in order to have a better degree of freedom by setting the distance between elements in the array. (G. Adamiuk et al, 2008). Figure 3.3 shows the aperture coupled feed method for Vivaldi matching and feed design and its main design parameters.

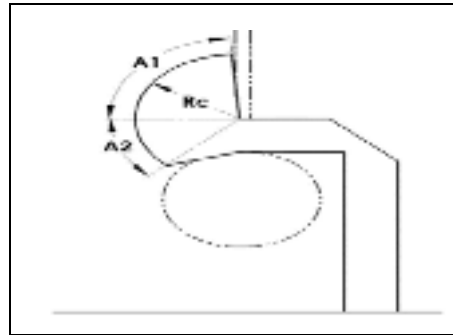


Figure 3.3 Main parameters for Vivaldi feed design  
Adapted from Y. Yang, etal (2008)

The width of microstrip line is designed for a 50 ohms line as shown in figure 3.4.

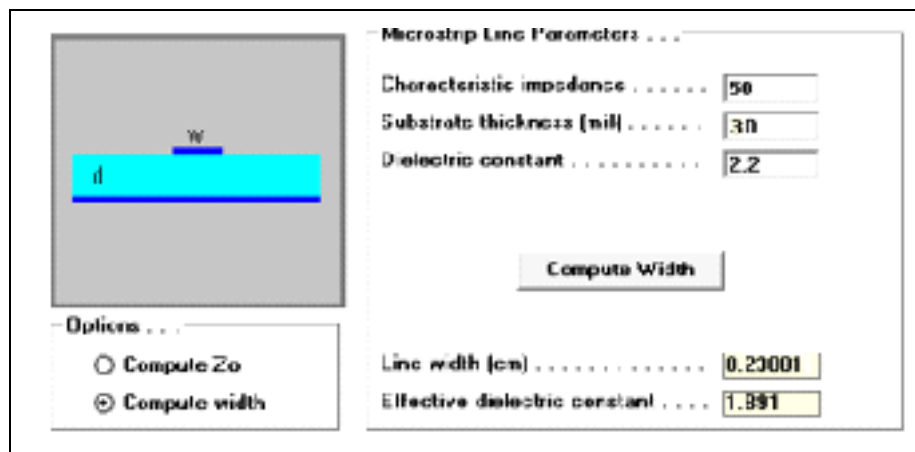


Figure 3.4 50 ohms microstrip line width calculation

The exponential microstrip lines is designed to obtain a good impedance matching over 8-12 GHz frequency range. This can be seen obviously in figure 3.5.

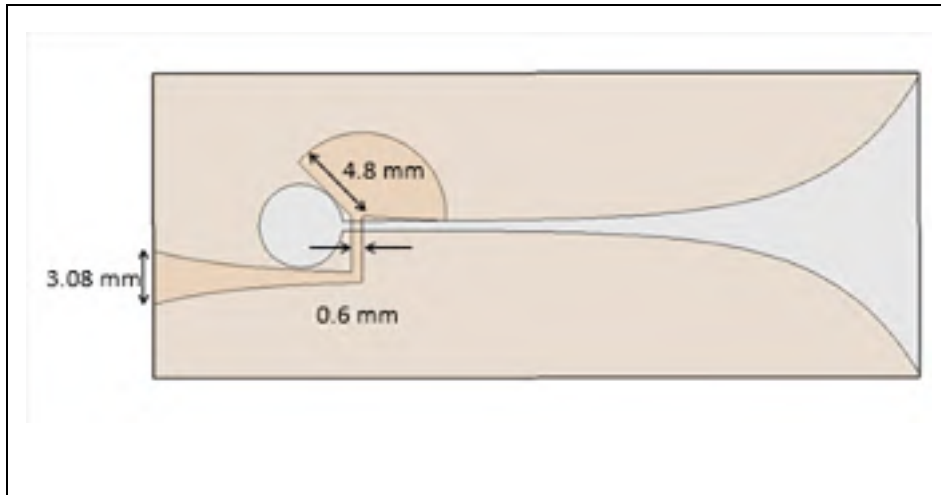


Figure 3.5 Vivaldi antenna with its impedance matching and feed in HFSS

It should be noted that this antenna is designed in HFSS with all parametric drawing. These parameters are shown in figure 3.6. We have done many optimization on these parameters to improve S11. It should be noted that getting a good matching over 8-12 GHz was the most time consuming part during this antenna design.



Project Variables | Intrinsic Variables | Constraints

Value
  Optimization
  Tuning
  Sensitivity
  Statistics

Name	Value	Unit	Evaluated Value	Description	Read-only	Hidden
Sr_c	2.4	mm	2.4mm	circle	<input type="checkbox"/>	<input type="checkbox"/>
Sr_c	13.5	mm	13.5mm	circle	<input type="checkbox"/>	<input type="checkbox"/>
Sr_sub	44	mm	44mm	substrate	<input type="checkbox"/>	<input type="checkbox"/>
Sy_sub	17.5	mm	17.5mm	substrate	<input type="checkbox"/>	<input type="checkbox"/>
Sh_sub	1	mm	1mm	substrate	<input type="checkbox"/>	<input type="checkbox"/>
Sdel_a	0.25	mm	0.25mm	start point for slot	<input type="checkbox"/>	<input type="checkbox"/>
Sdel_b	0.25	mm	0.25mm	end point for slot	<input type="checkbox"/>	<input type="checkbox"/>
Sy <sup>1</sup>	3.081/2	mm	1.5405mm	for feed	<input type="checkbox"/>	<input type="checkbox"/>
Sw50	0	mm	0mm	width	<input type="checkbox"/>	<input type="checkbox"/>
Sl <sub>1</sub>	12	mm	12mm	feed	<input type="checkbox"/>	<input type="checkbox"/>
Sl <sub>2</sub>	0	mm	0mm	width	<input type="checkbox"/>	<input type="checkbox"/>
Sl <sub>1</sub>	3.0	mm	3.0mm	feed	<input type="checkbox"/>	<input type="checkbox"/>
Sradius	1.8	mm	1.8mm	circle in bottom	<input type="checkbox"/>	<input type="checkbox"/>
Sd <sub>1</sub>	3		3	width	<input type="checkbox"/>	<input type="checkbox"/>
Sdel <sub>1</sub>	0	deg	0deg	width	<input type="checkbox"/>	<input type="checkbox"/>
Sl <sub>sub</sub>	0.5	mm	0.5mm	width	<input type="checkbox"/>	<input type="checkbox"/>
Sdel <sub>1</sub>	10	deg	10deg	bottom layer	<input type="checkbox"/>	<input type="checkbox"/>
Sdel <sub>2</sub>	180	deg	180deg	bottom layer	<input type="checkbox"/>	<input type="checkbox"/>
S <sub>1</sub>	0	mm	0mm	width	<input type="checkbox"/>	<input type="checkbox"/>
SA	-2000		-2000	EXP for slot (top layer)	<input type="checkbox"/>	<input type="checkbox"/>
Sy <sub>2</sub>	0.3	mm	0.3mm	for feed	<input type="checkbox"/>	<input type="checkbox"/>
SH	2000		2000	EXP value for feed	<input type="checkbox"/>	<input type="checkbox"/>
Sd <sub>feed</sub>	3	mm	3mm	for feed	<input type="checkbox"/>	<input type="checkbox"/>
Sin <sub>power</sub>	0	mm	0mm	width	<input type="checkbox"/>	<input type="checkbox"/>

Show Hidden

Figure 3.6 Optimized parameters for desired S11

### 3.5 Simulation results of designed Vivaldi antenna in two software “HFSS and CST”

Finally the Vivaldi antenna with the mentioned specifications (Figure 3.6) is designed and simulated. Figures 3.8 show the radiation pattern for the single element of antenna for 8, 10, 12 GHz. The Vivaldi antenna has linear polarization. In figure 3.7 the antenna radiates in E-plane (ZY plane) direction.

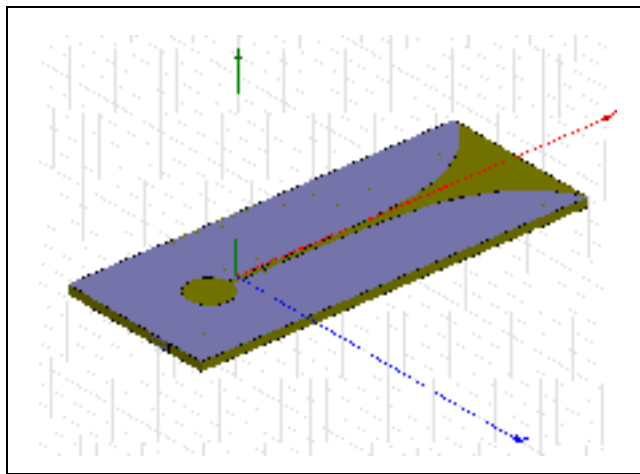


Figure 3.7 Vivaldi element in HFSS

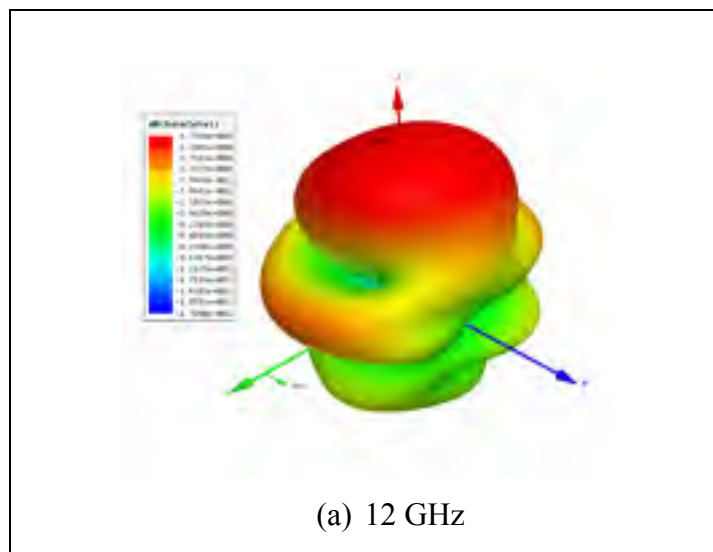


Figure 3.8 3D radiation pattern for designed Vivaldi antenna (a) 12 GHz

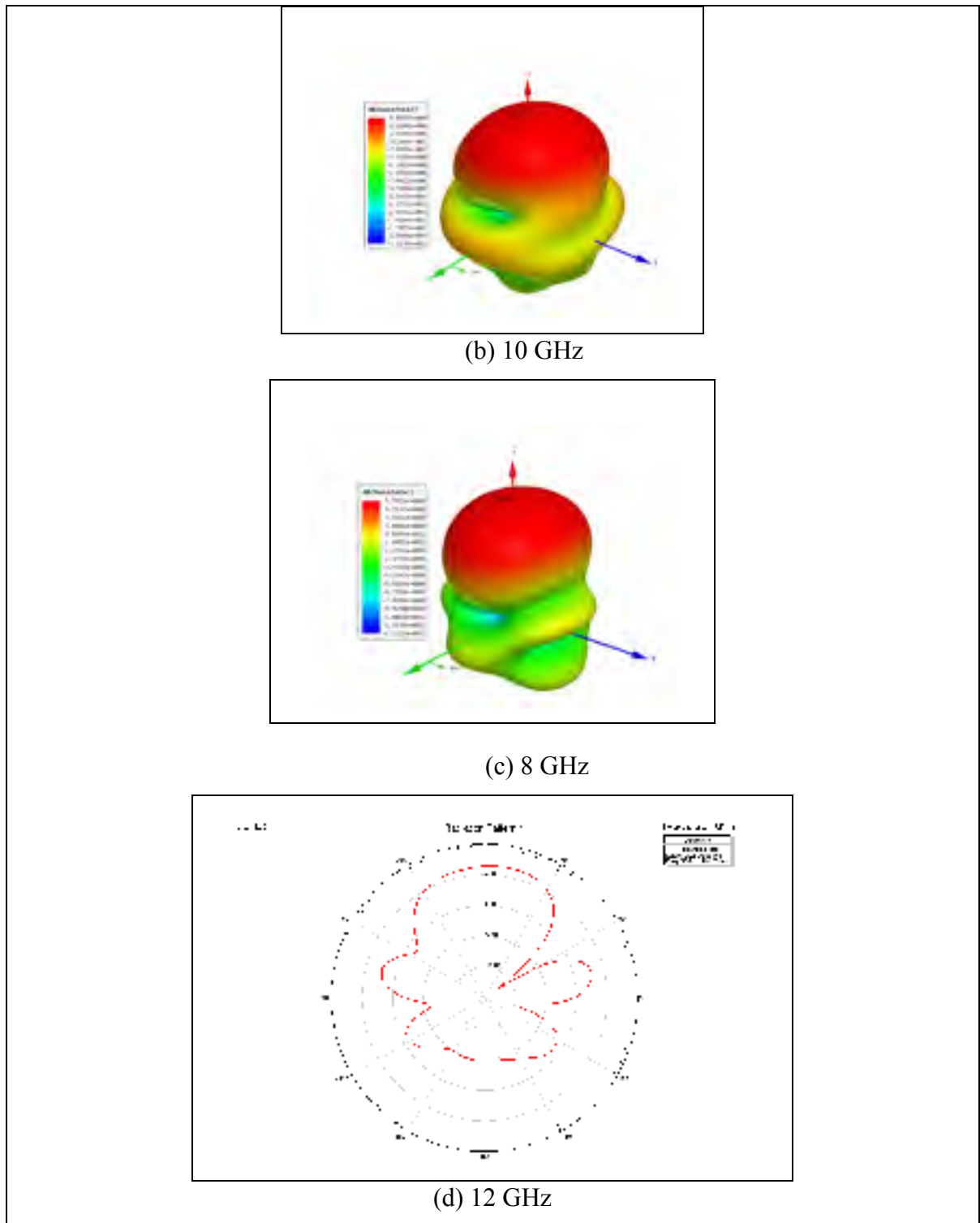
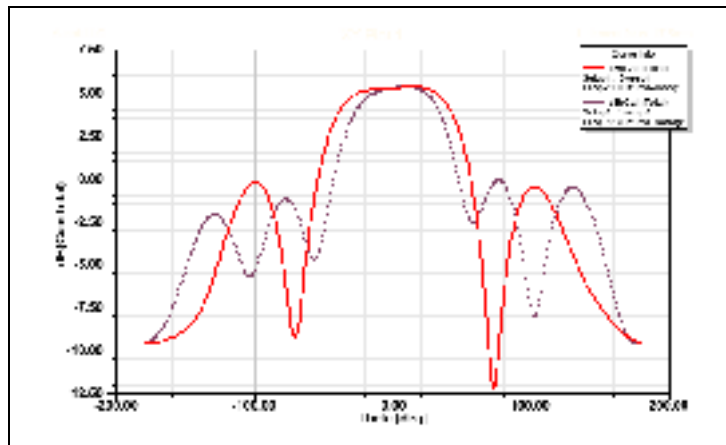
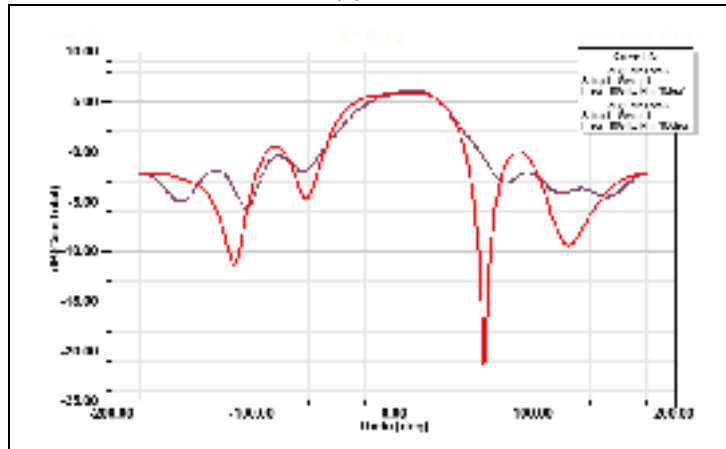


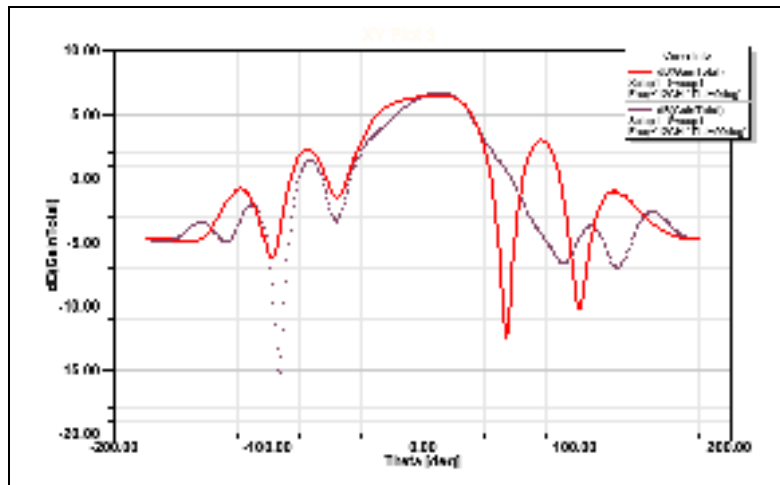
Figure 3.8 3D radiation pattern for designed Vivaldi antenna (b) 10 GHz, (C) 8 GHz, and (d) 2D radiation pattern at 12GHz



(a) 8 GHz



(b) 10 GHz



(c) 12 GHz

Figure 3.9 Radiation pattern in E-plane and H-plane

Table 3.2 show the simulation results in  $\phi=90$  plane (E-plane) in different frequencies. Figure 3.10 show the cross polarization (gain X) at frequency 8, 10, 12GHz.

Table 3. 2 Simulation results in  $\phi=90$  plane (E-palne)

Frequency(GHz)	Gain(dB)	SLL(dB)	HP_BW(degrees)
8	5.35	5.42	78
10	6.06	5.75	85
12	6.73	4.97	80

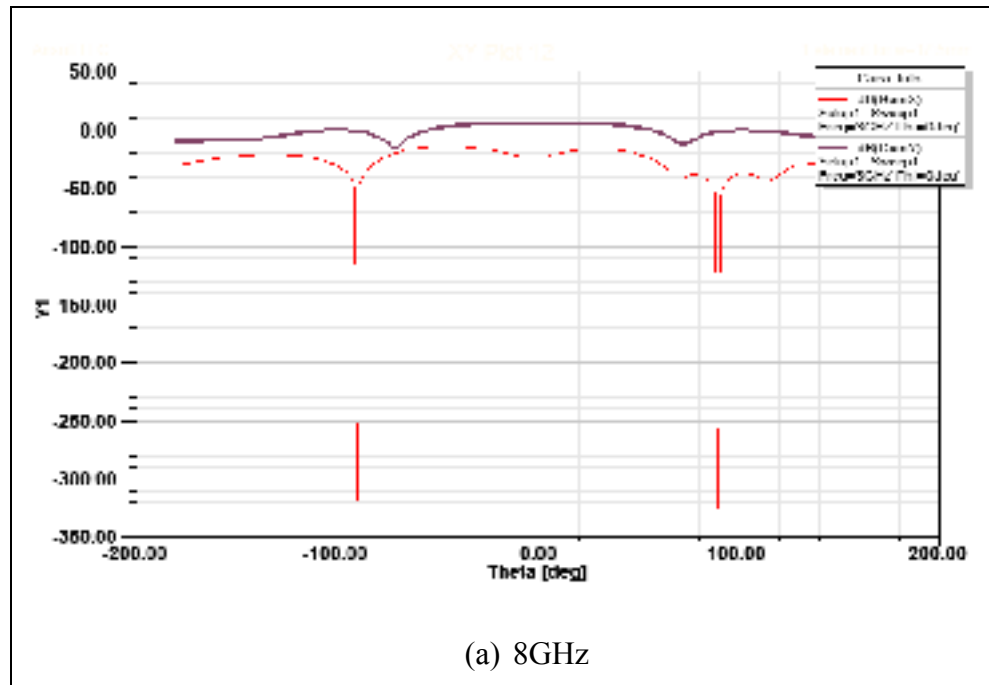


Figure 3.10 (a) Cross polarization at 8GHz

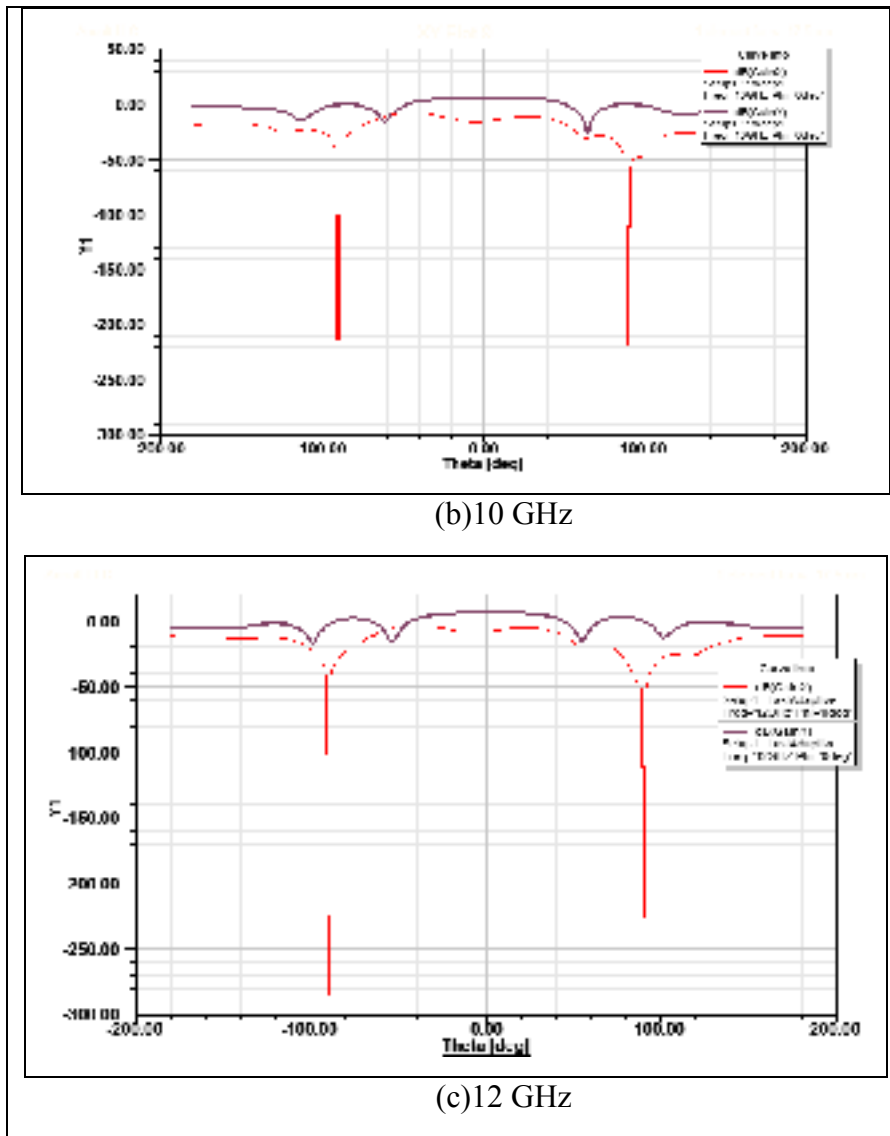


Figure 3.10 Cross polarization at (b) 10GHz, (c) 12GHz

We have also simulated this antenna in CST to just compare the results and make sure to have robust results. It has shown in figures 3.11.

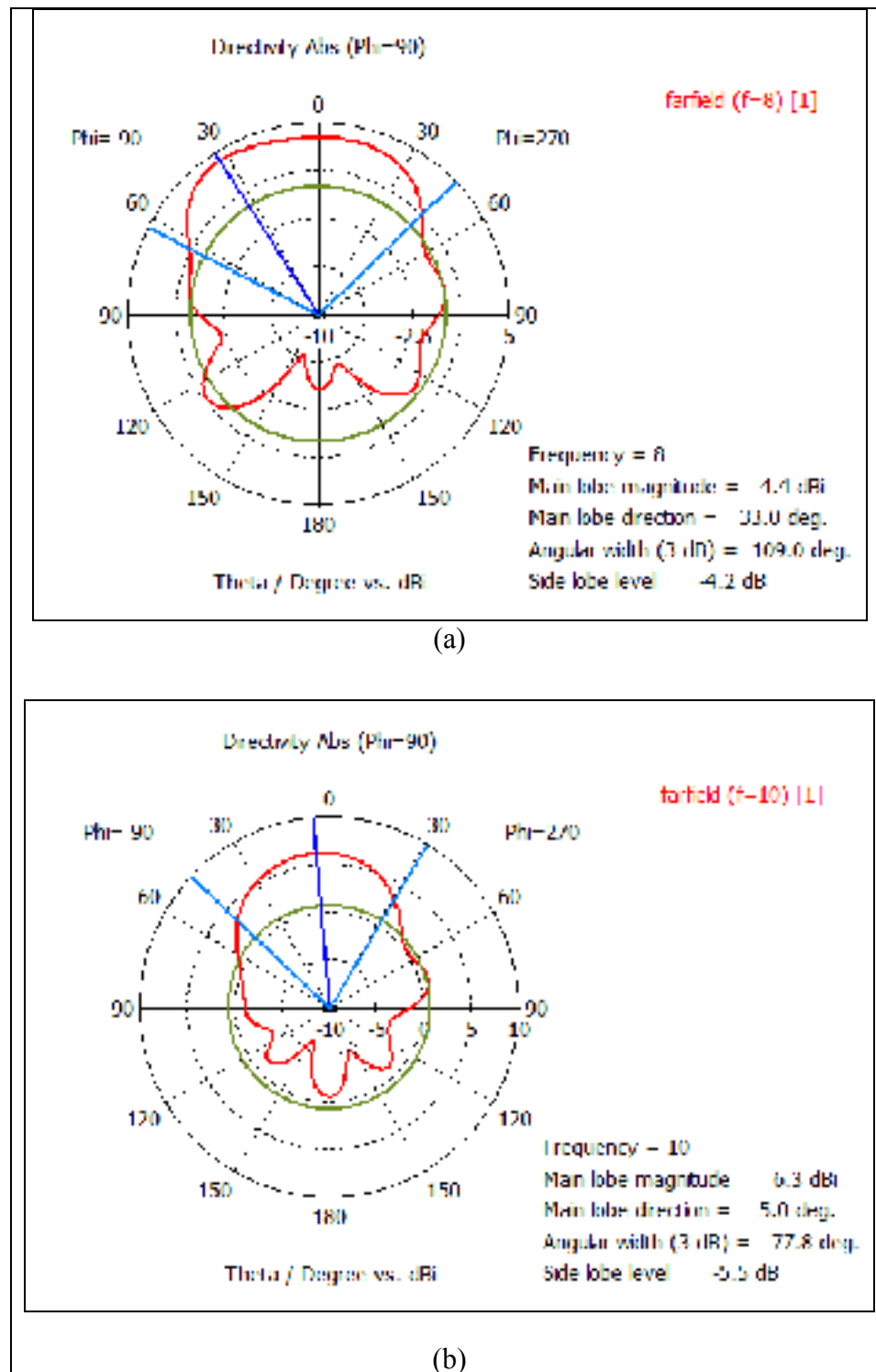


Figure 3.11 Simulation results of Vivaldi antenna in CST

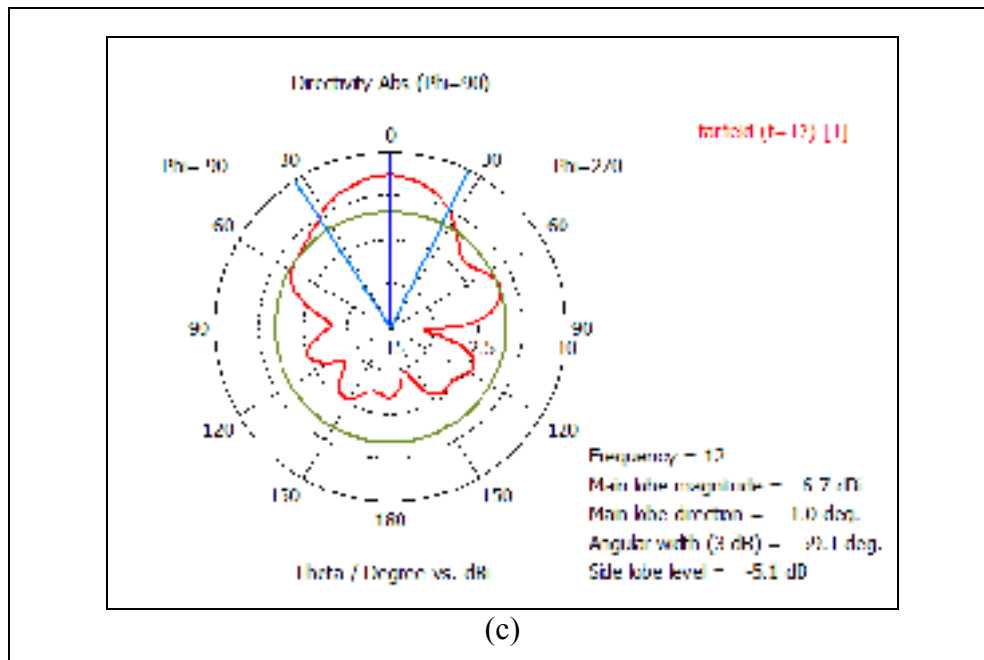


Figure 3.11 Simulation results of Vivaldi antenna in CST

Comparing the radiation pattern and gain of this antenna in HFSS and CST, it can be seen that there are good agreement between them.



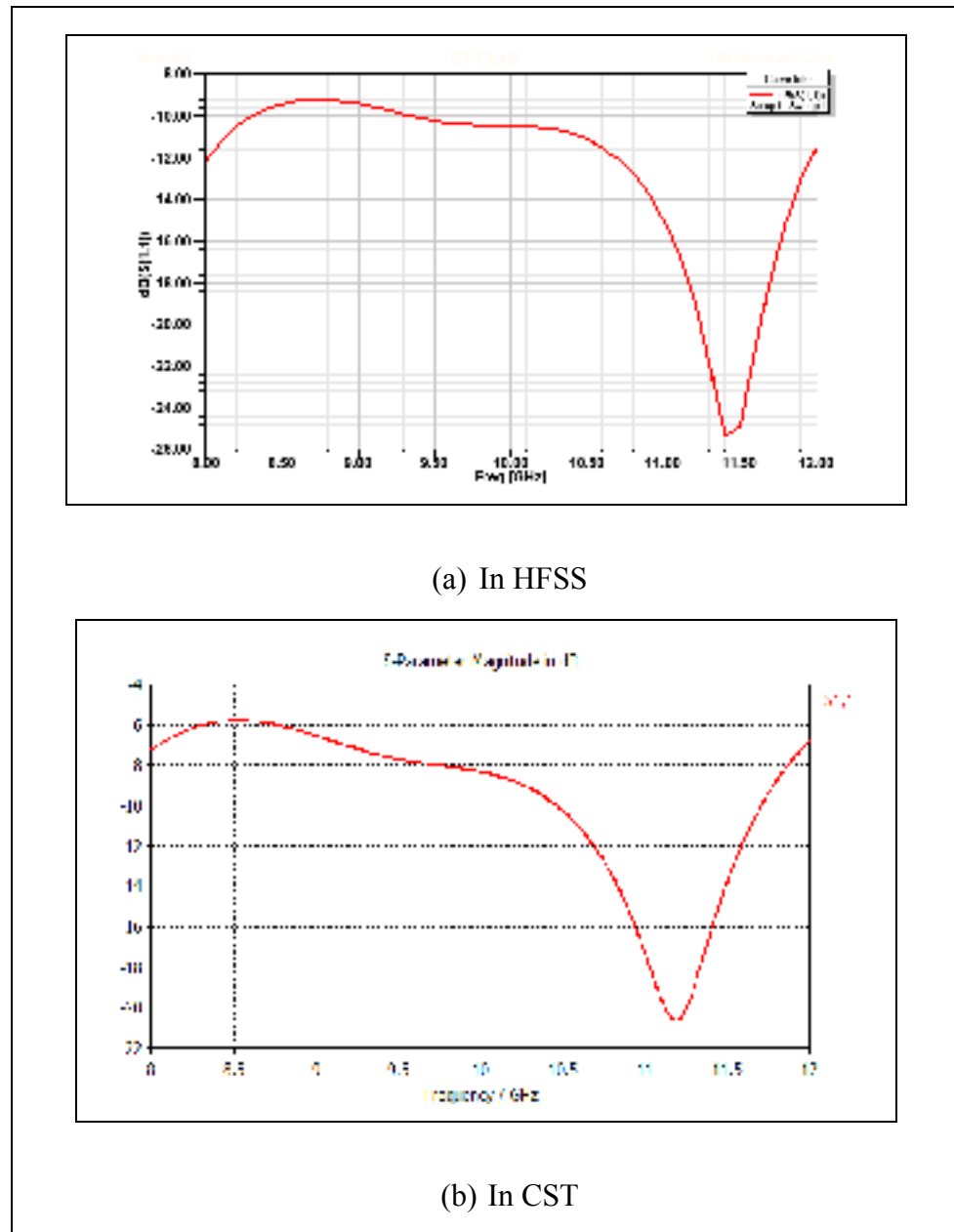


Figure 3.12 Input matching with lumped port excitation in HFSS and CST

It should be noted that the  $S_{11}$  is less than -10 dB at some frequencies, but as mentioned before the  $S_{11}$  will be further improved due to mutual coupling between elements in array. M.Wang et al (2010)

### 3.6 Radiation efficiency of Vivaldi antenna

We changed the top and bottom metals of Vivaldi antenna from PEC (Perfect Electric Conductor) to Copper to make the simulations more accurate. Figure 3.13 shows maximum antenna gain versus frequency and as you can see we have a smooth change over frequencies. Figure 3.14 shows efficiencies at different frequencies. Antenna efficiency determines how much of power can the antenna will radiate the energy. The antenna efficiency should be high as possible. As it can be seen the efficiency is more that 98% at different frequencies.

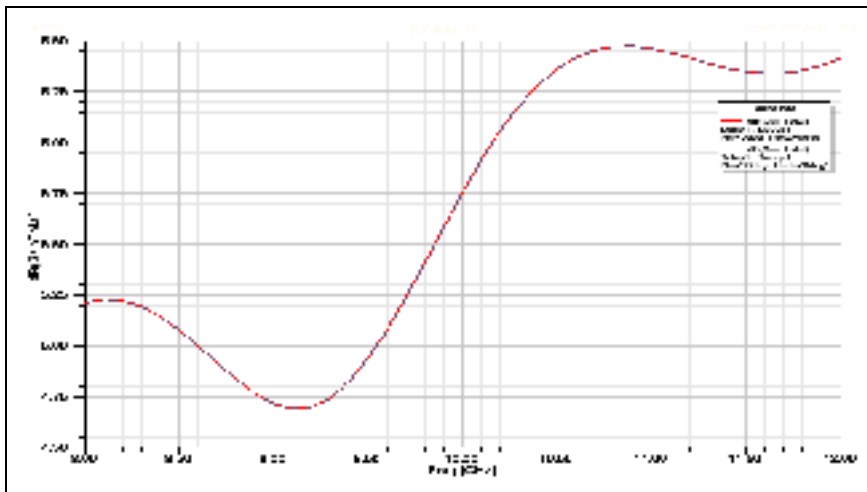


Figure 3.13 Maximum antenna gain vs frequency

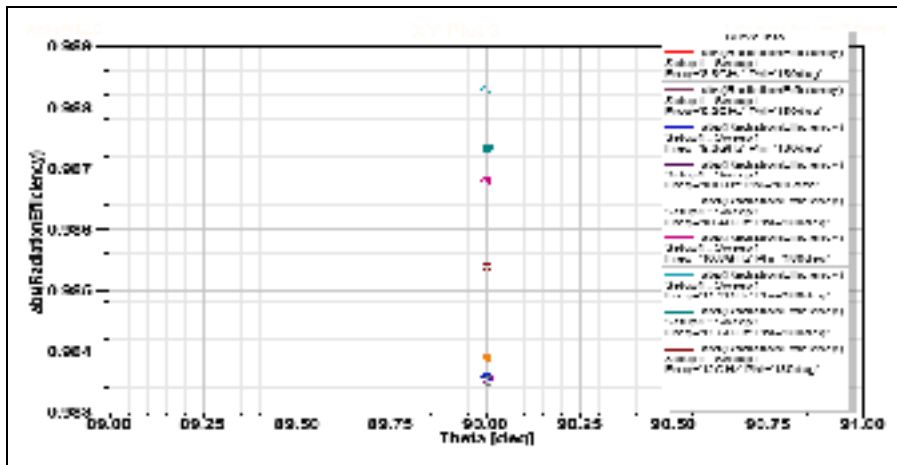


Figure 3.14 Pattern efficiency at different frequencies

### 3.7 Design and simulation of Vivaldi antenna linear array

In this section the design and simulation of a linear array of Vivaldi element will be presented. The Vivaldi antenna element has theoretically unlimited bandwidth. But the upper frequency operation ( $\lambda_{min}$ ) is limited by the transition, also in Vivaldi antenna array, it is limited by starting of grating lobes, which is determined by the element spacing (M.Wang et al, 2010). With increasing the space between elements, we will have more gain but degrading grating lobes, and also less mutual coupling, so better in matching. Therefore, first we have to choose the element spacing and then optimize antenna parameters to get desired bandwidth of the antenna array.

With changing the element spacing, the mutual coupling between elements (S12) will be changed smoothly. The reflection coefficient of each element (S11) will be cancelled by S12, therefore the bandwidth will be increased (M.Wang et al, 2010). Here we chose the element spacing equal to 15mm, which is also the element width. We have used the below formula which shows the limitation of  $d$  (element spacing) due to grating lobes. In this formula  $\lambda$  is minimum wavelength in our frequency operation and  $\theta_m$  is maximum scanning angle which we used 40 degrees.

$$\frac{d}{\lambda} < \frac{1}{1 + \sin\theta_m}$$

$$\theta_m = 40^\circ \quad \rightarrow \quad \frac{d}{\lambda} = 0.608 \quad \text{and} \quad \lambda_{min} = 24mm$$

Therefore we will have the element spacing  $d = 15mm$ . By this, we have  $\pm 40^\circ$  beam scanning without grating lobes.

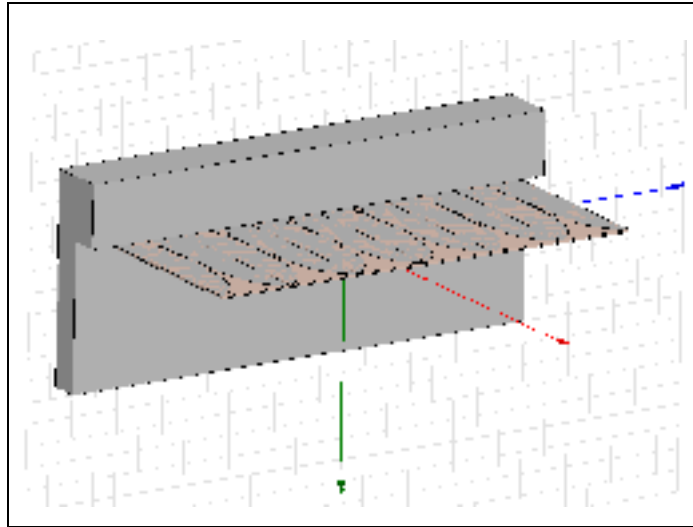


Figure 3.15 Vivaldi antenna array in HFSS

Figure 3.15 shows the linear arrays with Vivaldi elements. In this design we have used a mechanical structure to hold our array antenna which makes measuring to be easier and also it can improve the gain due to decreasing the back lobes. Figure 3.16 also shows the 3D radiation pattern of this array. It can be seen that we have 12.5dB gain. We can see that we have still some grating lobes. If we want to eliminate the grating lobes, we have to decrease our element spacing which cause reducing gain, so this is a trade off between having more gain or grating lobes.

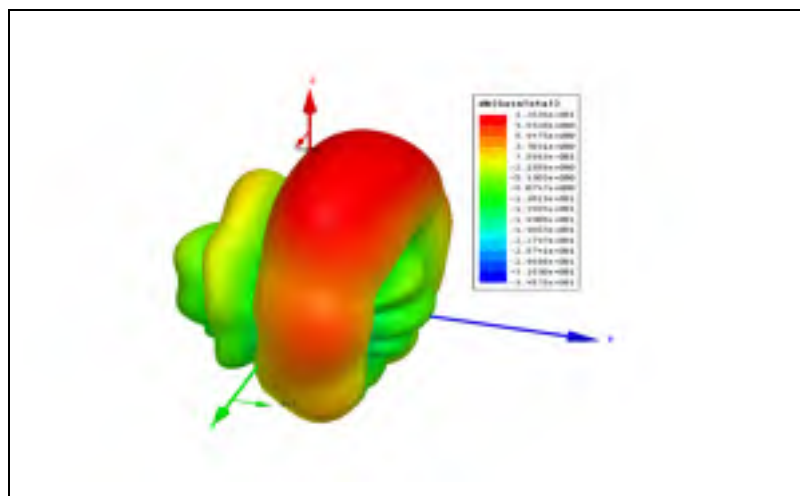


Figure 3.16 Vivaldi linear array 3D radiation pattern

### **3.8 Conclusion**

In this chapter, we talked about a single elements of Vivaldi antenna and the parameters which effect its performance. We designed one element in HFSS and CST at operation frequency (8GHz-12GHz) with desired SLL and gain and bandwidth. Also we talked about the array antenna and the limitation of the size and we used HFSS to design an  $1 \times 6$  array antenna, which is suitable to integrate with our designed Rotman Lens ( $6 \times 6$ ) in chapter two due to ultra-wide band Vivaldi behavior.



## CONCLUSION

In this thesis, wide-band wide-scan phased arrays have been investigated by utilizing a beamforming network that is based on a microstrip Rotman Lens. A wide beam scanning capability of  $\pm 40^\circ$  for the frequency range 8-12 GHz has been demonstrated. The most crucial part was to design a wide beam scanning Rotman Lens in conjunction with a good impedance matching over the entire frequency band. To do so, a technique has been proposed to place the dummy ports between input ports and output ports of Rotman Lens such that the mutual coupling between ports has been reduced significantly which resulted in improving the performance of the Rotman Lens. Three different Rotman Lenses were designed using fullwave simulation in CST and HFSS. One of three designs was fabricated and tested to verify the simulations. Good agreement between simulation and measurement was achieved.

Rotman-Vivaldi phased arrays offer a good option for achieving both wide-scanning and wideband coverage. With the Rotman Lens having been designed in microstrip, a single Vivaldi radiation element and a Vivaldi antenna array were also designed in microstrip technology but were not fabricated and tested. The full wave simulation results obtained by CST and HFSS were consistent giving confidence in the design.

As future work, it is recommended that Vivaldi antenna array be fabricated and tested. A final integration of the Rotman Lens with the Vivaldi array should be pursued to complete the work and demonstrate the wide-band wide-scan capabilities of the proposed design.





## APPENDIX I

### INPUT PARAMETERS FOR MATLAB CODE

Table-A I-1 Input parameters for MATLAB code  
Taken from J. Dong et al (2009)

<b>Input Parameter</b>	<b>Description</b>
eps	Dielectric permittivity ( $\epsilon_r$ )
e	Input contour eccentricity parameter
gamma	Scan angle over focal angle
r	Array amplitude array
n	Number of output ports
ap	Focal angle
g	Focal ratio
phim	Maximum angle of input ports on input contours
Num	Number of input ports



## APPENDIX II

### MATLAB CODE FOR ROTMAN DESIGN

Algorithm-A II.1 MATLAB code for Rotman design  
Taken from J. Dong et al (2009)

#### MATLAB Code

```
function [xb,yb,xr,yr,w]=RotmBRW(eps,e,gama,r,n,ap,g,phim,Num)
% eps dielectric constants for cavity region
% e The eccentricity of the beam contour
% gama Ray to beam angle ratio
% r 1/D inverse of the size of array
% n Number of receiving ports
% ap Off center focal angle
% g Focal ratio
% phim maximum subtended angle for beam port phase centers
% Num Number of beam ports
% xb yb locus of beam ports contour
% xr yr locus of receivingcontour
% w transmission lines length

% Deriving the beam ports contour
be=1/g;
phimax=phim*pi/180;
ap=ap*pi/180;
a=1/2*(-be^2*cos(ap)^2+2*be*cos(ap)+be^2*sin(ap)^2*e^2-1-...
be^2*sin(ap)^2)/(1-e^2)^(1/2)/(be*cos(ap)-1);
b=(1-e^2)^0.5*a;
Theta0=linspace(0,phim,Num);
Theta=linspace(0,phimax,Num);
xb=(0.5)./(a^2+tan(Theta).^2*b^2).*(-2*a+2*a*b-...
2*(b^2*a^2+2*tan(Theta).^2*b^3-tan(Theta).^2*b^2).^(1/2))*a;
yb=-xb.*tan(Theta);
% Deriving the receivingcontour
```

```

D=1/r;
y3=linspace(0,D/2,n)/sqrt(eps);
ze=y3*gama;
C=cos(ap);S=sin(ap);
a2=1-((1-be)/(1-be*C))^2-(ze/be).^2;
b2=-2+2.*ze.^2/be+2*(1-be)/(1-be*C)-(1-be).*(S.*ze./(1-be*C)).^2;
c2=-ze.^2+(S.*ze).^2/(1-be*C)-((S.*ze).^2./(1-be*C)/2).^2;
Bcd=b2.^2-4.*a2.*c2;
w=(-b2-(Bcd).^0.5)./a2/2;
xr=((ze.*sin(ap)).^2-2*be.*w+2*w)/(be.*cos(ap)-1)/2;
yr=ze.*(1-w./be);
end.

```





```

br=zeros(1,n-1);
cr=zeros(1,n-1);
ar=zeros(1,n-1);

for j=1:n-1
    xmr(j)=(xr(j)+xr(j+1))/2;
    ymr(j)=(yr(j)+yr(j+1))/2;
    mr(j)=ymr(j)/(xmr(j)+1);
    ar(j)=1+mr(j)^2;
    br(j)=2*mr(j)^2-2*xmr(j)-2*mr(j)*ymr(j);
    cr(j)=mr(j)^2-2*mr(j)*ymr(j)+(xmr(j)^2)+(ymr(j)^2)-hr^2;
    deltar(j)=sqrt(br(j)^2-4*ar(j)*cr(j));
    xrp(j)=(-br(j)+deltar(j))/2*ar(j);
    yrp(j)=mr(j)*(1+xrp(j));

    xr0(j)=xrp(j)+wh/(sqrt(1+(1/mr(j)^2)));
    yr0(j)=yrp(j)+(xrp(j)-xr0(j))/(mr(j));
    xr00(j)=xrp(j)-wh/(sqrt(1+(1/mr(j)^2)));
    yr00(j)=yrp(j)+(xrp(j)-xr00(j))/(mr(j));

end

% output ports
pol=[xr0' yr0']; po2=[xr00' yr00']; co=[xr' yr'] ;

for i=1 : length(co)-1
    B=[co(i,:) ; pol(i,:) ; po2(i,:) ; co(i+1,:) ; co(i,:)];
    C=B;
    C(:,2)=-B(:,2);
    eval(['portout_up_',num2str(i),'=',mat2str(B),';'])
    eval(['portout_down_',num2str(i),'=',mat2str(C),';'])

    plot(B(:,1),B(:,2))
    plot(C(:,1),C(:,2))

    dlmwrite(['portout_up_',num2str(i),'.txt'],B, 'newline','pc')
    dlmwrite(['portout_down_',num2str(i),'.txt'],C, 'newline','pc')

end

% input ports

for i=1:length(xb)-1
    xb_m(i)=0.5*(xb(i)+xb(i+1));
    yb_m(i)=0.5*(yb(i)+yb(i+1));
end

% middle input port
x_1=xb_m(1);
y_1=-yb_m(1);

```

```

temp=[x_1 y_1];

temp1=[xb_m' yb_m'];
temp2=[-1-hb wh];
temp3=[-1-hb -wh];

temp4=[x0' y0'];
temp5=[x00' y00'];
temp4(1,:)=[];
temp5(1,:)=[];

ci=[temp;temp1]; pi1=[temp3;temp5] ; pi2=[temp2;temp4];

fin1=length(xb);
fin2=length(ci);

m=(yb(fin1)-ci(fin2,2))/(xb(fin1)-ci(fin2,1));
distance=sqrt((yb(fin1)-ci(fin2,2))^2+(xb(fin1)-ci(fin2,1))^2);
x=xb(fin1)+distance/sqrt(m^2+1);
y=m*(x-xb(fin1))+yb(fin1);
temp6=[x y];

ci=[ci;temp6];

for i=1 : length(ci)-1
    if i==1
        B=[ci(i,:);pi1(i,:);pi2(i,:);ci(i+1,:);ci(i,:)];
        eval(['portinput_',num2str(i),'=',mat2str(B),';'])
        plot(B(:,1),B(:,2))
        dlmwrite(['portinput_',num2str(i),'.txt'],B, 'newline','pc')

    else
        B=[ci(i,:);pi1(i,:);pi2(i,:);ci(i+1,:);ci(i,:)];
        C=B;
        C(:,2)=-B(:,2);
        eval(['portinput_up_',num2str(i),'=',mat2str(B),';'])
        eval(['portinput_down_',num2str(i),'=',mat2str(C),';'])

        plot(B(:,1),B(:,2))
        plot(C(:,1),C(:,2))

        dlmwrite(['portinput_up_',num2str(i),'.txt'],B, 'newline','pc')
        dlmwrite(['portinput_down_',num2str(i),'.txt'],C, 'newline','pc')

    end
end

line([-1 0],[0 0],'LineStyle','--')
text(-.7,0,[num2str(2*Num-1),'x',num2str(2*(n-1)),'Rotman Lens'])

```





## APPENDIX IV

### VALUE FOR TABLE 2.2

Value for table 2.2 are calculated from using the formula (1.7) and the formulas came in section (1.2.3), and then optimised them for better performance.

$$\gamma = \text{ray to beam abgle ratio} = \frac{\sin(\Psi_{\alpha})}{\sin\alpha} \quad \Psi = \text{array scan angle}$$

$$g = 1 + \frac{\alpha^2}{2} \quad (\text{A IV-1})$$

In this design  $\alpha$  is  $6^\circ$  and array scan angle is  $12^\circ$ . Therefore we will have:

$$\gamma = \frac{\sin(\Psi_{\alpha})}{\sin\alpha} = 1.989 = 1.99$$

$$g = 1 + \frac{\alpha^2}{2} = 1.005$$



## APPENDIX V

### VALUE FOR TABLE 2.5

Value for table 2.5 are calculated from using the formula (1.7) and the formulas came in section (1.2.3), and then optimised them for better performance.

$$\gamma = \text{ray to beam abgle ratio} = \frac{\sin(\Psi_{\alpha})}{\sin\alpha} \quad \Psi = \text{array scan angle}$$
$$g = 1 + \frac{\alpha^2}{2} \quad (\text{A V-1})$$

In this design  $\alpha$  is  $40^\circ$  and array scan angle is  $80^\circ$ . Therefore we will have:

$$\gamma = \frac{\sin(\Psi_{\alpha})}{\sin\alpha} = 1.53$$

$$g = 1 + \frac{\alpha^2}{2} = 1.24$$



## APPENDIX VI

### VALUE FOR TABLE 2.8

Value for table 2.8 are calculated from using the formula (1, 7) and the formulas came in section (1.2.3), and then optimised them for better performance.

$$\gamma = \text{ray to beam abgle ratio} = \frac{\sin(\Psi_{\alpha})}{\sin\alpha} \quad \Psi = \text{array scan angle}$$
$$g = 1 + \frac{\alpha^2}{2} \quad (\text{A VI-1})$$

In this design  $\alpha$  is  $40^{\circ}$  and array scan angle is  $80^{\circ}$ . Therefore we will have:

$$\gamma = \frac{\sin(\Psi_{\alpha})}{\sin\alpha} = 1.53$$

$$g = 1 + \frac{\alpha^2}{2} = 1.24$$



## LIST OF REFERENCES

- F. C. Commission, "Commission's Rules Regarding Ultra-Wideband Transmission Systems." vol. FCC-0248, FCC, Ed., 2002.
- J. Wells, " Multigigabit wireless technology at 70 GHz, 80 GHz, and 90 GHz, " RFDESIGN, www.rfdesign.com 2006.
- Steven Christie et al, "Rotman Lens-Based Retrodirective Array," IEEE TRANSACTION ON ANTENNAS AND PROPAGATION, VOL. 60, NO. 3, MARCH 2012.
- M. Ranjbar Nikkhah, P. Loghmanni, J. Rashed-Mohassel, and A. A. Kishk, "Theory of ESPAR Design with Aperture Coupled Dielectric Resonators and Their Implementation in Large Arrays," *IEEE Trans. Antennas Propag.*, vol. 62, no. 6, pp. 3359-3364, June 2014.
- Woosung Lee et al, "Compact Two-Layer Rotman Lens-Fed Microstrip Antenna Array at 24 GHz," *IEEE Transactions on Antennas and Propagation*, VOL. 59, NO. 2, FEBRUARY 2011.
- M. Ranjbar Nikkhah, M. Hiranandani, A. A. Kishk and K. Wu, "Fast Design of Rotman Lens and its Application in Rotman-DRA Phased array," *in Proc. IEEE APS Int. Symp., Jul. 2015, Vancouver, Canada.*
- R. C. Hansen, *Phased Array Antennas*. New York: John Wiley& Sons, Inc., 1998.
- J. Brown, *Microwave Lens*: Methuen, 1953.
- J. Brown, Jones, S.S., "Microwave Lenses," *Electronic Engineering*, vol.22, p.6, Apr-Oct 1950.
- R.M.Cox and J.R.Sebring, "MLS-A practical application of microwave technology," *IEEE Transactions on Microwave Theory and Techniques*, vol. MTT-24, p. 8, Dec. 1976.
- K. Jaeheung, "Developments of Rotman Lenses at Micro/Millimeter-wave Frequencies," in *Electrical Engineering*. vol. Ph.D. Boulder: University of Colorado, 2003.
- J. Dong and A. I. Zaghoul, "Implementation of Microwave Lens for 360-Degree Scanning," in *IEEE International Symposium on Antennas Propagation* Charleston, South Carolina, 2009.
- O. Kilic and R. Dahlstrom, "Rotman Lens Beam Formers for Army Multifunction RF Antenna Applications," in *IEEE Antennas and Propagation Society International Symposium*, 2005, pp. 43-46 vol. 2B .



- J. Dong, A. I. Zaghoul, and C. J. Reddy, "Quaduple Bandwidth True Time Delay Printed Microwave Lens Beam Former for Ultra Wideband Multifunctional Phased Array Applications," in *IEEE International Symposium on Antennas and Propagation*, North Charleston, South Carolina, 2009.
- J. Dong, A. I. Zaghoul, R. Sun, C. J. Reddy, and S. Weiss, "Accurate Simulation of Rotman-Lens Using FEKO," in *Applied Computational Electromagnetics Society (ACES) Conference* Monterey, California 2009.
- C. W. Penney, R. J. Luebbers, and E. Lenzing, "Broad band Rotman Lens simulations in FDTD,"  
" 2005, pp. 51-54 vol. 2B.
- S. Weiss, S. Keller, and C. Ly, "Development of Simple Affordable Beamformer for Army Platforms," in *Proceedings of GOMACTech-07 Conference* Lake Buena Vista, FL, 2006.
- W. Rotman and R. Turner, "Wide-angle microwave lens for line source applications," *IEEE-Trans. Antennas Prpag.*, vol. AP-11, no.6, pp. 623-632, Nov.1963.
- Hansen R. C., "Design Trades for Rotman Lenses," *IEEE Transactions on Antennas and Propagation*, vol. 39, no. 4, April 1991.
- Y. Yang, Y. Wang, and A. E. Fathy "DESIGN OF COMPACT VIVALDI ANTENNA ARRAYS FOR UWB SEE THROUGH WALL APPLICATION" *Progress In Electromagnetics Research*, PIER 82, 401–418, 2008.
- C. Rappaport and A. Zaghoul, "Optimized three-dimensional lenses for wide-angle scanning" in *IEEE Transactions on Antennas and Propagation*, vol. 33, no. 11, pp. 1227-1236, E Nov 1985.doi: 10.1109/TAP.1985.1143519
- R. Dhawan\* and Gurkirandeep Kaur "VIVALDI ANTENNA SIMULATION ON DEFINING PARAMETERS, PARAMETRIC STUDY AND RESULTS" *Progress In International Science Press*, pp. 5129-5138, 9(11) 2016, I J C T A
- J. Shin and D. H. Schaubert, "A parameter study of stripline-fed Vivaldi notch-antenna arrays," in *IEEE Transactions on Antennas and Propagation*, vol. 47, no. 5, pp. 879-886, May 1999.doi: 10.1109/8.774151

G. Adamiuk, T. Zwick and W. Wiesbeck, "Dual-orthogonal polarized Vivaldi antenna for ultra wideband applications," MIKON 2008 - 17th International Conference on Microwaves, Radar and Wireless Communications, Wroclaw, 2008, pp. 1-4

Min Wang, Wen Wu, Zhongxiang shen "Bandwidth Enhancement of antenna arrays utilizing mutual coupling between antenna elements" Hindawi Publishing Corporation International Journal of Antennas and Propagation Volume 2010, Article ID 690713

Mike Stasiowski and Dan Schaubert "BROADBAND ARRAY ANTENNA"

Nurhayati, E. Setijadi and G. Hendranto, "Comparison study of S-Band Vivaldi-based antennas," 2016 IEEE Region 10 Symposium (TENSYMP), Bali, 2016, pp. 188-193.doi: 10.1109/TENCONSpring.2016.7519402